REPORT DOCUMENTATION PAGE

AFRL-SR-BL-TR-00-

0490

1. AGENCY USE ONLY *(Leave blank)*	2. REPORT DATE	3. RE
	December, 1998	

4. TITLE AND SUBTITLE
1998 Summer Research Program (SRP), High School Apprenticeship Program (HSAP), Final Reports, Volume 14, Phillips Laboratory

5. FUNDING NUMBERS
F49620-93-C-0063

6. AUTHOR(S)
Gary Moore

7. PERFORMING ORGANIZATION NAME(S) AND ADDRESS(ES)
Research & Development Laboratories (RDL)
5800 Uplander Way
Culver City, CA 90230-6608

8. PERFORMING ORGANIZATION REPORT NUMBER

9. SPONSORING/MONITORING AGENCY NAME(S) AND ADDRESS(ES)
Air Force Office of Scientific Research (AFOSR)
801 N. Randolph St.
Arlington, VA 22203-1977

10. SPONSORING/MONITORING AGENCY REPORT NUMBER

11. SUPPLEMENTARY NOTES

12a. DISTRIBUTION AVAILABILITY STATEMENT
Approved for Public Release

12b. DISTRIBUTION CODE

13. ABSTRACT *(Maximum 200 words)*

The United States Air Force Summer Research Program (USAF-SRP) is designed to introduce university, college, and technical institute faculty members, graduate students, and high school students to Air Force research. This is accomplished by the faculty members (Summer Faculty Research Program, (SFRP)), graduate students (Graduate Student Research Program (GSRP)), and high school students (High School Apprenticeship Program (HSAP)) being selected on a nationally advertised competitive basis during the summer intersession period to perform research at Air Force Research Laboratory (AFRL) Technical Directorates, Air Force Air Logistics Centers (ALC), and other AF Laboratories. This volume consists of a program overview, program management statistics, and the final technical reports from the HSAP participants at the Phillips Laboratory.

14. SUBJECT TERMS
Air Force Research, Air Force, Engineering, Laboratories, Reports, Summer, Universities, Faculty, Graduate Student, High School Student

15. NUMBER OF PAGES

16. PRICE CODE

17. SECURITY CLASSIFICATION OF REPORT	18. SECURITY CLASSIFICATION OF THIS PAGE	19. SECURITY CLASSIFICATION OF ABSTRACT	20. LIMITATION OF ABSTRACT
Unclassified	Unclassified	Unclassified	UL

UNITED STATES AIR FORCE

SUMMER RESEARCH PROGRAM -- 1998

HIGH SCHOOL APPRENTICESHIP PROGRAM FINAL REPORTS

VOLUME 14

PHILLIPS LABORATORY

RESEARCH & DEVELOPMENT LABORATORIES

5800 Uplander Way

Culver City, CA 90230-6608

Program Director, RDL
Gary Moore

Program Manager, AFOSR
Colonel Jan Cerveny

Program Manager, RDL
Scott Licoscos

Program Administrator, RDL
Johnetta Thompson

Program Administrator, RDL
Rebecca Kelly-Clemmons

Submitted to:

AIR FORCE OFFICE OF SCIENTIFIC RESEARCH

Bolling Air Force Base

Washington, D.C.

December 1998

PREFACE

Reports in this volume are numbered consecutively beginning with number 1. Each report is paginated with the report number followed by consecutive page numbers, e.g., 1-1, 1-2, 1-3; 2-1, 2-2, 2-3.

This document is one of a set of 15 volumes describing the 1998 AFOSR Summer Research Program. The following volumes comprise the set:

VOLUME	TITLE
1	Program Management Report
	Summer Faculty Research Program (SFRP) Reports
2	Armstrong Laboratory
3	Phillips Laboratory
4	Rome Laboratory
5A & 5B	Wright Laboratory
6	Arnold Engineering Development Center, Air Logistics Centers, United States Air Force Academy and Wilford Hall Medical Center
	Graduate Student Research Program (GSRP) Reports
7	Armstrong Laboratory
8	Phillips Laboratory
9	Rome Laboratory
10	Wright Laboratory
11	Arnold Engineering Development Center, and Wilford Hall Medical Center
	High School Apprenticeship Program (HSAP) Reports
12	Armstrong Laboratory
13	Phillips Laboratory
14	Rome Laboratory
15A, 15B & 15C	Wright Laboratory

SRP Final Report Table of Contents

SRP Final Report Table of Contents

SRP Final Report Table of Contents

SRP Final Report Table of Contents

SRP Final Report Table of Contents

SRP Final Report Table of Contents

SRP Final Report Table of Contents

SRP Final Report Table of Contents

SRP Final Report Table of Contents

1. INTRODUCTION

The Summer Research Program (SRP), sponsored by the Air Force Office of Scientific Research (AFOSR), offers paid opportunities for university faculty, graduate students, and high school students to conduct research in U.S. Air Force research laboratories nationwide during the summer.

Introduced by AFOSR in 1978, this innovative program is based on the concept of teaming academic researchers with Air Force scientists in the same disciplines using laboratory facilities and equipment not often available at associates' institutions.

The Summer Faculty Research Program (SFRP) is open annually to approximately 150 faculty members with at least two years of teaching and/or research experience in accredited U.S. colleges, universities, or technical institutions. SFRP associates must be either U.S. citizens or permanent residents.

The Graduate Student Research Program (GSRP) is open annually to approximately 100 graduate students holding a bachelor's or a master's degree; GSRP associates must be U.S. citizens enrolled full time at an accredited institution.

The High School Apprentice Program (HSAP) annually selects about 125 high school students located within a twenty mile commuting distance of participating Air Force laboratories.

AFOSR also offers its research associates an opportunity, under the Summer Research Extension Program (SREP), to continue their AFOSR-sponsored research at their home institutions through the award of research grants. In 1994 the maximum amount of each grant was increased from $20,000 to $25,000, and the number of AFOSR-sponsored grants decreased from 75 to 60. A separate annual report is compiled on the SREP.

The numbers of projected summer research participants in each of the three categories and SREP "grants" are usually increased through direct sponsorship by participating laboratories.

AFOSR's SRP has well served its objectives of building critical links between Air Force research laboratories and the academic community, opening avenues of communications and forging new research relationships between Air Force and academic technical experts in areas of national interest, and strengthening the nation's efforts to sustain careers in science and engineering. The success of the SRP can be gauged from its growth from inception (see Table 1) and from the favorable responses the 1997 participants expressed in end-of-tour SRP evaluations (Appendix B).

AFOSR contracts for administration of the SRP by civilian contractors. The contract was first awarded to Research & Development Laboratories (RDL) in September 1990. After completion of the 1990 contract, RDL (in 1993) won the recompetition for the basic year and four 1-year options.

2. PARTICIPATION IN THE SUMMER RESEARCH PROGRAM

The SRP began with faculty associates in 1979; graduate students were added in 1982 and high school students in 1986. The following table shows the number of associates in the program each year.

YEAR	SRP Participation, by Year			TOTAL
	SFRP	GSRP	HSAP	
1979	70			70
1980	87			87
1981	87			87
1982	91	17		108
1983	101	53		154
1984	152	84		236
1985	154	92		246
1986	158	100	42	300
1987	159	101	73	333
1988	153	107	101	361
1989	168	102	103	373
1990	165	121	132	418
1991	170	142	132	444
1992	185	121	159	464
1993	187	117	136	440
1994	192	117	133	442
1995	190	115	137	442
1996	188	109	138	435
1997	148	98	140	427
1998	85	40	88	213

Beginning in 1993, due to budget cuts, some of the laboratories weren't able to afford to fund as many associates as in previous years. Since then, the number of funded positions has remained fairly constant at a slightly lower level.

3. RECRUITING AND SELECTION

The SRP is conducted on a nationally advertised and competitive-selection basis. The advertising for faculty and graduate students consisted primarily of the mailing of 8,000 52-page SRP brochures to chairpersons of departments relevant to AFOSR research and to administrators of grants in accredited universities, colleges, and technical institutions. Historically Black Colleges and Universities (HBCUs) and Minority Institutions (MIs) were included. Brochures also went to all participating USAF laboratories, the previous year's participants, and numerous individual requesters (over 1000 annually).

RDL placed advertisements in the following publications: *Black Issues in Higher Education, Winds of Change,* and *IEEE Spectrum.* Because no participants list either *Physics Today* or *Chemical & Engineering News* as being their source of learning about the program for the past several years, advertisements in these magazines were dropped, and the funds were used to cover increases in brochure printing costs.

High school applicants can participate only in laboratories located no more than 20 miles from their residence. Tailored brochures on the HSAP were sent to the head counselors of 180 high schools in the vicinity of participating laboratories, with instructions for publicizing the program in their schools. High school students selected to serve at Wright Laboratory's Armament Directorate (Eglin Air Force Base, Florida) serve eleven weeks as opposed to the eight weeks normally worked by high school students at all other participating laboratories.

Each SFRP or GSRP applicant is given a first, second, and third choice of laboratory. High school students who have more than one laboratory or directorate near their homes are also given first, second, and third choices.

Laboratories make their selections and prioritize their nominees. AFOSR then determines the number to be funded at each laboratory and approves laboratories' selections.

Subsequently, laboratories use their own funds to sponsor additional candidates. Some selectees do not accept the appointment, so alternate candidates are chosen. This multi-step selection procedure results in some candidates being notified of their acceptance after scheduled deadlines. The total applicants and participants for 1998 are shown in this table.

1998 Applicants and Participants			
PARTICIPANT CATEGORY	TOTAL APPLICANTS	SELECTEES	DECLINING SELECTEES
SFRP	382	85	13
(HBCU/MI)	(0)	(0)	(0)
GSRP	130	40	7
(HBCU/MI)	(0)	(0)	(0)
HSAP	328	88	22
TOTAL	840	213	42

4. SITE VISITS

During June and July of 1998, representatives of both AFOSR/NI and RDL visited each participating laboratory to provide briefings, answer questions, and resolve problems for both laboratory personnel and participants. The objective was to ensure that the SRP would be as constructive as possible for all participants. Both SRP participants and RDL representatives found these visits beneficial. At many of the laboratories, this was the only opportunity for all participants to meet at one time to share their experiences and exchange ideas.

5. HISTORICALLY BLACK COLLEGES AND UNIVERSITIES AND MINORITY INSTITUTIONS (HBCU/MIs)

Before 1993, an RDL program representative visited from seven to ten different HBCU/MIs annually to promote interest in the SRP among the faculty and graduate students. These efforts were marginally effective, yielding a doubling of HBCI/MI applicants. In an effort to achieve AFOSR's goal of 10% of all applicants and selectees being HBCU/MI qualified, the RDL team decided to try other avenues of approach to increase the number of qualified applicants. Through the combined efforts of the AFOSR Program Office at Bolling AFB and RDL, two very active minority groups were found, HACU (Hispanic American Colleges and Universities) and AISES (American Indian Science and Engineering Society). RDL is in communication with representatives of each of these organizations on a monthly basis to keep up with the their activities and special events. Both organizations have widely-distributed magazines/quarterlies in which RDL placed ads.

Since 1994 the number of both SFRP and GSRP HBCU/MI applicants and participants has increased ten-fold, from about two dozen SFRP applicants and a half dozen selectees to over 100 applicants and two dozen selectees, and a half-dozen GSRP applicants and two or three selectees to 18 applicants and 7 or 8 selectees. Since 1993, the SFRP had a two-fold applicant increase and a two-fold selectee increase. Since 1993, the GSRP had a three-fold applicant increase and a three to four-fold increase in selectees.

In addition to RDL's special recruiting efforts, AFOSR attempts each year to obtain additional funding or use leftover funding from cancellations the past year to fund HBCU/MI associates.

SRP HBCU/MI Participation, By Year				
YEAR	SFRP		GSRP	
	Applicants	Participants	Applicants	Participants
1985	76	23	15	11
1986	70	18	20	10
1987	82	32	32	10
1988	53	17	23	14
1989	39	15	13	4
1990	43	14	17	3
1991	42	13	8	5
1992	70	13	9	5
1993	60	13	6	2
1994	90	16	11	6
1995	90	21	20	8
1996	119	27	18	7

6. SRP FUNDING SOURCES

Funding sources for the 1998 SRP were the AFOSR-provided slots for the basic contract and laboratory funds. Funding sources by category for the 1998 SRP selected participants are shown here.

1998 SRP FUNDING CATEGORY	SFRP	GSRP	HSAP
AFOSR Basic Allocation Funds	67	38	75
USAF Laboratory Funds	17	2	13
Slots Added by AFOSR (Leftover Funds)	0	0	0
HBCU/MI By AFOSR (Using Procured Addn'l Funds)	0	0	N/A
TOTAL	84	40	88

7. COMPENSATION FOR PARTICIPANTS

Compensation for SRP participants, per five-day work week, is shown in this table.

1998 SRP Associate Compensation

PARTICIPANT CATEGORY	1991	1992	1993	1994	1995	1996	1997	1998
Faculty Members	$690	$718	$740	$740	$740	$770	$770	$793
Graduate Student (Master's Degree)	$425	$442	$455	$455	$455	$470	$470	$484
Graduate Student (Bachelor's Degree)	$365	$380	$391	$391	$391	$400	$400	$412
High School Student (First Year)	$200	$200	$200	$200	$200	$200	$200	$200
High School Student (Subsequent Years)	$240	$240	$240	$240	$240	$240	$240	$240

The program also offered associates whose homes were more than 50 miles from the laboratory an expense allowance (seven days per week) of $52/day for faculty and $41/day for graduate students. Transportation to the laboratory at the beginning of their tour and back to their home destinations at the end was also reimbursed for these participants. Of the combined SFRP and GSRP associates, 65 % claimed travel reimbursements at an average round-trip cost of $730.

Faculty members were encouraged to visit their laboratories before their summer tour began. All costs of these orientation visits were reimbursed. Forty-three percent (85 out of 188) of faculty associates took orientation trips at an average cost of $449. By contrast, in 1993, 58 % of SFRP associates elected to take an orientation visits at an average cost of $685; that was the highest percentage of

associates opting to take an orientation trip since RDL has administered the SRP, and the highest average cost of an orientation trip.

Program participants submitted biweekly vouchers countersigned by their laboratory research focal point, and RDL issued paychecks so as to arrive in associates' hands two weeks later.

This is the third year of using direct deposit for the SFRP and GSRP associates. The process went much more smoothly with respect to obtaining required information from the associates, about 15% of the associates' information needed clarification in order for direct deposit to properly function as opposed to 7% from last year. The remaining associates received their stipend and expense payments via checks sent in the US mail.

HSAP program participants were considered actual RDL employees, and their respective state and federal income tax and Social Security were withheld from their paychecks. By the nature of their independent research, SFRP and GSRP program participants were considered to be consultants or independent contractors. As such, SFRP and GSRP associates were responsible for their own income taxes, Social Security, and insurance.

8. CONTENTS OF THE 1998 REPORT

The complete set of reports for the 1998 SRP includes this program management report (Volume 1) augmented by fifteen volumes of final research reports by the 1998 associates, as indicated below:

1998 SRP Final Report Volume Assignments

LABORATORY	SFRP	GSRP	HSAP
Armstrong	2	7	12
Phillips	3	8	13
Rome	4	9	14
Wright	5A, 5B	10	15
AEDC, ALCs, USAFA, WHMC	6	11	

APPENDIX A – PROGRAM STATISTICAL SUMMARY

A. Colleges/Universities Represented

Selected SFRP associates represented 169 different colleges, universities, and institutions, GSRP associates represented 95 different colleges, universities, and institutions.

B. States Represented

SFRP -Applicants came from 47 states plus Washington D.C. Selectees represent 44 states.

GSRP - Applicants came from 44 states. Selectees represent 32 states.

HSAP - Applicants came from thirteen states. Selectees represent nine states.

Total Number of Participants	
SFRP	85
GSRP	40
HSAP	88
TOTAL	213

Degrees Represented			
	SFRP	GSRP	TOTAL
Doctoral	83	0	83
Master's	1	3	4
Bachelor's	0	22	22
TOTAL	186	25	109

SFRP Academic Titles	
Assistant Professor	36
Associate Professor	34
Professor	15
Instructor	0
Chairman	0
Visiting Professor	0
Visiting Assoc. Prof.	0
Research Associate	0
TOTAL	85

Source of Learning About the SRP		
Category	Applicants	Selectees
Applied/participated in prior years	177	47
Colleague familiar with SRP	104	24
Brochure mailed to institution	101	21
Contact with Air Force laboratory	101	39
IEEE Spectrum	12	1
BIIHE	4	0
Other source	117	30
TOTAL	616	162

APPENDIX B – SRP EVALUATION RESPONSES

1. OVERVIEW

Evaluations were completed and returned to RDL by four groups at the completion of the SRP. The number of respondents in each group is shown below.

Table B-1. Total SRP Evaluations Received

Evaluation Group	Responses
SFRP & GSRPs	100
HSAPs	75
USAF Laboratory Focal Points	84
USAF Laboratory HSAP Mentors	6

All groups indicate unanimous enthusiasm for the SRP experience.

The summarized recommendations for program improvement from both associates and laboratory personnel are listed below:

A. Better preparation on the labs' part prior to associates' arrival (i.e., office space. computer assets, clearly defined scope of work).

B. Faculty Associates suggest higher stipends for SFRP associates.

C. Both HSAP Air Force laboratory mentors and associates would like the summer tour extended from the current 8 weeks to either 10 or 11 weeks; the groups state it takes 4-6 weeks just to get high school students up-to-speed on what's going on at laboratory. (Note: this same argument was used to raise the faculty and graduate studen participation time a few years ago.)

2. 1998 USAF LABORATORY FOCAL POINT (LFP) EVALUATION RESPONSES

The summarized results listed below are from the 84 LFP evaluations received.

1. LFP evaluations received and associate preferences:

Table B-2. Air Force LFP Evaluation Responses (By Type)

		How Many Associates Would You Prefer To Get ? (% Response)											
		SFRP				GSRP (w/Univ Professor)				GSRP (w/o Univ Professor)			
Lab	Evals Recv'd	0	1	2	3+	0	1	2	3+	0	1	2	3+
AEDC	0	-	-	-	-	-	-	-	-	-	-	-	-
WHMC	0	-	-	-	-	-	-	-	-	-	-	-	-
AL	7	28	28	28	14	54	14	28	0	86	0	14	0
USAFA	1	0	100	0	0	100	0	0	0	0	100	0	0
PL	25	40	40	16	4	88	12	0	0	84	12	4	0
RL	5	60	40	0	0	80	10	0	0	100	0	0	0
WL	46	30	43	20	6	78	17	4	0	93	4	2	0
Total	**84**	**32%**	**50%**	**13%**	**5%**	**80%**	**11%**	**6%**	**0%**	**73%**	**23%**	**4%**	**0%**

LFP Evaluation Summary. The summarized responses, by laboratory, are listed on the following page. LFPs were asked to rate the following questions on a scale from 1 (below average) to 5 (above average).

2. LFPs involved in SRP associate application evaluation process:
   a. Time available for evaluation of applications:
   b. Adequacy of applications for selection process:
3. Value of orientation trips:
4. Length of research tour:
5. a. Benefits of associate's work to laboratory:
   b. Benefits of associate's work to Air Force:
6. a. Enhancement of research qualifications for LFP and staff:
   b. Enhancement of research qualifications for SFRP associate:
   c. Enhancement of research qualifications for GSRP associate:
7. a. Enhancement of knowledge for LFP and staff:
   b. Enhancement of knowledge for SFRP associate:
   c. Enhancement of knowledge for GSRP associate:
8. Value of Air Force and university links:
9. Potential for future collaboration:
10. a. Your working relationship with SFRP:
    b. Your working relationship with GSRP:
11. Expenditure of your time worthwhile:

(Continued on next page)

12. Quality of program literature for associate:
13. a. Quality of RDL's communications with you:
    b. Quality of RDL's communications with associates:
14. Overall assessment of SRP:

Table B-3. Laboratory Focal Point Reponses to above questions

	AEDC	*AL*	*USAFA*	*PL*	*RL*	*WHMC*	*WL*
# Evals Recv'd	0	7	1	14	5	0	46
Question #							
2	-	86 %	0 %	88 %	80 %	-	85 %
2a	-	4.3	n/a	3.8	4.0	-	3.6
2b	-	4.0	n/a	3.9	4.5	-	4.1
3	-	4.5	n/a	4.3	4.3	-	3.7
4	-	4.1	4.0	4.1	4.2	-	3.9
5a	-	4.3	5.0	4.3	4.6	-	4.4
5b	-	4.5	n/a	4.2	4.6	-	4.3
6a	-	4.5	5.0	4.0	4.4	-	4.3
6b	-	4.3	n/a	4.1	5.0	-	4.4
6c	-	3.7	5.0	3.5	5.0	-	4.3
7a	-	4.7	5.0	4.0	4.4	-	4.3
7b	-	4.3	n/a	4.2	5.0	-	4.4
7c	-	4.0	5.0	3.9	5.0	-	4.3
8	-	4.6	4.0	4.5	4.6	-	4.3
9	-	4.9	5.0	4.4	4.8	-	4.2
10a	-	5.0	n/a	4.6	4.6	-	4.6
10b	-	4.7	5.0	3.9	5.0	-	4.4
11	-	4.6	5.0	4.4	4.8	-	4.4
12	-	4.0	4.0	4.0	4.2	-	3.8
13a	-	3.2	4.0	3.5	3.8	-	3.4
13b	-	3.4	4.0	3.6	4.5	-	3.6
14	-	4.4	5.0	4.4	4.8	-	4.4

3. 1998 SFRP & GSRP EVALUATION RESPONSES

The summarized results listed below are from the 120 SFRP/GSRP evaluations received.

Associates were asked to rate the following questions on a scale from 1 (below average) to 5 (above average) - by Air Force base results and over-all results of the 1998 evaluations are listed after the questions.

1. The match between the laboratories research and your field:
2. Your working relationship with your LFP:
3. Enhancement of your academic qualifications:
4. Enhancement of your research qualifications:
5. Lab readiness for you: LFP, task, plan:
6. Lab readiness for you: equipment, supplies, facilities:
7. Lab resources:
8. Lab research and administrative support:
9. Adequacy of brochure and associate handbook:
10. RDL communications with you:
11. Overall payment procedures:
12. Overall assessment of the SRP:
13. a. Would you apply again?
    b. Will you continue this or related research?
14. Was length of your tour satisfactory?
15. Percentage of associates who experienced difficulties in finding housing:
16. Where did you stay during your SRP tour?
    a. At Home:
    b. With Friend:
    c. On Local Economy:
    d. Base Quarters:
17. Value of orientation visit:
    a. Essential:
    b. Convenient:
    c. Not Worth Cost:
    d. Not Used:

SFRP and GSRP associate's responses are listed in tabular format on the following page.

Table B-4. 1997 SFRP & GSRP Associate Responses to SRP Evaluation

	Arnold	Brooks	Edwards	Eglin	Griffis	Hanscom	Kelly	Kirtland	Lackland	Robins	Tyndall	WPAFB	average
# res	6	48	6	14	31	19	3	32	1	2	10	85	257
1	4.8	4.4	4.6	4.7	4.4	4.9	4.6	4.6	5.0	5.0	4.0	4.7	4.6
2	5.0	4.6	4.1	4.9	4.7	4.7	5.0	4.7	5.0	5.0	4.6	4.8	4.7
3	4.5	4.4	4.0	4.6	4.3	4.2	4.3	4.4	5.0	5.0	4.5	4.3	4.4
4	4.3	4.5	3.8	4.6	4.4	4.4	4.3	4.6	5.0	4.0	4.4	4.5	4.5
5	4.5	4.3	3.3	4.8	4.4	4.5	4.3	4.2	5.0	5.0	3.9	4.4	4.4
6	4.3	4.3	3.7	4.7	4.4	4.5	4.0	3.8	5.0	5.0	3.8	4.2	4.2
7	4.5	4.4	4.2	4.8	4.5	4.3	4.3	4.1	5.0	5.0	4.3	4.3	4.4
8	4.5	4.6	3.0	4.9	4.4	4.3	4.3	4.5	5.0	5.0	4.7	4.5	4.5
9	4.7	4.5	4.7	4.5	4.3	4.5	4.7	4.3	5.0	5.0	4.1	4.5	4.5
10	4.2	4.4	4.7	4.4	4.1	4.1	4.0	4.2	5.0	4.5	3.6	4.4	4.3
11	3.8	4.1	4.5	4.0	3.9	4.1	4.0	4.0	3.0	4.0	3.7	4.0	4.0
12	5.7	4.7	4.3	4.9	4.5	4.9	4.7	4.6	5.0	4.5	4.6	4.5	4.6
Numbers below are percentages													
13a	83	90	83	93	87	75	100	81	100	100	100	86	87
13b	100	89	83	100	94	98	100	94	100	100	100	94	93
14	83	96	100	90	87	80	100	92	100	100	70	84	88
15	17	6	0	33	20	76	33	25	0	100	20	8	39
16a	-	26	17	9	38	23	33	4	-	-	-	30	
16b	100	33	-	40	-	8	-	-	-	-	36	2	
16c	-	41	83	40	62	69	67	96	100	100	64	68	
16d	-	-	-	-	-	-	-	-	-	-	-	0	
17a	-	33	100	17	50	14	67	39	-	50	40	31	35
17b	-	21	-	17	10	14	-	24	-	50	20	16	16
17c	-	-	-	-	10	7	-	-	-	-	-	2	3
17d	100	46	-	66	30	69	33	37	100	-	40	51	46

4. 1998 USAF LABORATORY HSAP MENTOR EVALUATION RESPONSES

Not enough evaluations received (5 total) from Mentors to do useful summary.

5. 1998 HSAP EVALUATION RESPONSES

The summarized results listed below are from the 23 HSAP evaluations received.

HSAP apprentices were asked to rate the following questions on a scale from 1 (below average) to 5 (above average)

1. Your influence on selection of topic/type of work.
2. Working relationship with mentor, other lab scientists.
3. Enhancement of your academic qualifications.
4. Technically challenging work.
5. Lab readiness for you: mentor, task, work plan, equipment.
6. Influence on your career.
7. Increased interest in math/science.
8. Lab research & administrative support.
9. Adequacy of RDL's Apprentice Handbook and administrative materials.
10. Responsiveness of RDL communications.
11. Overall payment procedures.
12. Overall assessment of SRP value to you.
13. Would you apply again next year? Yes (92 %)
14. Will you pursue future studies related to this research? Yes (68 %)
15. Was Tour length satisfactory? Yes (82 %)

	Arnold	Brooks	Edwards	Eglin	Griffiss	Hanscom	Kirtland	Tyndall	WPAFB	Totals
# resp	5	19	7	15	13	2	7	5	40	113
1	2.8	3.3	3.4	3.5	3.4	4.0	3.2	3.6	3.6	3.4
2	4.4	4.6	4.5	4.8	4.6	4.0	4.4	4.0	4.6	4.6
3	4.0	4.2	4.1	4.3	4.5	5.0	4.3	4.6	4.4	4.4
4	3.6	3.9	4.0	4.5	4.2	5.0	4.6	3.8	4.3	4.2
5	4.4	4.1	3.7	4.5	4.1	3.0	3.9	3.6	3.9	4.0
6	3.2	3.6	3.6	4.1	3.8	5.0	3.3	3.8	3.6	3.7
7	2.8	4.1	4.0	3.9	3.9	5.0	3.6	4.0	4.0	3.9
8	3.8	4.1	4.0	4.3	4.0	4.0	4.3	3.8	4.3	4.2
9	4.4	3.6	4.1	4.1	3.5	4.0	3.9	4.0	3.7	3.8
10	4.0	3.8	4.1	3.7	4.1	4.0	3.9	2.4	3.8	3.8
11	4.2	4.2	3.7	3.9	3.8	3.0	3.7	2.6	3.7	3.8
12	4.0	4.5	4.9	4.6	4.6	5.0	4.6	4.2	4.3	4.5
Numbers below are percentages										
13	60%	95%	100%	100%	85%	100%	100%	100%	90%	92%
14	20%	80%	71%	80%	54%	100%	71%	80%	65%	68%
15	100%	70%	71%	100%	100%	50%	86%	60%	80%	82%

CHARACTERIZATION OF THE CO2 LASER

Lauren A. Ferguson

Moriarty High School
PO Box 2000
Moriarty, NM 87035

Final Report for:
High School Apprenticeship Program
AFRL/Phillips Laboratory

Sponsored by:
Air Force Office of Scientific Research
Bolling Air Force Base, DC

And

Phillips Laboratory

August 1998

CHARACTERIZATION OF THE CO_2 LASER

Lauren A. Ferguson
Moriarty High School

Abstract

A carbon dioxide laser was characterized. To characterize the laser, a series of tests were run to determine the laser's P- branch wavelength capabilities, power vs. temperature relationship, and overall stability. Experimental results indicated that the laser runs more efficiently at lower temperatures. The laser also seems to be more stable at the P(20) wavelength instead of at P(22). The tests also showed that to use the laser in an experimental setup, the laser needed to be refurbished.

CHARACTERIZATION OF THE CO_2 LASER

Lauren A. Ferguson

Introduction

Satellites play a big role in our lives: from cable television and mobile phone services to global positioning, weather forecasting, and even surveillance. However, the traditional way of tracking them is not very precise. Currently, satellites are tracked with the use of radar. Unfortunately, radar can only provide a general position, not an exact location, of the satellite. In order to alleviate this potential problem, the idea of using lasers to track satellites has been considered. Because lasers have a smaller focus, they can pinpoint exactly where the satellite can be found. With enough research, lasers might even be able to determine a satellite's velocity and speed, the direction it's pointing, and even to whom it belongs. This information can be used to maintain United States satellites and to monitor those belonging to other nations.

Currently, no one is using lasers to track satellites and the United States is the only country doing research for that purpose. Part of the reason may be that lasers are still relatively new and their full capabilities have not yet been discovered. Therefore, this project is not only to determine whether lasers can track satellites, but also to learn more about the lasers themselves. Since lasers are so new, there is limited knowledge about them. For this reason, the project itself is mainly trial and error. However, the system continues to be tested and improved upon.

The laser setup needed for this project requires two main parts: the transmitter and the receiver. In this case, the transmitter is the laser (or lasers) itself. When the laser beam is directed out into space and comes in contact with the satellite, some of the light photons will be reflected off of the satellite and back to Earth. However, since the beam is so spread out by the time it reaches the satellite, the remainder of the photons will miss the satellite and continue out into space. The reflected photons are picked up by a detector (the receiver) and then fed into a computer or oscilloscope to be analyzed.

Before this process can be understood, however, it is first necessary to understand how lasers work. Laser stands for light amplification by stimulated emission of radiation. The picture below (fig. 1) shows the three main components of a laser: the pumping source, the active medium, and the reflecting mirrors (or cavity). When the active medium is pumped (in this case, carbon dioxide is repeatedly shocked with an electric discharge), the CO_2 molecules absorb the energy and are excited to a higher energy level. When one of the molecules decays back to the ground state, it emits a photon of light. This photon, in turn, stimulates other molecules to emit photons at the same wavelength as the first photon, creating stimulated emission. Many of the photons pass out of the cavity and are absorbed by the laser head casing. However, some of the photons run parallel with the cavity and reflect off the mirrors as they continue to stimulate more molecules to emit photons. Eventually, there are enough photons with enough energy for some to pass through the partial mirror and create a beam.

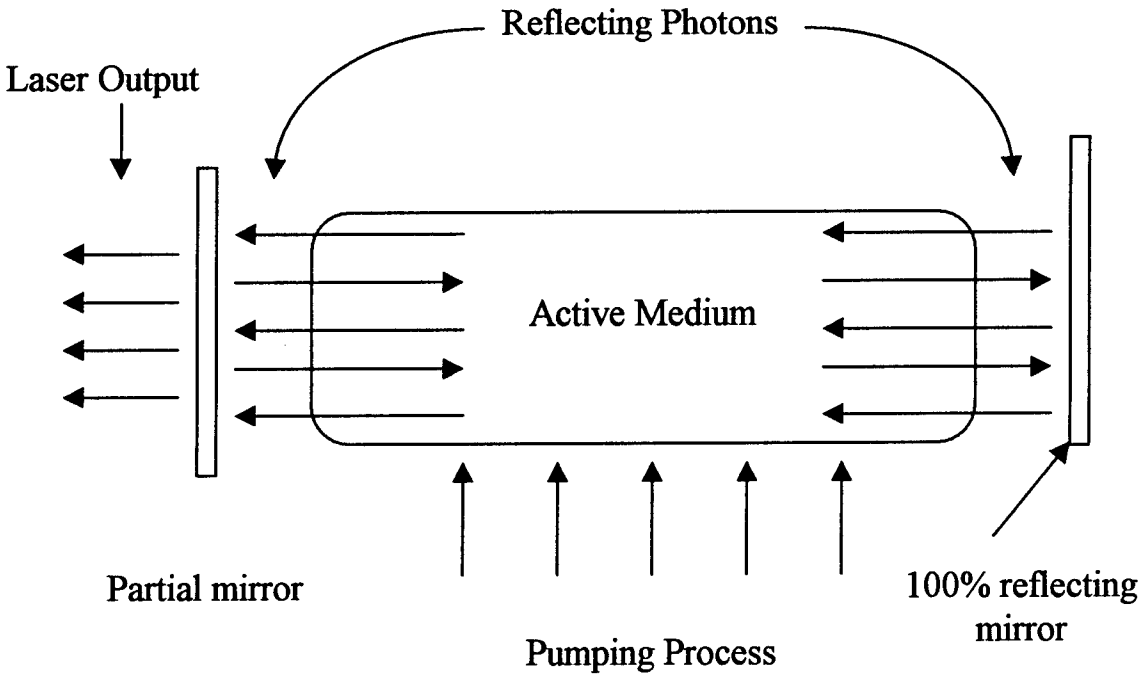

Figure 1. Schematic of the inside of a laser

Now that the lasers themselves have been discussed, it is important to understand the actual setup of the system that is currently being tested. The system consists of four lasers. The main laser is a carbon dioxide laser made by Laser Science Inc. (LSI) which is used for illuminating the targets. It is positioned on an optical breadboard next to two other CO_2 lasers that serve as the master and local oscillators. The fourth laser is a helium laser. It is used for alignment because the CO_2 lasers have invisible beams. A schematic of the system is shown below (fig. 2).

The master and local oscillators also serve a purpose. When the return beam comes back from the site, it enters a detector. Unfortunately, the detector creates a lot of noise, which, together with the fact that the return beam is greatly decreased in power, makes it hard to interpret the information that is received. To solve these problems, the local oscillator beam is mixed with the return beam before it enters the detector. In this way, the power of the beam is increased, but the noise stays the same. Another difficulty is that it is very hard to control the wavelength of the LSI laser. To overcome this dilemma, the master oscillator beam is shot into the LSI laser head. The smaller laser is easier to control and it stimulates the LSI to run at the same wavelength as the master oscillator.

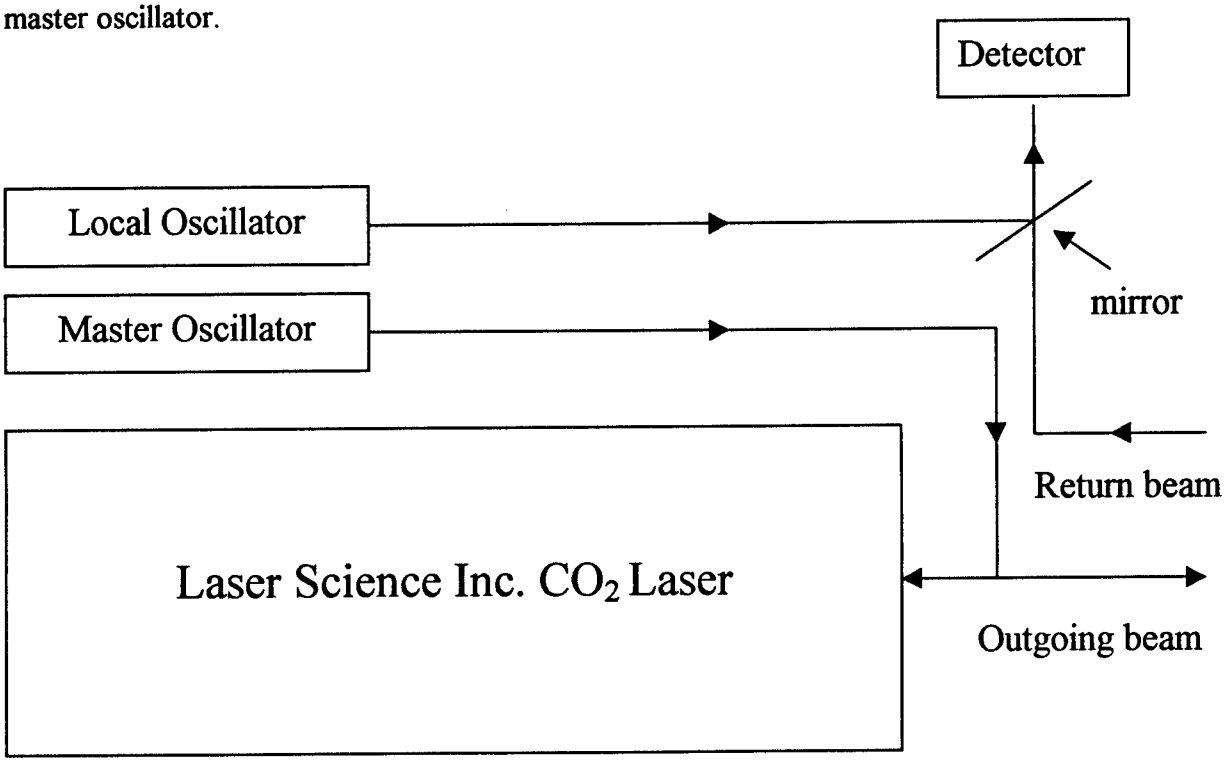

Figure 2. Schematic of the main system

Discussion of Problem

The laser that was being used as the master oscillator was not performing very well. It was hard for the master oscillator to stay at one transverse electromagnetic mode (TEM). Some of the transverse electromagnetic modes are shown below (fig. 3). The master oscillator would also waver between P(20) and P(22). (Note: P(x) represents the wavelength of the laser in the P-branch vibrational-rotational band.) Although the master oscillator could still be used, it was apparent that a replacement was needed. To avoid having to wait for a month to get the master oscillator fixed, a spare CO_2 laser was considered. Before the spare could be used in the setup, however, it had to be characterized to see if it was capable of being the master oscillator. To characterize the spare laser, five tests were performed on it. The first was a general test of which wavelengths could be reached in the P-branch vibrational-rotational band. There was also a power vs. temperature test and a stability test for both P(20) and P(22).

Methodology

To run the tests, a small optical breadboard was set up with the spare laser head, spectrum analyzer, power meter, laser power supply, frequency stabilizer, and flat reflecting mirrors as shown on the next page (fig. 4). Also included in the setup were a recirculating water cooler (chiller), a thermal image plate, a beam block, and a black light. While blocked, the spare laser was turned on for one hour before each test to allow the laser to warm up and stabilize. After one hour, the block was removed and the laser beam was reflected from mirror A to mirror B and into the spectrum analyzer. There, the P-branch wavelength was read and recorded. Next, mirror A was removed and the beam went into the power meter. There the voltage was read and recorded. Finally, the thermal image plate was placed in front of the beam and, with the help of the black light, the TEM was determined. (Note: While the spare laser was being characterized, experiments were also being run on the master oscillator in the main setup.)

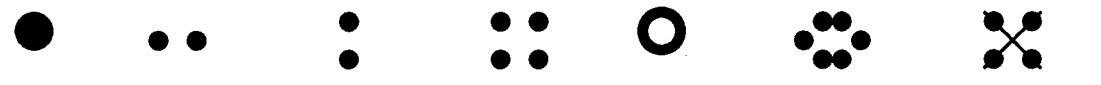

Figure 3. Picture of the transverse electromagnetic modes that have been encountered during this project.

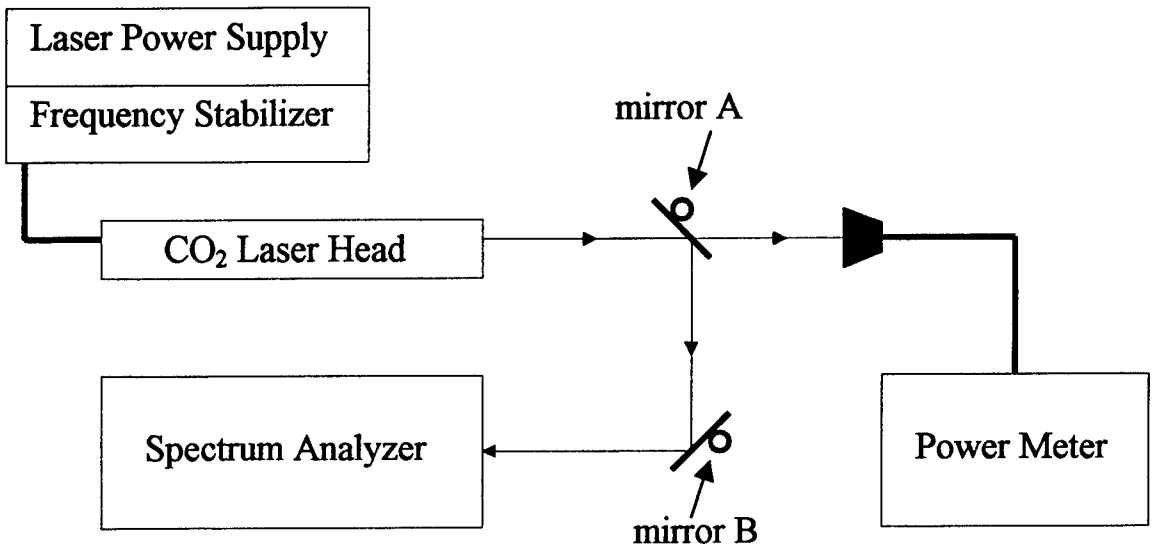

Figure 4. Schematic of the system used to characterize the spare CO_2 laser

The first test on the spare laser determined the maximum power output at each P-branch wavelength that could be reached. The temperature was kept constant at 21.5 degrees celsius. The micrometer on the laser head was used to adjust to the different wavelengths and the DC Bias knob on the frequency stabilizer was adjusted to achieve maximum power from the laser. The spare laser was stable at only six wavelengths (see table 1). Normally, the master oscillator is kept at P(22) and at this wavelength the spare laser emitted the most power and had a strong, stable beam. However, the beam quality at P(22) was poor. At this wavelength, the beam profile was TEM_{01} instead of the ideal mode, TEM_{00} (see fig. 3).

Since the master oscillator was already running at P(22) and the master oscillator needs to have high power readings, the next two tests on the spare laser were run at P(22). The first test focused on the relationship between power and temperature. The temperature is controlled by the chiller. After the laser had been running for one hour, the temperature and maximum power output were recorded. The first data point was taken at ten degrees celsius. Next, the temperature was set at 10.5°C and the spare laser was allowed to sit for fifteen minutes in order to stabilize. After the wait, the DC Bias knob was readjusted and the power was recorded again.

This procedure was repeated as the temperature was increased by .5 degree increments until 22°C was reached. The different temperatures produced significant variation in the maximum power output (see fig. 6). This test also determined the temperatures at which the laser would run best.

Based upon system considerations, the next test was run at 18.5°C. This test was used to determine if the spare laser would maintain a stable power output over an extended period of time. The power output was measured at thirty-minute intervals, each data point being taken after the DC Bias knob was adjusted for maximum output. Contrary to the first characterization test, the stability test proved the spare laser to have low power readings at P(22) and 18.5°C (see fig. 7).

During the characterization tests, the master oscillator was also being tested. The master oscillator was beginning to fluctuate in power at P(22) and was found to be more stable at P(20). For this reason, the power vs. temperature and stability tests were rerun on the spare laser at P(20). The power vs. temperature test showed that the spare laser worked well at 13.5°C (see fig. 8) and that the power readings were much higher at P(20) than at P(22). The stability test was rerun at 13.5°C and was stable compared to the P(22) stability test (see fig. 9).

Line	Power (watts)	TEM	Micrometer	DC Bias Voltage	Water Temp (°C)
P(10)	2	00	854	60.4	21.5
P(16)	1.6	01	880	45.1	21.5
P(20)	1.3	00	920	40.7	21.5
P(22)	2.8	01	916	62	21.5
P(24)	1	00	927	-4.1	21.5
P(28)	0.5	01	1033	56	21.5

Table 1. Data from first characterization test

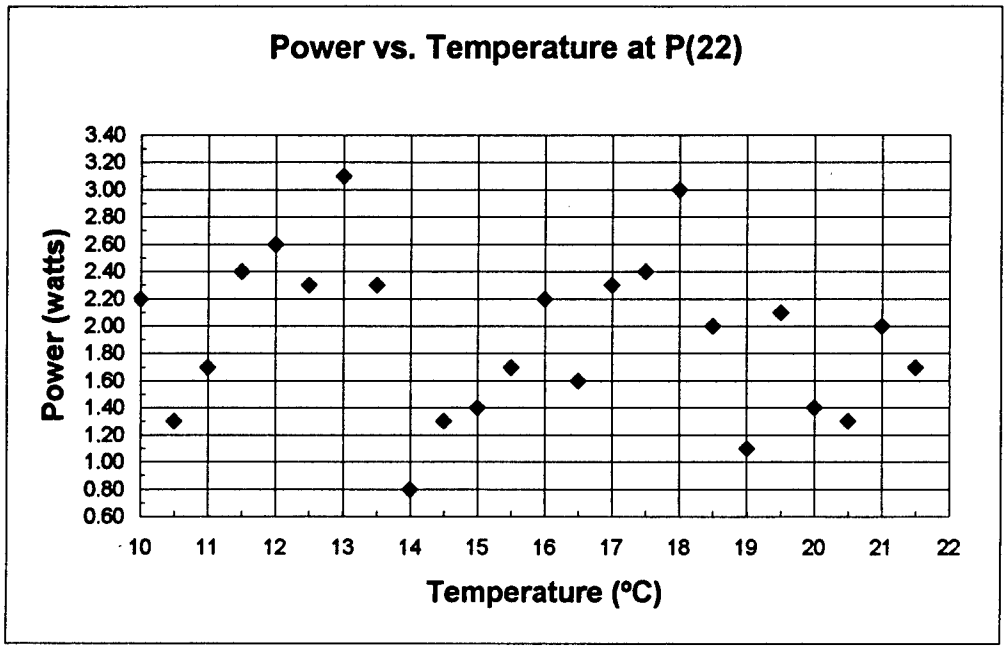

Figure 6. Data from second characterization test

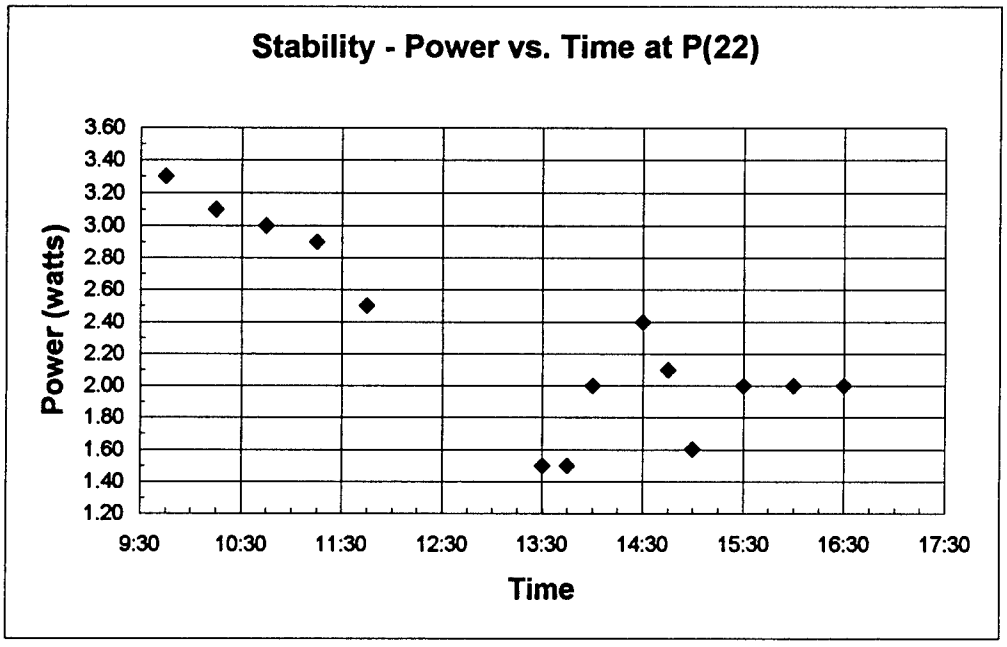

Figure 7. Data from third characterization test. Note: the gap in the data between 12:00 and 13:15 is due to the fact that the beam disappeared, making it impossible to take a data point.

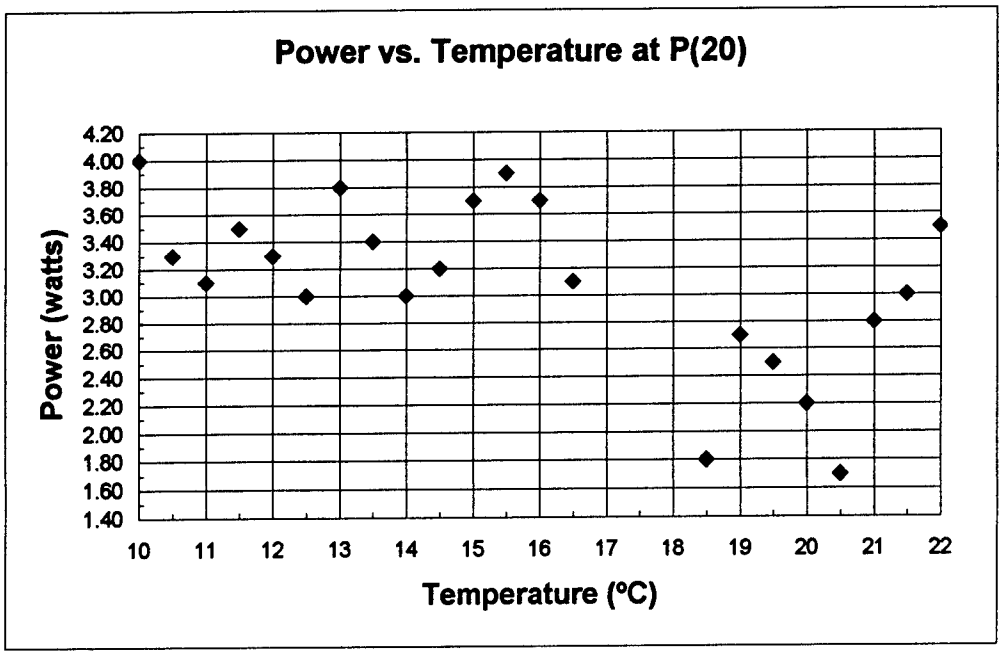

Figure 8. Data from fourth characterization test. Note: the gap in the data at 17°, 17.5°, and 18°C is due to the fact that the beam disappeared at these temperatures, making it impossible to take a data point.

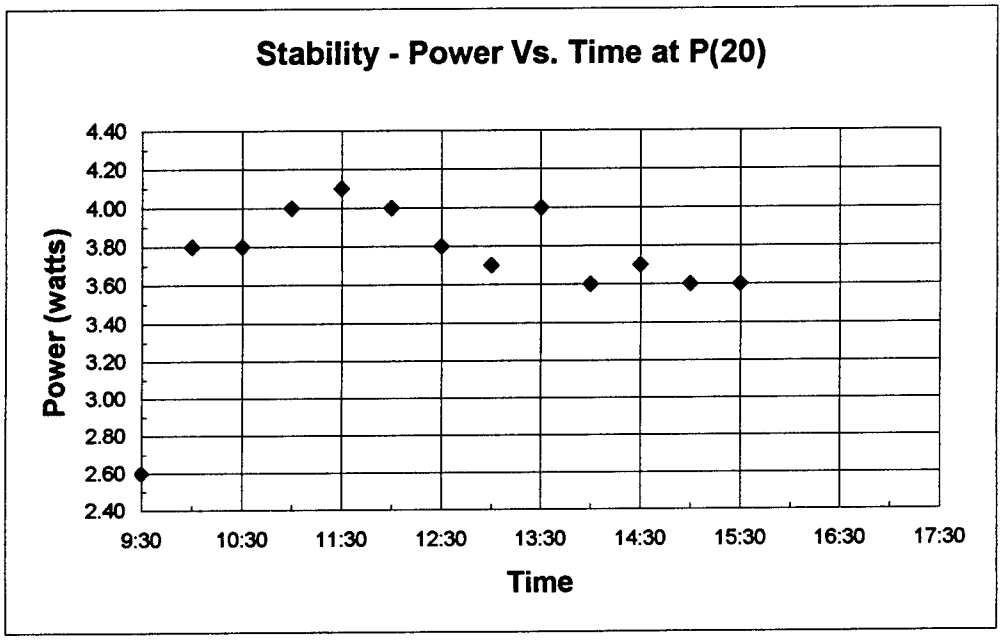

Figure 9. Data from fifth characterization test.

Results

The results of the first characterization test were used to determine which wavelength to run the remaining tests on. Ironically, of the six wavelengths that were found during this test, P(22) had the highest power reading but a lower beam quality (TEM_{01}), while P(20) had the ideal mode (TEM_{00}) but a lower power reading than at P(22). Since the master oscillator needs to have a beam with TEM_{00} and high power readings, the power vs. temperature and stability tests were run at both P(20) and P(22). Since each laser is different, the next four tests were used to determine the spare laser's average power output and overall stability.

The power vs. temperature test at P(22) had good power readings, but they were low compared with the same test taken at P(20). Part of the problem may be that during the tests taken at P(22), the chiller was inside the same room as the spare laser and was most likely throwing off the ambient temperature in the room. To mitigate this problem, the chiller was moved outside of the room for the P(20) tests. The results of the tests could have been thrown off due to this change. Although the master oscillator is usually used at 21.5°C, the P(22) temperature test showed that the spare laser works even better at either 13°C or 18°C. The test at P(20) confirmed that the spare laser works better at lower temperatures. In addition, the power readings taken at P(20) were more consistent between temperature changes.

The P(22) stability test indicated that the spare laser was unstable at this wavelength because the laser kept decreasing in power over time. In the first two hours the power decreased by nearly one watt. That is a significant decrease in comparison with the stability test at P(20). Not only did the P(20) test have higher power readings, but the stability was excellent, fluctuating between only 3.6 and 4.1 watts.

Conclusions

The test results indicate that the spare CO_2 laser has much higher power readings at P(20) than at P(22). Since the master oscillator also has higher power readings at P(20), both lasers will be run at P(20) in the future. In addition, the tests indicated that the spare laser runs much better at lower temperatures. However, the experimental results determined that although the spare CO_2

laser performed very well at P(20), the beam did not emit enough power to be used as a replacement for the master oscillator. Instead of buying a new laser or refurbishing the master oscillator, it was decided that the spare laser would be refurbished so that the master oscillator could still be used while the replacement was being fixed.

References

1. Schawlow, Arthur L., "Optical Masers" June 1961. Lasers and Light. San Francisco: W. H. Freeman and Company. ©1969. Pgs. 224-233
2. Schawlow, Arthur L., "Advances in Optical Masers" July 1963. Lasers and Light. San Francisco: W. H. Freeman and Company. ©1969. Pgs. 234-245
3. Patel, C. K. N., "High-Power Carbon Dioxide Lasers" August 1968. Lasers and Light. San Francisco: W. H. Freeman and Company. ©1969. Pgs. 264-275
4. Siegman, A. E., An Introduction to Lasers and Masers. New York: McGraw-Hill Book Company. ©1971

SATELLITE ORBIT DETERMINATION FROM OPTICAL SIGHTINGS

Kevin L. Grimes

Albuquerque Academy
6400 Wyoming NE
Albuquerque, NM 87109

Final Report for:
High School Apprentice Program
Air Force Research Laboratory
Phillips Research Site

Sponsored by:
Air Force Office of Scientific Research
Bolling Air Force Base, DC

and

Air Force Research Laboratory
Phillips Research Site

September 1998

SATELLITE ORBIT DETERMINATION FROM OPTICAL SIGHTINGS

Kevin L. Grimes
Albuquerque Academy

Abstract

An investigation of the nature of satellite orbits was conducted. Based on time-exposures of satellites taken from a remote telescope, and mapped against a star background, angles for the topocentric right ascension and declination system were obtained. An investigation of the methods for analyzing this data was then conducted. Based on the angles, an existing orbit could be improved through a least squares polynomial, or an entirely new orbit could be calculated. In either case, a model for predicting the position of a satellite at a future point is created, affecting applications such as remote signal interaction between the satellite and a point on the surface of the earth.

SATELLITE ORBIT DETERMINATION FROM OPTICAL SIGHTINGS

Kevin L. Grimes
Albuquerque Academy

Introduction

Satellite orbits generally require six or more orbital elements in order to describe the shapes and other vital information pertaining to their paths. These can be used to determine a satellite's current position, as well as predict where a satellite will appear at some point in the future. This can be useful when attempting to send or receive signals or determining where to place a second satellite such that it does not collide with any other objects. Due to factors such as the non-spherical shape of the earth, the positions of the moon, planets, and other large bodies, and other unforeseen effects, the orbits change, or rather degrade, over time. Should a satellite be allowed to continue without being tracked, it would eventually be lost. Thus, updating satellite orbits is essential to utilizing any functionality the satellite may serve.

Methodology

Data can be collected and processed from a remote location, and with minimal intervention by the user. Software designed to operate the telescope is programmed with the coordinates of the telescope, and given access to a clock accurate to a small fraction of a second. It then accepts recent two-line element sets and propagates an orbit for the desired satellites such that a rough position is known for each satellite at any given time. The telescope then accepts scripts, which instruct it to automatically slew to any number of satellites, and obtain a ten-second time exposure for each. By turning at the same rate as the stars move across the sky, the telescope creates images in which the stars appear as fixed points and the satellites streak through. Another program can then automatically determine the ends of the streak. Due to the fact that the relative positions of the stars show little variation even at six-month intervals, these points can be mapped against the star background in order to determine the unit vectors in terms of the topocentric right ascension and declination system. With these angles, the satellite orbit can be improved by making a least squares polynomial to fit the data, or a completely new orbit can be calculated from the unit vectors and the respective times (see appendix A).

Results

The data obtained from analysis of telescope photographs of satellites showed a slight deviation from the initial orbit. Over time, the calculated orbit degrades to the point where a satellite would no longer be traceable. Thus it becomes important to track, and update the progress of satellites so that they may remain in contact and serve some useful purpose, and not collide with a newly launched projectile.

Conclusion

While satellite orbits change over time, it is possible to update or even recalculate these orbits based solely on telescope photographs. Since the telescope can be operated remotely, data from any location can be collected and processed. A telescope would simply need to be deployed and programed with its coordinates. A high-accuracy mount is not required, thus reducing the cost of satellite tracking should the telescope replace the current method of satellite tracking. The computer system controlling the telescope would be able to use a two-line element set to predict the position of a satellite, tell the telescope to slew to it and take a time-exposure, then process the data, correcting the orbit in order to produce an updated two-line element set. This process could continue indefinitely and with little human intervention.

References

Bate, Roger, et. al.. Fundamentals of Astrodynamics. New York: Dover Publications, Inc., 1971.

Appendix A: Orbit Determination Based on Line of Sight Unit Vectors[1]

Based on exposures at three separate times, the six angles α_1, δ_1, α_2, δ_2, α_3, δ_3 of the topocentric right ascension and declination of a satellite can easily be determined. If we let $\mathbf{L}_1$, $\mathbf{L}_2$, and $\mathbf{L}_3$ be the unit vectors along the line-of-sight to the satellite at the three observation times, then

$$\mathbf{L}_i = \begin{vmatrix} L_I \\ L_J \\ L_K \end{vmatrix}_i = \begin{vmatrix} \cos\delta_i & \cos\alpha_i \\ \cos\delta_i & \sin\alpha_i \\ \sin\delta_i & \end{vmatrix}_i, \quad i = 1, 2, 3 \tag{1}$$

Since $\mathbf{L}_i$ are unit vectors along the slant range vector ρ,

$$\mathbf{r} = \rho\mathbf{L} + \mathbf{R} \tag{2}$$

where ρ is the slant range to the satellite, $\mathbf{r}$ is the vector from the center of the earth to the satellite, and $\mathbf{R}$ is the vector from the center of the earth to the observation site. Differentiating twice produces:

$$\dot{\mathbf{r}} = \dot{\rho}\mathbf{L} + \rho\dot{\mathbf{L}} + \dot{\mathbf{R}} \tag{3}$$

$$\ddot{\mathbf{r}} = 2\dot{\rho}\dot{\mathbf{L}} + \ddot{\rho}\mathbf{L} + \rho\ddot{\mathbf{L}} + \ddot{\mathbf{R}} \tag{4}$$

From the equation of motion we have the dynamical relationship

$$\ddot{\mathbf{r}} = -\frac{\mu\mathbf{r}}{r^3}$$

Substituting this into equation (4) and simplifying yields:

$$\mathbf{L}\ddot{\rho} + 2\dot{\mathbf{L}}\dot{\rho} + (\ddot{\mathbf{L}} + \frac{\mu\mathbf{L}}{r^3})\rho = -(\ddot{\mathbf{R}} + \frac{\mu\mathbf{R}}{r^3}) \tag{5}$$

At a specified time, the above vector equation represents three component equations in 10 unknowns. The vectors $\mathbf{L}$, $\mathbf{R}$, and $\ddot{\mathbf{R}}$ are known at time t; $\dot{\mathbf{L}}$, $\ddot{\mathbf{L}}$, ρ, $\dot{\rho}$, $\ddot{\rho}$, and r are not known. Since the value of $\mathbf{L}$ is known at three times, t_1, t_2, and t_3, we can numerically differentiate to obtain $\dot{\mathbf{L}}$ and $\ddot{\mathbf{L}}$ at the central time, t_2, provided the three observations are not too far apart in time. Using the Lagrange interpolation formula to write a general analytical expression for $\mathbf{L}$ as a function of time produces:

$$\mathbf{L}(t) = \frac{(t-t_2)(t-t_3)}{(t_1-t_2)(t_1-t_3)}\mathbf{L}_1 + \frac{(t-t_1)(t-t_3)}{(t_2-t_1)(t_2-t_3)}\mathbf{L}_2 + \frac{(t-t_1)(t-t_2)}{(t_3-t_1)(t_3-t_2)}\mathbf{L}_3$$

This second order polynomial in t reduces to $\mathbf{L}_1$ when $t = t_1$, $\mathbf{L}_2$ when $t = t_2$, and $\mathbf{L}_3$ when $t = t_3$.

[1] Bate, Roger, et. al.. Fundamentals of Astrodynamics. New York: Dover Publications, Inc., 1971. pp. 117-122.

Differentiating this equation twice yields:

$$\dot{\mathbf{L}}(t) = \frac{2t-t_2-t_3}{(t_1-t_2)(t_1-t_3)}\mathbf{L}_1 + \frac{2t-t_1-t_3}{(t_2-t_1)(t_2-t_3)}\mathbf{L}_2 + \frac{2t-t_1-t_2}{(t_3-t_1)(t_3-t_2)}\mathbf{L}_3 \tag{6}$$

$$\ddot{\mathbf{L}}(t) = \frac{2}{(t_1-t_2)(t_1-t_3)}\mathbf{L}_1 + \frac{2}{(t_2-t_1)(t_2-t_3)}\mathbf{L}_2 + \frac{2}{(t_3-t_1)(t_3-t_2)}\mathbf{L}_3 \tag{7}$$

By setting $t = t_2$ in equations (6) and (7), numerical values for $\dot{\mathbf{L}}$ and $\ddot{\mathbf{L}}$ for the central time can be obtained. If there are more than three observations available, more accurate values of $\dot{\mathbf{L}}$ and $\ddot{\mathbf{L}}$ may be obtained by making a least squares polynomial to fit the observations.

Equation (5) now represents three component equations in four unknowns, ρ, $\dot{\rho}$, $\ddot{\rho}$, and r. Solving the equation for ρ using Cramer's rule, the determinant of the coefficients is:

$$D = \begin{vmatrix} L_I & 2\dot{L}_I & \ddot{L}_I + \frac{\mu L_I}{r^3} \\ L_J & 2\dot{L}_J & \ddot{L}_J + \frac{\mu L_J}{r^3} \\ L_K & 2\dot{L}_K & \ddot{L}_K + \frac{\mu L_K}{r^3} \end{vmatrix}$$

Since the value of the determinant is not changed when $\frac{\mu}{r^3}$ times the first column is subtracted from the third column, D reduces to:

$$D = 2\begin{vmatrix} L_I & \dot{L}_I & \ddot{L}_I \\ L_J & \dot{L}_J & \ddot{L}_J \\ L_K & \dot{L}_K & \ddot{L}_K \end{vmatrix} \tag{8}$$

Applying Cramer's rule to equation (5),

$$D_\rho = -\begin{vmatrix} L_I & 2\dot{L}_I & \ddot{R}_I + \frac{\mu R_I}{r^3} \\ L_J & 2\dot{L}_J & \ddot{R}_J + \frac{\mu R_J}{r^3} \\ L_K & 2\dot{L}_K & \ddot{R}_K + \frac{\mu R_K}{r^3} \end{vmatrix}$$

This determinant can then be split to produce:

$$D_\rho = -2\begin{vmatrix} L_I & \dot{L}_I & \ddot{R}_I \\ L_J & \dot{L}_J & \ddot{R}_J \\ L_K & \dot{L}_K & \ddot{R}_K \end{vmatrix} - \frac{2\mu}{r^3}\begin{vmatrix} L_I & \dot{L}_I & R_I \\ L_J & \dot{L}_J & R_J \\ L_K & \dot{L}_K & R_K \end{vmatrix} \tag{9}$$

For simplicity, let the first determinant be D_1 and the second be D_2.

$$\rho = \frac{-2D_1}{D} - \frac{2\mu}{r^3}\cdot\frac{D_2}{D}, \quad D \neq 0 \tag{10}$$

Provided D does not equal zero, we have an equation for ρ as a function of the still unknown r. From geometry, ρ and r are related by

$$\mathbf{r} = \rho\mathbf{L} + \mathbf{R} \tag{2}$$

Dotting this equation into itself yields:

$$r^2 = \rho^2 + 2\rho\mathbf{L}\cdot\mathbf{R} + R^2 \tag{11}$$

Equations (10) and (11) represent two equations in two unknowns, ρ and r. Substituting equation (10) into (11) leads to an eighth order equation in r which may be solved by iteration. Once the value of r at the central date is known, equation (10) may be solved for ρ, and the vector **r** may be obtained from equation (2).

Applying Cramer's rule again to equation (5) in much the same manner, $\dot{\rho}$ can be determined:

$$D\dot{\rho} = -\begin{vmatrix} L_I & \ddot{R}_I & \dddot{L}_I \\ L_J & \ddot{R}_J & \ddot{L}_J \\ L_K & \ddot{R}_K & \ddot{L}_K \end{vmatrix} - \frac{\mu}{r^3}\begin{vmatrix} L_I & R_I & \ddot{L}_I \\ L_J & R_J & \ddot{L}_J \\ L_K & R_K & \ddot{L}_K \end{vmatrix} \tag{12}$$

If we let the first determinant be D_3 and the second be D_4, then

$$\dot{\rho} = -\frac{D_3}{D} - \frac{\mu}{r^3}\cdot\frac{D_4}{D}, \quad D \neq 0 \tag{13}$$

Since r is known, equation (13) can be solved for $\dot{\rho}$. To obtain the velocity vector, **v**, at the central date we only need to differentiate **r** in equation (2):

$$\mathbf{v} = \dot{\mathbf{r}} = \dot{\rho}\mathbf{L} + \rho\dot{\mathbf{L}} + \dot{\mathbf{R}} \tag{14}$$

MSX-OBSERVED OBJECTS WIHG UNUSUAL INFRARED EMISSION

Andrea Hunt

Phillips Academy
180 Main Street
Andover, MA 01810

Final Report for:
High School Apprenticeship Program
AFRL/Phillips Laboratory

Sponsored by:
Air Force Office of Scientific Research
Bolling Air Force Base, DC

And

Phillips Laboratory

August 1998

MSX-OBSERVED OBJECTS WITH UNUSUAL INFRARED EMISSION

Andrea Hunt
Phillips Academy

Abstract

The MSX measurements of the infrared emission of point sources in the galactic plane were examined. Color-color diagrams were created and used to locate point sources with unusually high infrared emission levels. Point sources possessing unusual infrared emission levels were identified by their abnormal positions on the color-color diagrams. A search of the SIMBAD database was conducted using the MSX-recorded coordinates. The references to each object provided by SIMBAD were researched in an attempt to find an explanation of the unusually high levels of infrared radiation emitted by these objects. These reasons, when found, are discussed.

MSX-OBSERVED OBJECTS WITH UNUSUAL INFRARED EMISSION

Andrea Hunt

Introduction

Recently, the ability to observe astronomical objects from outside the Earth's obscuring atmosphere by use of telescope-carrying satellites has significantly increased the number of objects in space that have been identified and studied. In particular, the **I**nfrared **A**stronomy **S**atellite (IRAS) has been the means of substantial cataloguing of sources of infrared emission in the galactic plane. To identify the infrared sources missed by IRAS's observations in the 1980's, the **M**idcourse **S**pace **E**xperiment (MSX) was launched in 1996. Using data recorded during the MSX survey of sources of infrared emission in the galactic plane, color-color diagrams were created as a tool to identify noteworthy objects located during this survey.

The data used consisted of a list of each of the sources of infrared radiation, accompanied by measurements of how much radiation was emitted by each of the point sources in the different band widths: A, B1, B2, C, D, and E. Using these data, color-color diagrams in which different band combinations were plotted against each other were composed. These diagrams make it possible for individual objects to be located on the basis of how much radiation they emit in each band. For example, to find objects that have high emission levels in the B1 bandwidth, a plot with (Fb1-Fb2)/Fd on the x-axis was created. The point sources which were located farther to the right on the x-axis were those objects that had the highest emission in the B1 bandwidth--because the operation of (Fb1-Fb2)/Fd yielded a larger number. This procedure is useful because once the amount and type of radiation emitted by each point source is determined, conclusions about that object's physical properties can be drawn. The data colors were compared to expected colors of various types of astronomical objects.

In addition, statistics to measure the success of MSX's data-gathering activities were compiled.

Methodology

The various graphs of the MSX data were compared to graphs of identical scale that had been created with model data, intended to predict where "typical" objects in the MSX data should appear on the plots. The classes of objects represented by the models include main sequence stars, giant stars, supergiant stars, carbon-rich stars (AGB-C), oxygen-rich stars (AGB-O), planetary nebulae, reflection nebulae, and HII regions. For example, the below graph of X=(Fa-Fc)/Fc, Y=(Fc-Fd)/Fe was created using the actual data recorded by MSX.

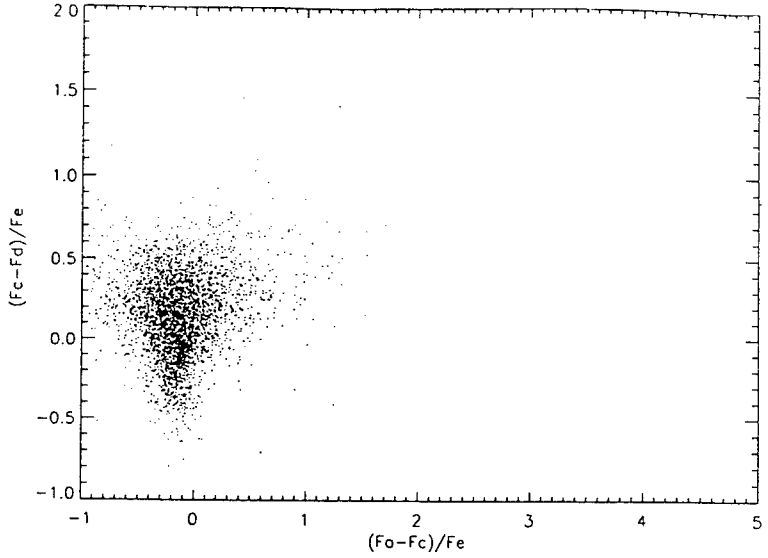

Next, another graph of X=(Fa-Fc)/Fe, Y=(Fc-Fd)/Fe was created, but using the model data.

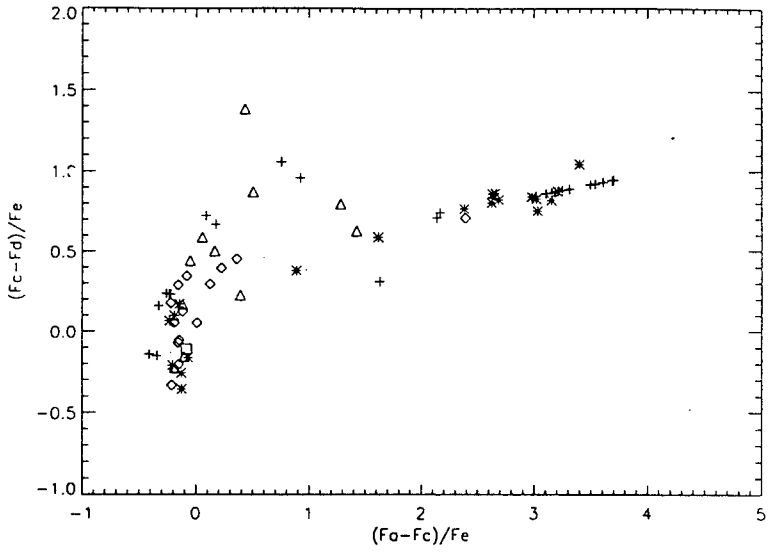

The two graphs are compared, and the plot of the models is overlaid on top of the data plot. In this case, the data's location on the graph concurs with the models' prediction.

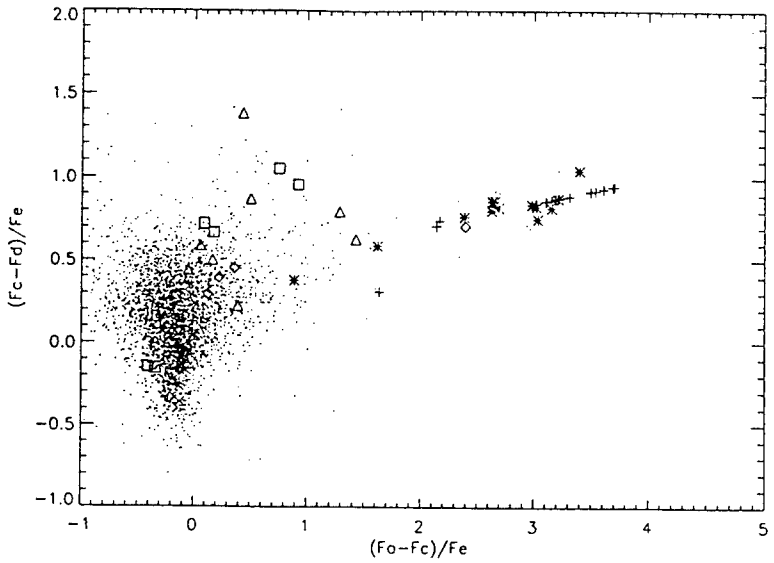

Much experimentation with different band width combinations was done to find the combinations that would produce "useful" plots, in which enough separation between the data points existed to allow points to be examined individually. Three graphs that proved particularly useful for identifying individual objects with unusual emission levels included:

Graph	*X*	*Y*	*Range*
A	(Fe-Fa)/Fd	(Fe-Fd)/Fd	X=[-3.5,11.5] Y=[-1.5,11.5]
B	(Fb1-Fb2)/Fd	(Fc-Fd)/Fd	X=[-1.0,1.5] Y=[-0.5,1.0]
C	(Fa-Fc)/Fd	(Fa-Fd)/Fd	X=[-4.1, 8.5] Y=[-2.0,10.0]

To identify objects with unusual emission levels, point sources whose locations on the plots were not in accordance with the model data's locations were singled out. To determine the reason for this deviation, the dissenting points were located by isolating the area of the graph in which they appeared and finding the galactic coordinates of the objects represented. These coordinates were then converted into the format accepted by the SIMBAD database search engine, and a search

was conducted. Typically, these searches were done using a radius of 10 arcseconds. The radius was increased gradually in increments of 5 until an object was located. In cases where no object was located within 1 arcminute of the specified coordinates, the search radius was increased in increments of 1 arcminute until an object was located.

Results

Of particular interest are some objects that were found to stand out on *Graph A* (see page 4-13). The objects that were researched fall inside the square drawn in the bottom left corner of the graph. The square contains sources that are located just above the predicted grouping of main sequence and carbon (AGB-C) stars. When the coordinates of these 26 point sources were looked up in the SIMBAD database, a majority of 17 were listed simply as sources of infrared radiation first identified by IRAS. The searches for the remaining points yielded 4 stars and 5 sets of coordinates with inconclusive results.

Table A-1--Conclusive Identifications

RA(2000)	Dec(2000)	Object	Search Radius
10 23 50	-57 57 13	Variable Star	15 arcseconds
11 20 27	-61 52 44	Mira-Cet Variable Star	25 arcseconds
13 30 25	-63 24 46	Carbon Star	0arcseconds
17 24 44	-36 48 38	Star in Double System	10 arcseconds

The **Variable Star**, identified by SIMBAD as HD90289, is associated with unusual infrared emissions because it is located inside giant HII region RCW 49. It was located during an X-ray observation of RCW 49 by the ROSAT satellite. The X-ray detection of HD90289 by ROSAT is of note because the star would then be located beyond the "dividing line" in the color-magnitude diagram, where no X-ray emission is expected. (Belloni & Meghretti, 1996)

The **Mira-Cet Variable**, identified in SIMBAD as HD98678, is located quite near to, and was once thought to be part of, the Be/X-ray transient system A 1118-616. The infrared measurements of the system confirm it to be a source of bright infrared emission, with levels comparable to those of similar Be/X-ray systems.

A 1118-616 is characterized as being at the extreme end of the possible range of values observed in similar systems. The source of this system's excess infrared emission is believed to be the hot plasma in the Be star's circumstellar disk. (Coe et al, 1994)

The **Carbon Star**, identified as C*2095 by SIMBAD, is correctly identified as C*3398 in A General Catalog of Cool Galactic Carbon Stars, Second Edition (Stephenson, 1989). An explanation of its unusual emission levels could not be found.

The **Star in a Double System**, identified as CCDM J17247-3649B by SIMBAD, is located in the galactic center. A reason for the excess emission could not be found, but one possible explanation does exist. Since it is located in the dense galactic center, it is possible that the infrared emissions associated with it are actually a combination of emissions of other nearby objects that were not discernible.

A SIMBAD database search using the following coordinates was conducted; however, the resulting identifications are questionable because the nearest objects to the specified coordinates are unusually far away. There is, however, some uncertainty as to the accuracy of the coordinates recorded during the IRAS identification of the two infrared sources on the below list. The margin of error in the IRAS coordinates might be the reason for the larger search radii needed to locate the infrared sources in the SIMBAD database. This could warrant further investigation.

Table A-2--Inconclusive Identifications

RA(2000)	Dec(2000)	Object	Search Radius
09 5.6 36	-48 9.7 44	Star	7 arcminutes
14 5.8 50	-61 56 1.3	Infra-red Source	5 arcminutes
18 5.4 24	-21 23 36	Infra-red Source	9 arcminutes
18 33 27	-9.3 23 42	Radio Source	3 arcminutes
20 4.1 10	+29 48 38	Emission-Line Star	3 arcminutes

Graph B also contained some point sources that are of interest because of their atypical emission levels. The model plot for this graph predicts that on the x-axis, the data will be concentrated around 0, ranging up to about 0.7.

Many of the actual data, however, fell between 1.0 and 1.5--the area enclosed in the rectangle drawn onto the attached *Graph B* (see page 4-14). The point sources located between 1.0 and 1.5 were researched in the same manner as discussed above. Since the x-axis shows (Fb1-Fb2)/Fd, the objects in the 1.0 to 1.5 area have particularly strong emissions in the B1 band.

Again, the majority of the 22 points that were researched--12--were identified by the SIMBAD database simply as infrared sources discovered by IRAS. The remaining points yielded 4 stars, 1 cloud, 1 radio source, and 4 sets of coordinates with inconclusive results.

Table B-1--Conclusive Identifications

RA(2000)	Dec(2000)	Object	Search Radius
16 53 4.5	-43 32 50	Molecular Cloud	15 arcseconds
16 58 6.2	-42 19 26	Carbon Star	5 arcseconds
17 21 36	-36 15 56	Star	15 arcseconds
17 29 44	-33 50 34	Radio Source	20 arcseconds
18 2.1 4.2	-23 37 39	Wolf-Rayet Star	5 arcseconds
20 53 52	+44 24 6.1	Star	0 arcseconds

The **Molecular Cloud** is identified by SIMBAD as OH 342.00+0.25. It was thought to be the site of an OH maser; however, this possibility was ruled out and no definitive reason could be found to explain its excess emission in the B1 band. (Bowers & Knapp, 1989)

The **Carbon Star** is identified by SIMBAD as IRAS 16545-4214. It is classified as an infrared carbon star--one of a class of stars which are characterized by a dominant emission by the dust grains contained in their circumstellar envelopes. IRAS 16545-4214 is an infrared carbon star with excess emission *above* its dust emission. This excess is believed to be the result of free-free emission originating in the inner parts of its circumstellar shell. (Groenwegen, 1995)

The **Star**, identified by SIMBAD as RHI 848-42 and as spectral type M3, has a unique case. The reference provided by SIMBAD is from a journal that, after three attempts, could not be located! Therefore, it is quite possible that an explanation of this star's unusually high B1 emission levels exists in this paper.[1]

The **Radio Source**, identified by SIMBAD as GPSR5, is located near the galactic center. It was located during a 5GHz VLA survey of the galactic plane. During this survey, the possibility of it being a planetary nebula or HII region was ruled out. Those who conducted this survey suppose it to actually be an extragalactic source that fell into the survey area. (Becker et al, 1994)

The **Wolf-Rayet Star** is identified by SIMBAD as WR 104 (and also Ve 2-45, as it is called in some references). This star is known to have a large infrared excess--and this excess emission is attributed to thermal emission from the graphite grains found in its circumstellar dust shell. (Dyck et al, 1984)

The **Star**, identified as StRs 383 by SIMBAD, is found in a listing of "highly reddened stars" that are, most likely, "distant luminous stars". (Stephenson, 1992) It is further asserted that this star's excess is not the result of circumstellar emission, as was the case in several previously discussed stars, but because of interstellar absorption.

When a SIMBAD search using the following coordinates was conducted, the resulting identifications were unreliable because of the unusually large search radii needed to locate an object. These points, again, might warrant further investigation.

Table B-2--Inconclusive Identifications

RA(2000)	Dec(2000)	Object	Search Radius
16 14 16	-51 2.5 30	Dark Nebula	4 arcminutes
17 35 31	-32 7.2 12	Star	2 arcminutes
20 2.4 29	+29 51 40	Star	5 arcminutes
20 3.1 10	+29 59 11	Star	3 arcminutes

One last remarkable point source was found in *Graph C* (see page 4-15), but in this instance, not because of its unusual location. Instead, when attempting to isolate point sources found in certain areas of the graph, a typographical error in the command line that was entered produced a set of coordinates that, when looked up in the SIMBAD database, turned out to be those of a maser. The coordinates were afterward verified to be those of a true point source located in *Graph C*. The maser, identified as BE83 Maser 298.22-00.34 in the database, is an H2O maser located in the extremely luminous HII region G298.22-00.34. (Simpson, 1995)

In addition to the above research of point sources with unusual emission levels recorded by MSX, DCE validation was conducted. While the majority were successful, many were unsuccessful as a result of one of three possible occurrences.

In the instances in which "no valid data" appears instead of the number of measurements in each band, the explanation provided is:
"The beginning of the housekeeping file for this DCE segment ID overlaps with the beginning of the housekeeping file from the other segment. The time interval covered during this segment takes place during the camera turn on (macro RC) and hence, there are no data available."

In the instances where "no database found" appears instead of data, this is explained, quite simply, by:
"No GEO database was found."

When "no data available" is in place of data, this is explained by:
"The only valid data contained within the level 2a data files were minicals or no level 2a files were created. Both of these conditions are due to the current convert settings for DCEs of this type."

Conclusion

This brief research foray into just a small *sampling* of the noteworthy objects observed by MSX has produced a

handful of satisfactory explanations as to why certain objects emit excess infrared radiation. The other coordinates--those with inconclusive search results and those listed simply as infrared sources--are perhaps the most interesting. Allowing, of course, for the possibility of errors in the coordinates, there is a chance that at some of these coordinates exist objects that have not been identified--with a potentially remarkable explanation for their infrared excess. It is, in the author's opinion, worthwhile to further research these elusive emitters of infrared radiation.

The author wishes to thank Dr. Frank Clark, Dr. Michael Egan, and Dr. Russel Shipman of the Air Force Research Labs at Hanscom AFB, MA for their help, guidance and patience with the many questions of a beginner.

References

Belloni, T. and Meghretti, S. "ROSAT observations of giant HII region RCW 49." Astronomy and Astrophysics 286 (1996): 935

Becker, R.H. et al. "A 5 GHz VLA survey of the galactic plane." Astrophysical Journal Supplement Series 91 (1994): 347

Bowers, P.F. and Knapp G. R. "A study of OH/IR stars and planetary nebula formation." Astrophysical Journal 347 (1989): 325

Coe, M.J., et al. "Multiwave band study of a major X-ray outburst from the Be/X-ray transient system A1118-616." Astronomy and Astrophysics 289 (1994): 784

Dyck, H.M. et al. "Infrared dust shell around the WC9 star Ve2-45." Astrophysical Journal 277 (1984):675

Groenwegen, M.A.T. "Dust shells around infrared carbon stars." Astronomy and Astrophysics 293 (1995):463

Simpson, J.P. et al. "Far-infrared lines from HII regions: abundance variations in the Galaxy." Astrophysical Journal 444 (1995): 721

Stephenson, C.B. A General Catalog of Cool Galactic Carbon Stars, Second Edition. Case Western Reserve University: Warner & Swasey Observatory, 1989

Stephenson, C.B. "A list of highly reddened stars likely to be distant luminous stars." Astronomical Journal 103 (1992): 263

[1] 1984 Annual Tokyo Astronomical Observatory 19 469 (as given by SIMBAD)

Graph A--MSX Data

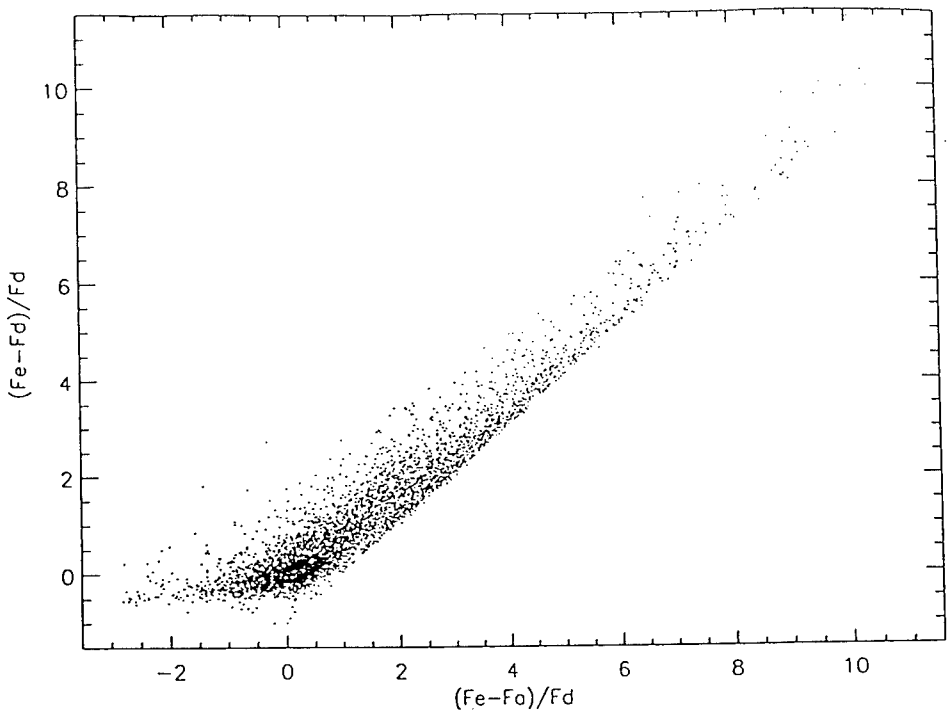

MSX Data , Model Data

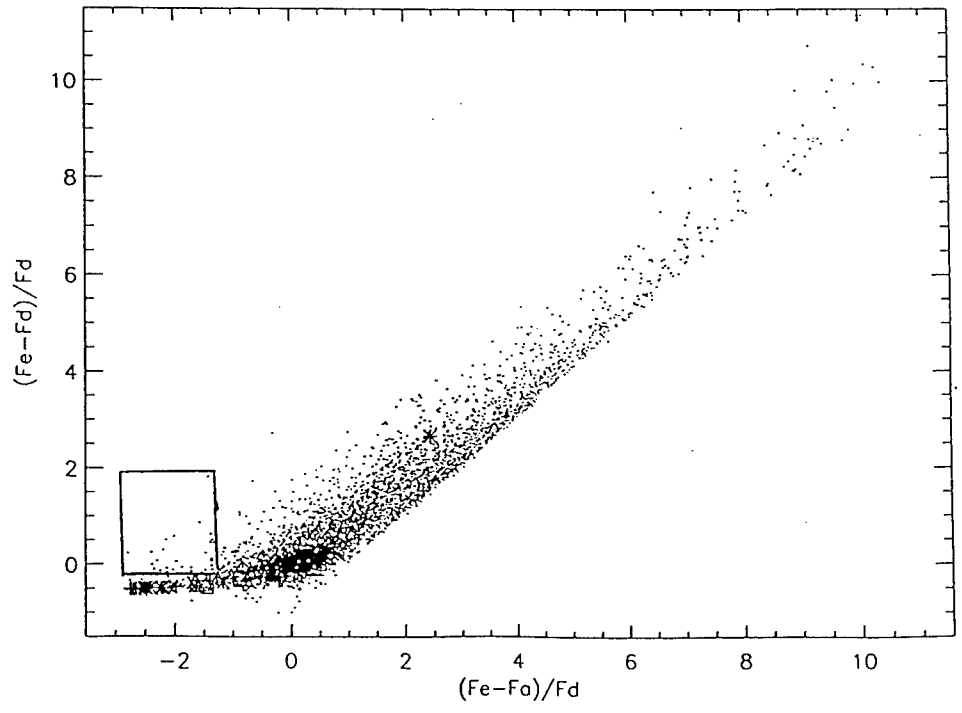

Graph B--MSX Data

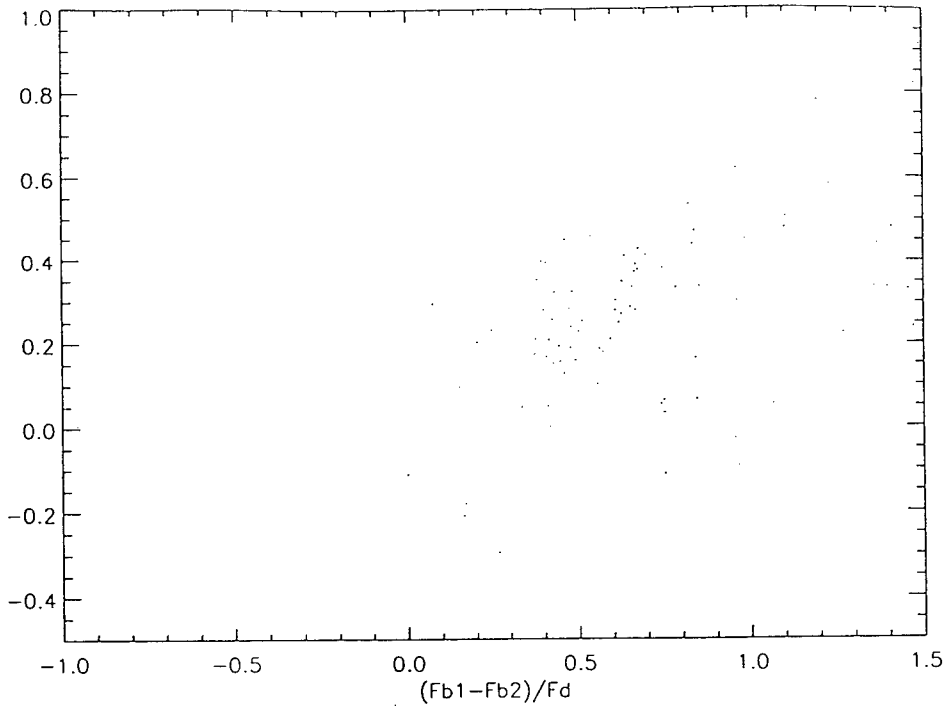

MSX Data , Model Data

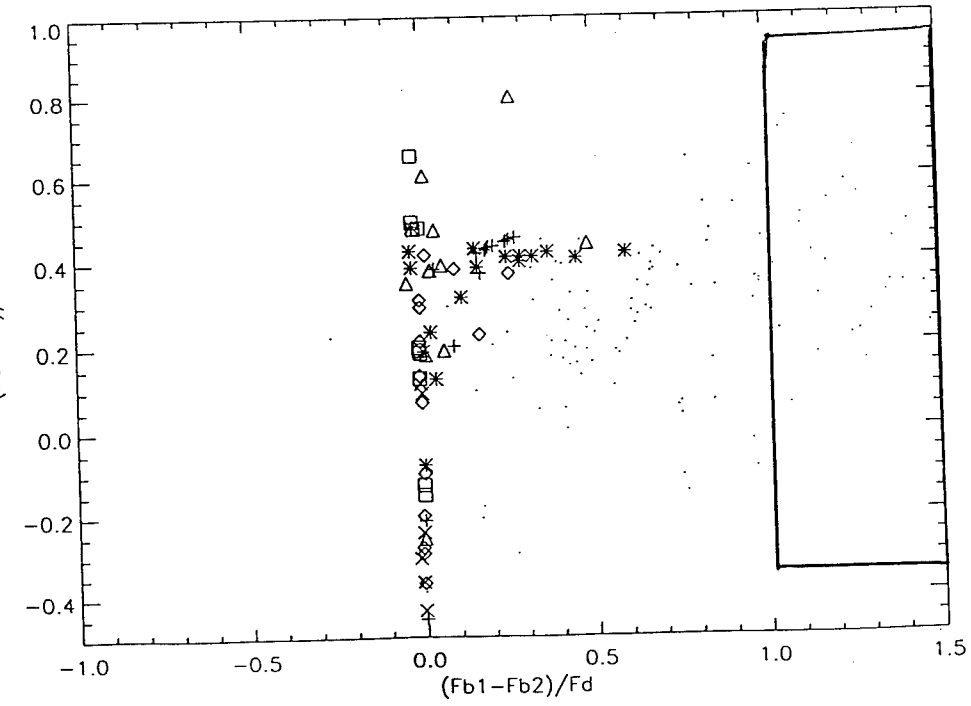

Graph C--MSX Data

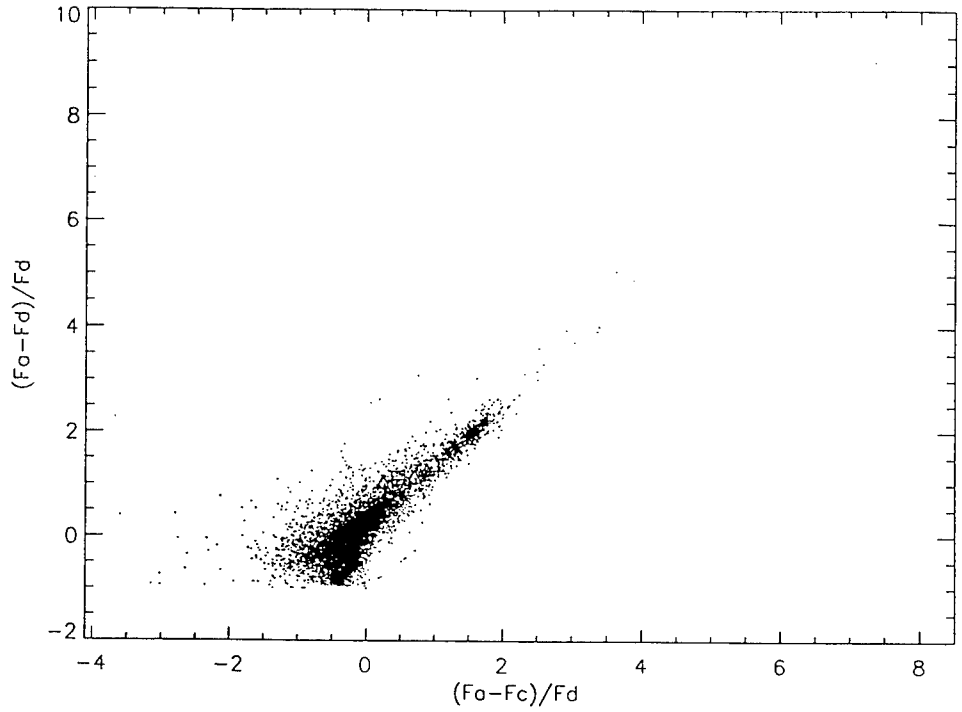

MSX Data , Model Data

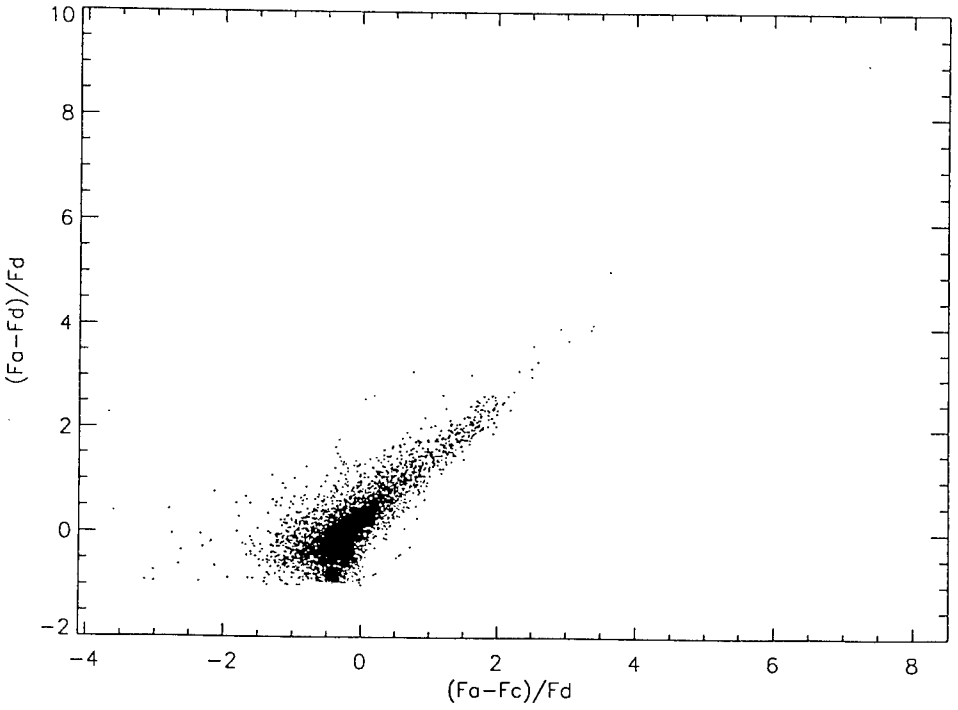

THE CHARGING AND DISCHARGING OF SPACECRAFT: AN INTRODUCTION

Mary H. Ly

Billerica Memorial High School
35 River St.
Billerica, MA 01821

Final Report for:
High School Apprenticeship Program
AFRL/Phillips Laboratory

Sponsored by:
Air Force Office of Scientific Research
Bolling Air Force Base, DC

And

Phillips Laboratory

August 1998

THE CHARGING AND DISCHARGING OF SPACECRAFTS: AN INTRODUCTION

Mary H. Ly
Billerica Memorial High School

Abstract

This report will present an introductory overview pertaining to spacecraft charging and discharging. If an object is subjected to an unequal flux of ions and electrons, it develops a net charge. The surfaces of the spacecraft, if charged to different potentions, result in differential charging. The current balance determines the charging state of the spacecraft in a steady state. Spacecraft in the geosynchronous region are of most concern since there are many satellites in this region where most spacecraft charging occurs. Options exist that can prevent and mitigate the charging of spacecraft. Photoemission and emissions of secondary and backscattered electrons often provide important currents. Beam emissions and other mitigation techniques also reduce the level of charging.

Introduction

A spacecraft operating in order to acquire accurate data and function properly must avoid any anomalies. One harmful risk that spacecraft encounter is spacecraft charging, which can cause incorrect electronic instrument measurements on board. The forecasting of spacecraft charging in time varying plasma environment in space is important. The prediction of onsets achieved ahead of time enable mitigation measures to be prepared and properly executed [1-2].

This report provides an introductory overview on the process of spacecraft charging and the mitigation techniques. The very phenomenon of why a spacecraft may become charged is also relevant to why the time between midnight and early dawn is the time a spacecraft is susceptible to charging. ABrief overview of the different kinds of charging and their harmful effects. The concepts of current balance and ambient electron energy in space plasmas are critical in understanding how the state of the environment contributes to the spacecraft's charge. The collection of current is essential in spacecraft charging concepts and will be discussed.

Over the last two decades, several techniques have been developed that eliminate and limit the worst effects of spacecraft charging. This report will present the natural, passive, and active approaches to mitigation and prevention techniques. The emission of electrons and beam emission will be presented as a more detailed approach of spacecraft discharging. The report will conclude with the importance of spacecraft charging analysis.

The Process of Spacecraft Charging

When an object in space, whether a dust grain, an asteroid, or a spacecraft, is exposed to the space environment, its surfaces are continually bombarded by charged particles and by photons [3]. The charges carried by the particles are then added to the object's. Electrons are lighter and faster than ions, and therefore are more probable to collide with objects. This causes the spacecraft to be negatively charged. If many electrons collide on the surface, the negative charging process begins.

The rate of charge transfer depends mainly on the charge already existing on the spacecraft and the environment conditions. The electric field arising from the distributed charge influences the motion of charged

particles moving towards or from the spacecraft. A positive charge attracts electrons and repels ions for example, and secondary or photoelectrons returns to the spacecraft instead of escaping. The charge transfer will continue and proceed until equilibrium is reached (when the net current to the surface diminishes).

Spacecraft Charging at Geosynchronous Altitudes

Space weather at geosynchronous altitudes varies. In quiet times, the plasma energy is very low (below 100 eV). Occasionally the plasma energy is energetic (hundreds and thousands of eV). The ambient plasma electrons and ions bombard the spacecraft surfaces. Ambient electrons are much more important than ions, because electrons are much faster and therefore the electron flux is much higher than that of ions. Depending on the secondary and backscattered electron coefficients of the surface material, the charging level may become significant (hundreds or thousands of V).

Secondary electrons are more important because they are more abundant than backscattered electrons. The secondary emission coefficient may exceed unity at an intermediate energy range (about 60 to 1200 eV of incoming electron energy) for many surface materials including metals and plastics. When the coefficient exceeds unity, there are more secondary electrons (which are outgoing) than primary electrons (which are incoming). Below the first cross-over energy and above the second, there are more incoming electrons than outgoing ones, and therefore negative charging occurs. When the incoming electrons are of thousands of eV which exceeds the second cross-over energy, negative charging of the surface material is likely. However, when the surface is in sunlight, the charging level is likely low because of the high outgoing electron flux of photoemission. In fact, charging in sunlight is often positive and near zero (a few V positive), because the photoemission flux often exceeds that of the incoming ambient plasma electrons.

Therefore, significant surface charging is expected when the ambient plasma is energetic while the surface is not on the sunlit side of a spacecraft. The ambient plasma energy depends on the local time of the day and the solar and geomagnetic conditions. Most often, the weather at geosynchronous altitudes is quiet, meaning low plasma energy. The Sun interacts with the magnetosphere, which is the Earth's electromagnetic atmosphere.

Without the Sun, the Earth's magnetic field lines would be in a dipole pattern. A perfect dipole pattern would be symmetric about the north-south axis. However, because of Solar wind interactions, the Earth's magnetic field pattern is not symmetric. The Sun emits plasma continuously and in all directions. The plasma so emitted is called Solar wind. It controls the Earth's space weather. The Solar wind speed varies. When the Solar wind is strong, the Earth's magnetic field line is stretched out in an elongated geomagnetic tail (in analogy with a cometary tail) to distances of several hundred Earth radii. Later, when the Solar wind weakens, the tail snaps back (in analogy to the snap back of a stretched rubber band). When the tail snaps back, the electrons and ions inside the stretched tail are accelerated to high energies and move towards the Earth. When they arrive at very low altitudes (below a few hundreds of km), they lose most of their energy. High energy electrons, of course, can cause spacecraft charging. Since these high energy electrons travel from the long tail, which is on the night side of the Earth, the night hours are expected to be the most likely local time for spacecraft charging.

The hours after midnight are more likely for spacecraft charging to occur than those before midnight. The reason is because there is a slight asymmetry between the dawn and dusk side of the magnetosphere. When the Solar wind blows past the Earth's magnetic field lines, the wind electron velocity tends to bend according to the right hand fingers rule of the vector directions of the velocity and the magnetic field line. The wind ions, however, tend to turn towards the opposite directions. This mechanism results in a complicated electric field pattern in the magnetosphere. In this pattern, a so called "cross tail electric field" exists. The electric field is on the night side of the magnetosphere and is pointing from the dawn side towards the dusk side. When the energetic electrons from the tail are traveling along the elongated field lines towards the Earth, their velocities are affected by to the "cross tail electric field". Since an electron is attracted towards the opposite direction of an electric field, the velocity tends to bend towards the dawn side. Therefore, the early morning hours (i.e., the dawn side of midnight) are expected to be the most likely time for spacecraft to occur.

The CCS Experiment on DSCS

An Phillips Laboratory (now Air Force Research Laboratory) experiment, CCS, was conducted on a DSCS satellite a few years ago. It was a geosynchronous satellite. The potentials of two surfaces (kapton and quartz) were measured almost continuously everyday. When either of the potentials reached 500 V, a trigger was on

automatically. The trigger released a partially ionized neutral gas from a device on the spacecraft to form a low energy plasma surrounding the spacecraft. The low energy plasma ions return to the highly negatively charged surface thereby lowering the potential, while the low energy plasma electrons are repelled from the negatively charged spacecraft thereby carrying away negative charges. This mechanism mitigates the negative charging on the surfaces.

The measurements of potentials of the surfaces provides a good opportunity for obtaining statistical results on the most likely hours for spacecraft charging to occur.

The Different Kinds of Charging

Several terms are used to describe the different kinds of spacecraft charging. Natural charging is the interaction of the spacecraft surfaces with the natural plasma or radiation environment. When the entire spacecraft potential relative to the ambient plasma is changed uniformly, absolute charging results. Artificial charging is due to emission of electrons, ion beams, and other processes [2]. Differential charging occurs when parts of the spacecraft are charged to different potentials relative to each other.

Differential charging is considered very harmful and undesirable because it forms local potential wells and barriers. It also generates electrostatic noise and sparks when discharging occurs. One way to prevent this type of charging is to cover a spacecraft entirely with a conducting coating, therefore letting the potential be uniform in all areas. However, most sensors and instruments on the surfaces would not function properly if covered. The potential distribution formed a barrier that prevented secondary electrons from escaping the spacecraft [3].

The Importance of Equilibrium

When it is raining, rain drops raise the water level in a pool until some leaking current drains water away as fast as the raining rate. This goes to show that at equilibrium, currents must balance. Kirchloff's law states that at equilibrium, every junction in a circuit must satisfy current balance in electricity. As an analogy, a spacecraft surface is a junction in a circuit in space. Currents must flow in and out of the surface. The sum of the currents must

equal zero with current balance:

$$\sum_n I_n = 0 \qquad \text{Eq. 1}$$

where In is the nth current.

Understanding equilibrium charge on a body is important in this field. In a plasma, emission processes are nonsignificant. The equilibrium charge is negative because of the higher flux of electrons to an uncharged surface. The charge is positive where photoemission is most dominant. The flux of ions and electrons are exposed to a significant loss mechanism for the charged particles in the medium [3]. In the solar system, the motion of the charged spacecraft depends on the magnetic and electric fields of the solar wind and by the fields surrounding the planets and their satellites.

Space Plasmas and the Geosynchronous Environment

As an example, if a surface is charged to -0.11 Volts, an incoming electron of 0.1 eV would not reach the surface. This example illustrates why low energy ambient plasmas cannot cause high level charging. In the 200-500 km range altitude from the Earth's surface (Low Earth Orbits), the plasma density is 10^5-10^6 cm^-3, a very high density, while the plasma energy is low, at about 0.1 eV. In LEO, no high level charging is expected. The only areas that would be susceptible to high level charging are the auroral regions where the electron energies could reach as high as keV.

Spacecraft and satellites that provide continuous communications services or weather data operate at geosynchronous orbit, about 22,282 miles from the Earth. The satellites circle the Earth at the same rate as the Earth's rotation, therefore appearing "fixed" with respect to a given spot on Earth. The plasma condition depends on the solar and geomagnetic activities. Spacecrafts in this region may encounter energetic plasmas associated with geomagnetic storms. These storms charged spacecraft s to as much as -20,000 volts [4]. In the geosynchronous region, contrary to LEO, the plasma density is low, 0.1 to 10 cm^-3 and the energy varies greatly between 20eV to 20keV. Because of the lower plasma density, the ambient current to the spacecraft is around 10nA/m^2 or higher.

The Emission of Electrons

Three different types of electron emissions play critical roles in spacecraft charging. These three are photoemission, secondary emission, and backscattering. They are included in the balance of currents because they provide significant outgoing electron currents.

Photoemission

Photoemission is the process of photons knocking electrons out from surfaces. The ultraviolet light from the sun is energetic enough (about 10.2 eV) to knock out electrons from surfaces. The emitted photoelectrons have only energies of a few eV. In the earth's upper atmosphere, the photoemission current depends on the surface material and the sunlight angle. However, atmospheric attenuation of the ultraviolet light becomes significant at low altitudes. At a great distance from the Earth, the light intensity should be considered as a function of distance from the sun. In GEO, the plasma properties (density and energy) vary, depending mainly on the geomagnetic activity. When the plasma is calm, the net plasma current encountered by the spacecraft is less than that of the photoelectrons emitted from the spacecraft surfaces. In that case, the spacecraft would charge to a few positive Volts in sunlight. The photoelectrons with only a few eV will not leave, therefore, higher voltages are not expected.

Secondary Electron Emission

When one pours tea from a pot to a cup, the tea may splash if the pot is positioned too high. One cannot predict exactly how many tea drops would be ejected in a splash.The number of drops ejected is a matter of probability, a probability that can be established after many trials. Electrons can be considered analogous to drops in this situation. When an electron impacts on a surface, emissions may occur depending on the electron energy. If the energy is below about 10eV, the electron may eject secondary electrons from the surface. At high energies, the electron interacts and shares its energy with nearby electrons in the surface. One or more of the neighboring electrons may gain sufficient energy to leave the surface as secondary electrons. Primary electrons are the incoming

electrons. A secondary electron has an energy of a few eV normally. The number of secondary electrons emitted is a matter of probability.

When the energy is too high, the primary electron may penetrate so deeply into the material that the probability of emission for the energized electrons is low. On the other hand, at too low energies, the primary electron may not be energetic enough to create secondary electrons and therefore the probability of emission is also low. The probability of yield of secondary electron emission must lie in an intermediate energy region. Sometimes, the probability of secondary electron emission in an intermediate energy rage of primary electrons may exceed 1.

$$\delta < 1 \qquad (E_1 < E < E_2)$$

The cross-over energies are normally 70 and 1200 eV respectively. When the primary electron energies lie in these values, one secondary electron will be emitted for every entering primary electron.

Backscattered Electrons

There is a probability that electrons may backscatter when a primary electron impacts on a surface material. The primary electron would then also become the secondary electron. The probability depends on the material, primary electron energy and the angle of incidence. Unlike secondary electrons, the probability cannot exceed unity. Also, the energy of a backscattered electron may have up to the same energy as the primary electron.

The Mitigation and Prevention of Spacecraft Charging

It is important to develop prevention and mitigation techniques to ensure the safety of the spacecraft's electronics and instruments so that they function effectively. Passive methods include surface coating while an

active method includes controlled beam emissions. Artificial electron or ion emissions can discharge a spacecraft to an extent. The four types of artificial emissions for mitigation are electron emission, low energy ion emission, neutral gas emission, and combinations of the previous three.

Mitigation by Coating

For high secondary electron emissions, the secondary electrons have too low energy and be emitted if a spacecraft is charged to more than a few eV positive. An energy that low can be considered harmless to certain onboard instruments. When the energy is low, it is reasonable too use a surface coating, which has high secondary electron emission coefficient. For example, on the SCATHA satellite, the outer tip of the SC10, an instrument, is coated with copper-beryllium. A potential of a few eV is common in the quiet GEO conditions .Under severe conditions in GEO, the ambient electrons become so energetic that even the copper-beryllium coating is charged negatively to high potentials [2]. This is because ambient electron energy exceeds the second cross-over energy.

It is impractical for a spacecraft to be completely coated, for most sensors and instruments on the surfaces would not be able to function properly if covered. However, partial coverage of spacecraft surfaces with conductive coating has been used with some success. On GEOS satellites, a conducting and transparent coating, indium oxide, coated on the solar cells transforms into a conducting one while still allowing the solar cells to continue functioning [5]. The disadvantage is that some instruments may not function if covered. If a spacecraft is partially covered, the little spaces between the panels or coating may still develop charging.

Active Control by Beam Emissions

Electron Emission

The simplest way to emit electrons is by field emission or hot filament emission. The field emission uses sharp spikes from a conducting surface and generates high electrostatic fields. At high fields, field emission of electrons occurs.

Electrons can also be emitted from hot filaments at high temperatures. By connecting the power source of the filament to the spacecraft ground, this method can mitigate spacecraft charging. This is an active method that is normally used when ground control senses an accumulation of spacecraft charge. Both field emission and hot filament emission emit low energy electrons. If high current is to be emitted, an electron beam would be most useful.

Field emission, hot filament emission, and electron beam emission can mitigate charging only partially. These methods emit electrons from the conducting ground of a spacecraft into space. They discharge the conductor ground but cannot discharge the dielectrics [8]. The potentials of the ground and the dielectrics would settle at different potentials, causing different charging. This causes low energy electrons from leaving the surface.

Ion Beam Emission

When low energy positive ions are emitted from a highly negatively charged spacecraft, the charging level decreases [1]. In an ion beam emission, the ions are pulled back to the spacecraft. This neutralizes some negative charge and also attracts to the areas where negative charge is affluent. This reduces differential charge. The ions may also create secondary electrons in the process. These electrons carry away negative charge from the spacecraft. The disadvantage of this method is the possibility of contamination of the satellite surfaces by the beam ions [5].

Neutral Gas Emission

The charging level of a spacecraft is often unaffected when neutral gas is emitted. On the other hand, electron impact may be able to ionize the gas if the energy required is abundant. If the gas is ionized, it may be able to reduce the spacecraft charging level if the ions return and generate secondary electrons.

A Combination

This is considered the most efficient emission discharge process. It is simply the sum of the processes

explained above. It is difficult to compare the efficiencies of any two types of emissions. A given electron beam current cannot be compared with the same unit of current of a mixed electron and ion current. A mixture of the same amount of currents of electrons and ions would amount to a net current of zero. As a result, a direct comparison of the efficiencies of spacecraft charging using different types of emissions is invalid. Also, most ion beam devices release ions and neutral gas.

Conclusion

There have been many major accomplishments of charging analysis. It is generally realized that spacecraft charging is important. Spacecraft charging analysis often enables space experimentalists to interpret measures on board. Spacecraft charging provides satellite designers with a better understanding of the necessities to properly design their satellites.

The basic reason for charging is due to a fundamental property of electrons and ions. The electron flux is higher in space plasmas, causing the imbalance of fluxes. This often charges spacecraft surfaces to negative voltages. The emissions of secondary electrons, backscattered electrons, photoelectrons and artificial beams all need to be considered. At equilibrium, the surface potential is governed by the equation of current balance (see equation 1). For a typical spacecraft surface to reach equilibrium of charging, the time needed is often negligible (milliseconds).

Acknowledgement

Thanks to Shu T. Lai for reviewing this report and helping with the analytic interpretations of Spacecraft Charging.

References

1. Lai, S.T., An Overview of Electron and Ion Beam effects in Charging and Discharging of Spacecraft, *IEEE Trans. Nucl. Sci.*, Vol. 19, pp. 1629-1634, 1989..

2. Lai, S.T., Spacecraft Charging Thresholds in Single and Double Maxwellian Space Environments, *IEEE Trans. Nucl. Sci.*, Vol. 19, 1629-1634, 1991a.

3. Whipple, E.C., Potentials of Surfaces in Space, *Rep. Prog. Phys.*, Vol. 44, 1197, 1981.

4. Tribble, Alan C., The Plasma Environment, in *The Space Environment*, Princeton University Press, 1995.

5. Garrett, H. B., The Charging of Spacecraft Surfaces, in *Handbook of Geophysics and the Space Environment*, J.S. Jursa (ed), AFGL, ADA 167000, 1985.

6. Frederickson, A.R., J.A. Wall, F.L. Bouquet, Spacecraft Dielectric Material Properties and Spacecraft Charging, *Progress in Astronautics and Aeronautics*, Vol. 107, 1986.

Spacecraft Charging in Geosynchronous Altitudes

Percentage of Spacecraft Charging in GEO Orbit

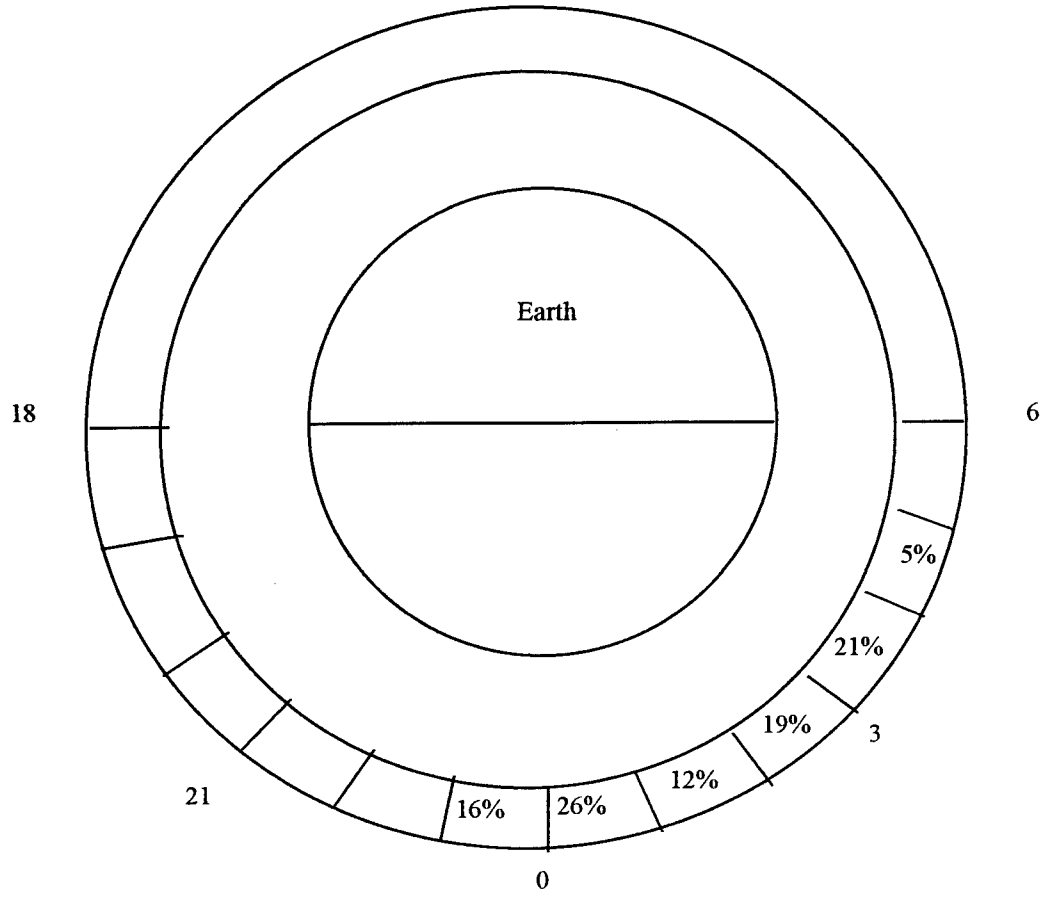

Spacecraft Charging in Geosynchronous Altitudes

The DCSC Data

Hrs	Number of Spacecraft Charging Incidents Within the Hour
1	XXXXXXXXXXXXXXXXX
2	XXXXXXXX
3	XXXXXXXXXXXX
4	XXXXXXXXXXXXX
5	XXX
6	
18	
19	
20	
21	
22	
23	
24	XXXXXXXXX

Radiometric and Radiation Characterization of Rockwell Science Center Detectors

Camden Mullen

Del Norte High School
5323 Montgomery NE
Albuquerque NM 87109

Final Report for:
High School Apprenticed Program
Philips Laboratory

Sponsored By:
Air Force Office of Scientific Research
Kirkland Air Force Base,
Albuquerque NM

And

Philips Laboratory

July 1998

Camden Mullen
Del Norte High School

Abstract

The Radiometric and Radiation Characterizations of Rockwell Science Center Detectors were studied. Two Photovoltaic HgCdTe detectors from the Long-wavelength Low Background Uniform Mercury Cadmium Telluride (LLUM) program were studied. The format of each consisted of several variable area conventional and lateral collection diodes and lateral collection arrays. The devices were identical in structure and format except one had an anti-reflection (AR) coating. The devices were held at a constant temperature and subject to radiometric and electrical characterization in both benign and radiation environments. The measurements performed in a benign environment were spectral and optical response dark and optical current-voltage.

Radiometric and Radiation Characterization of Rockwell Science Center Detectors

Camden Mullen

Introduction

The purpose of the Long-wavelength Low Background Uniform Mercury Cadmium Telluride (LLUM) program was to develop radiation hard, long-wavelength infrared (LWIR) high specific detectivity, uniform focal plane arrays that operated at strategic incident-photon-flux density levels.

Problem

The two diode arrays were identical except that one had an anti-reflection coating. Each detector was held at 40K or lower with no warm-up during testing. During testing, All diodes were shorted to each other and grounded. All measurements were made with the detector mounted in Janis, low background, side looking dewars configured with a cold finger directly under the chip carrier. Liquid nitrogen or helium fills the inner chamber, depending on the temperature of interest. Liquid nitrogen always fills the outer chamber. A 50 ohm resistor at the base of the cold finger provides heating as necessary. Calibrated platinum resistors monitor temperature at the base of the cold finger and near the detector.

In order to measure the spectral response the dewar is configured with a KRS-5 window and an optical path free from apertures or filters. A coax cable connects signal and ground pin from the dewar port to a Keithley 428 current amplifier. A Nicholet

Spectrometer bench is connected to the bench using an accessory box. OMIX E.S.P. software controls the entire system. The amplifier provides bias for the detector.

For evaluating the dark current, a metal plate covers the detector's optical area, witch is kept the temperature as the detector. To assure IR light is not penetrating the inner chamber, plates cover the nitrogen shield and replace the KRS-5 window. Triax cable connects the dewar electrical ports to a Keithley 707 switching matrix that consists of several Keithley 7174 8x12 Low Current Matrix Cards. A triax cable connects the 707 to a Keithley 236 source measure unit. The entire system is computer operated. The unit provides bias to the diodes and measures resulting current. Measurement of current is done in three steps. First the Keithley 236 varies bias from –300mV to –60mV in 10mV increments. Second, the unix varies the bias from –58 mV to 58mV in 2mV increments. Third, the unit varies the bias from 60mV to 300mV in 10 mV increments. LabView 4.o controls the entire system.

The graphs below show Photon Response and Dark current-voltage measurements.

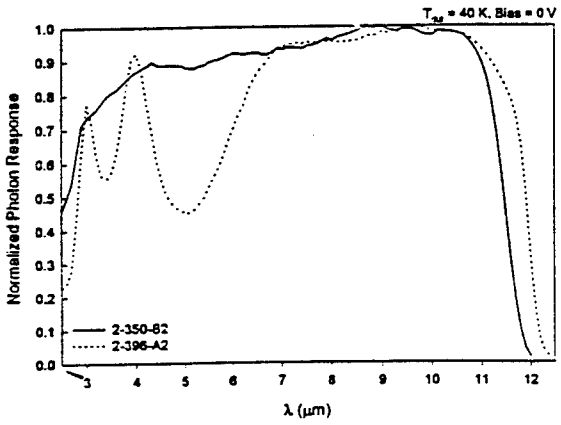

Figure 1-1 Photon Response

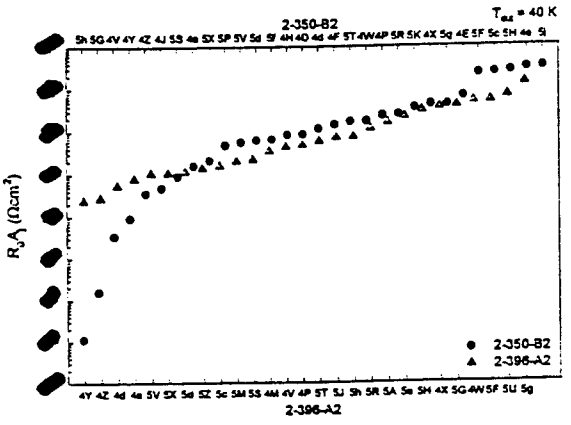

Figure 1-2 Dark R_oA_j

DEVELOPMENT OF A VISUALIZATION MODULES FOR ICEPIC

Kim Robinson

Sandia Preparatory School
532 Osuna Road. NE
Albuquerque, NM87113-1099

Final Report for:
High School Apprenticeship Program
AFRL/Phillips Laboratory

Sponsored by:
Air Force Office of Scientific Research
Bolling Air Force Base, DC

And

Phillips Laboratory

August 1998

DEVELOPMENT OF VISUALIZATION MODULES FOR ICEPIC

Kim Robinson
Sandia Prep School

Abstract

AVS/Express Developer's edition, by Advanced Visual Systems Inc. is a complex data visualization kit consisting of several hundred different modules, as well as a couple different editors, each serving a somewhat different function. In order to use this program, extensive training is required. In hopes of making things easier by designing a system with which people not familiar with the specifics of AVS can create visuals fairly quickly, an alternate method was developed. Through the custom designing of new modules specified to do certain things simply, graphs and movies are now considerably easier to make and include their own, easy to use, interfaces. This assists the computationalists at the Center for Plasma Theory and Computation by allowing them to view the results of their simulations more easily.

DEVELOPMENT OF VISUALIZATION MODULES FOR ICEPIC

Kim Robinson

Introduction

The computationalists at the Center for Plasma Theory and Computation (CPTC) run simulations with plasma physics software that create very complicated data. The easiest way of understanding this data is through the use of images created directly from the data. For this purpose, they purchased a software package called AVS/EXPRESS produced by AVS (Advanced Visual Systems), Inc [1]. It is multi-platform but runs very well on a Silicon Graphics machine due to the advanced graphics rendering hardware on that machine. Unfortunately, the learning curve associated with this software is fairly steep, so that a significant commitment of time is required to make even simple graphics. In order to significantly reduce the time required for members of the CPTC team to be able to create useful graphics, graphical interfaces and custom modules were developed that were specially tailored to the data created by the CPTC software packages. The process of creating specialized modules for the scientists took a bit of time, some C-coding, and a bit of creativity. Now there are modules that work exactly how they are needed to and contain specific interfaces that negate the need for one to understand the details of how AVS works. In this paper terms that are specific to AVS modules or pathnames will be Arial font while the underlined Arial represents modules that have been built, and terms that have a unique meaning in AVS will be in *italics*.

AVS Overview

The AVS software is based on groups of objects called modules. These modules often deal with data formatted in the AVS *field* format, which consist of a *mesh* combined with cell data. The AVS *fields* are not always the most convenient format to use. A *field* file can be read into AVS with the use of the AVS Read_Field module, but it has to be in a very specific format that involves a good deal of data post-processing before it can enter AVS. There are several other methods of reading in data that work better but most are still difficult to work with. The simplest of these is through the creation of a File_Import module. File_Import modules may be created and customized to the format of the files that are to be read in. Such modules read in multiple columns of data and export them as arrays. They can also be modified for specific files.

To build a File_Import module, a Workspace in the User_Workspaces library must be selected (see Figure 1). Usually, the User space should be reserved for modules that include user-provided source code. Under the Object menu on the menu bar is Add File_Import_Module. This opens an interface that prompts the user through the process, which includes naming the module, adding variables and assigning those variables to columns of data. It also wants to know if the file is ASCII or binary, which does make a difference. There is a bug in the ASCII reader: it prompts for how many bytes to skip, which does not work, so header lines do not work in ASCII files. It should be noted that these modules will only have the function of reading in data (user specified source code cannot be included.)

Data are passed and modified in AVS through a series of modules in a *network.* After the addition of several modules, this looks like a tangle of colored spaghetti. Each module has colored ports of what it can take in or put out. Modules are connected through colored tubes that eventually get tangled and provide a confused mess to work with. In general, the colors mean specific things, but depending on the module, a color can mean something different; black, for instance, can be several different things. Usually the colors correspond to the types of data as shown in Table 1.

Table 1. The color of the lines connecting modules corresponds to the types of data which may be transmitted along them.

Type of data	Color	Example
Renderable image	Red	*Mesh* output to viewer.
Field	Blue and Black stripes;	Output of *mesh* to input of data module
	All black;	(orthoslice).
	Blue, Black, green stripes	
Primitive data type	All black (single values, not *fields*)	
Float data type	Brown	Arrays of floats come from File_Import
Int data type	Pink	modules.
String data type	Blue	
Parent connection	Bright green	
UI connections	Pastels	Used primarily in UI

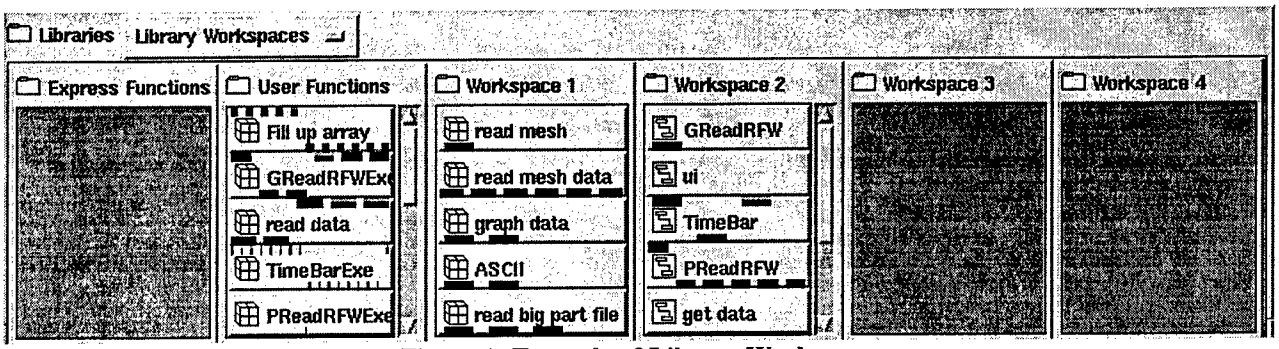

Figure 1: Example of Library Workspaces

Tools and Methods

AVS Applications are built in the *network editor* (An example is provided later in Figure 2). Typically, the first item in an AVS *network* is a module that is used to read in the data file. This can be hard to do for someone unfamiliar with AVS. As described above, the File_Import_Module is the simplest way of reading in a file with data in columns. The next step is to do something with that data. Most applications will require a *mesh* to be built; it is similar to a *field* and will often work the same way. A *mesh* may be created by inputting coordinate information into the appropriate module found under Main.Field_Mappers.Mesh_Mappers. There are several types of *mesh*es that can be used, but all are fairly straightforward. A point *mesh* tends to work best for plotting scattered particles. Where to go from here depends on the type of plot desired. AVS can make many different kinds of plots, all requiring different kinds of input. Images that are of particular interest to researchers at CPTC include contours of electric and magnetic fields, and the movement of particles through complex geometric shapes. Those plots will be focused on, since they were the ones developed.

Several tools were developed to visualize data produced by the plasma physics simulation software, ICEPIC [2]. ICEPIC is a particle-in-cell (PIC) code that was developed at the Air Force Research Laboratory (AFRL) primarily to assist in the development of high power microwave sources. ICEPIC produces a variety of data sets: each in independent files. These files include representations of the device geometry, electric and magnetic field information for all of the computational domain, charged particle positions and velocities, electrical current, transmitted power, etc. One of the projects accomplished this summer was a movie, which showed several of these data sets at once and their evolution with time. This allowed users to see the interaction of the data sets, giving them a "big picture" view of the simulation.

A picture of the geometry may be generated by viewing a quads output file. This file contains a series of quadrilaterals (four points in a plane) which are created by checking all of the faces of each cell within the problem and outputting those faces which lie on a physical boundary. The quads file is reduced to a workable size by a C code, quadreduce, written by Jerry Sasser of CPTC. It is read in using a macro (a collection of modules) called GReadRFW built by Kent Eschenberg from the Army Corps of Engineers Waterways Experiment Station (CEWES) Major Shared Resource Center (MSRC) in Vicksburg, Mississippi. GReadRFW includes a module built from C code with the Add_Module function that reads the geometry file and puts it into a point *mesh* format.

A PIC code tracks charged particles as they are moved through a computational mesh under the force of electric and magnetic fields. It is often interesting to view the location of these particles with respect to the device boundaries. Dr. Eschenberg also wrote a C program that makes this process much more efficient. Due to the number of particles that appear at each subsequent time step, around 1×10^6, it becomes very time-consuming to read them in as point *mesh*es one step at a time, so that it has to read and map every particle over and over again. The RF Particle Counter (rfpc) pre-processor breaks the problem domain into a 256x256x256 mesh of boolean data points. Each point is set to 1 if at least one of the particles exists in that region and 0 if none do. This array of booleans is then created for each time step and stored in a new file, which takes up considerably less space than the original data files. The rfpc program allows the Loop, which controls the movie, to run much faster. Those two modules are the basis of the development that is covered here.

Another image that was produced was a 2-dimensional contour plot of the radial electric fields in a cross-sectional cut through the volume. This technique is easily modified to view any component of the electric or magnetic field. This process is more complicated because the modules involved require an AVS *field* as input (in particular, one with a rectilinear or uniform *mesh*.) The electric field data output by ICEPIC is not compatible with the AVS *field* format and requires significant postprocessing. To understand the format of the electric field data consider the following example. The computational space in ICEPIC forms a parallelepiped (like a shoebox). This space is broken into rectangular cells by defining a grid as the intersection of an x-mesh with a y-mesh and a z-mesh, where each mesh is a 1D array that describes how that direction is to be divided. Now suppose that the device of interest is actually a cylinder

which fits within the computational space. ICEPIC only performs computations on cells which fall within the physical domain (in this case the cylinder, which has stair-stepped edges since the cells are rectangular) and no memory is allocated for the other cells. When ICEPIC outputs the electric field data, it goes through its list of real cells and prints the cell position (x, y, z) and then the components of the electric field (E_x, E_y, E_z). This is very different from the *field* format which would expect all of the x-mesh values, all of the y-mesh values, all of the z-mesh values, and then electric field values for every cell (including those outside the cylinder since AVS in not aware of its existence) in a particular order. Since reading in the files as a File_Import_Module was really too simple a format in this case, something else had to be created. It was necessary to build a new module, from scratch. This is similar to building a File_Import_Module: a library, preferably User, must be selected and the command (Add_Module) is found under the object menu. The interface prompts for variables and their roles in the module, but then it allows for the insertion of source code. Before generating source code, it is best to allow the new module interface to create a source code template given the desired inputs to and outputs from the module. This is done by clicking on *edit source* in the last window of the Add_Module tool before a file of the expected name exists. The template will contain all of the necessary Application Program Interfaces (APIs) required to communicate with AVS. In creating the module it is important to think ahead and carefully design the module. It is more difficult to add new APIs after the template has been created. These modules can be written in C, C++, or Fortran; the language option is the first thing that appears on opening the build module interface.

Converting ICEPIC data to AVS field format

As mentioned above, there are two steps involved in creating an AVS *field*: generating a *mesh* and assigning data to the *mesh*. The meshes that come from ICEPIC have to undergo several changes to get into AVS. Three files, xmesh, ymesh, and zmesh combine to make a range of values which may be contained in the ICEPIC field data file. Those are read into the *network* (see Figure 2) with three separate File_Import_Modules named read_mesh. Each array is interleaved with itself with the interleave_3_arrays module from Main.Mappers.Combiners. Finally, those three arrays are catenated to form an $[n_x+n_y+n_z][3]$ array of points that define the *mesh* that will be used in the AVS *field*. This is done with the concat_3_arrays module, which is found in the same menu as the interleave module. It does not matter if the three *mesh* dimensions are different because the interleaving takes care of that.

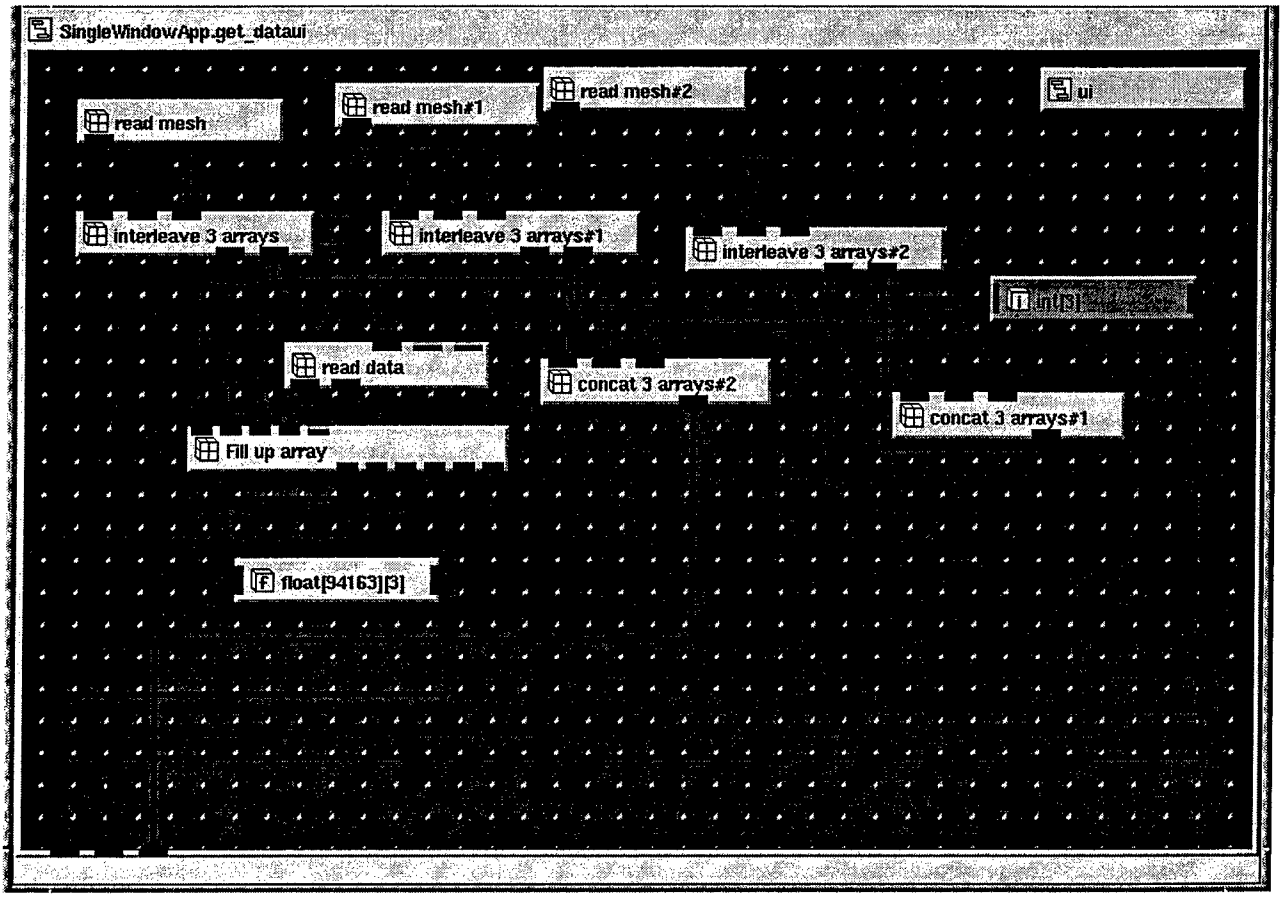

Figure 2: the read mesh network

The electric field data are read in with a custom module called read_data that reads in every line of the ICEPIC electric field file (x, y, z, E_x, E_y, E_z) and returns a single 1D array with all of this information grouped together. This array is then inserted in a custom module called Fill_up_array along with the mesh arrays. Within this module a large 1D array (n_x x n_y x n_z) is created to contain the data for the AVS *field*. This array is filled by using the position of the cell (x, y, z) to determine the indices in the mesh ($x=x_i$, $y=y_j$, $z=z_k$) which are used to inset the data into the array in the following way:

Data $[i+j*n_x+k*n_x*n_y]$ = Ex (at $x=x_i$, $y=y_j$, $z=z_k$)

In this example only one element of the electric field is used, which could be used to create an AVS field with scalar data (some of the AVS modules require that the data be scalar while others require vector data.) The format for vector data would be:

Data $[(i+j*n_x+k*n_x*n_y)*3+m]$ = E_m (at $x=x_i$, $y=y_j$, $z=z_k$)

Before the data are inserted in the large data array, the elements of the array are initialized to a value that is larger than any of the data (this value is referred to as the null value).

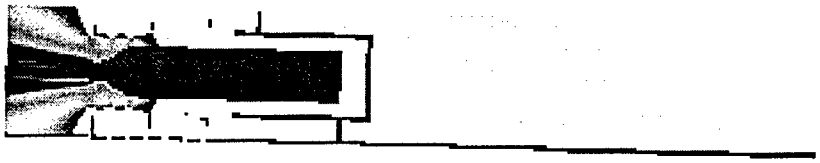

Figure 3: MILO

This will be used to take advantage of several useful AVS filter modules. The AVS *field* is created by piping the mesh array and the data array into a Rect_Scalar_field module, which creates a *field* consisting of a rectilinear *mesh* and scalar data. This module also requires dims, which is an array of the three mesh sizes. Points is the 2D array of the *mesh* points. Data is what came out of the Fill_up_array module. In this case it should be scalar, so E_x was chosen.

The Rect_scalar_field module outputs a field that can be fed into a module called orthoslice, under Mappers. Orthoslice shows a 2D plane of data in a cross-section which may be chosen to be in any of the 3 directions and may cut along any *mesh* point. If the shape of the object being simulated is not rectangular (for example, the cylinder discussed earlier), there will likely be null values surrounding the data that is wanted. These can be removed by using the threshold module, under Main.Filters. This was the purpose of the pre-initialization of the data array discussed above. When the null value is set everything with that value will disappear. The output of threshold feeds into orthoslice and orthoslice to the Uviewer (using the red pipe). The Uviewer should show a 2D plane colored in the shape of the device. This can be displayed over the device geometry by adding a GReadRFW module. Remember that when working with multiple images care must be taken not to edit the size or position of one of the images if it is important that they have a fixed position. This lesson is easily learned the first time a project has to be restarted after accidentally editing only one object's size or position. The results of an orthoslice and an image of a device are shown in Figure 3, where this is an early time step for the Magnetically Insulated Line Oscillator (MILO) [3].

The colors chosen for the contours are specified in the datamap. The colors are scaled to the data and if the null value used to preinitialize the electric field array is much larger than the real data, the image

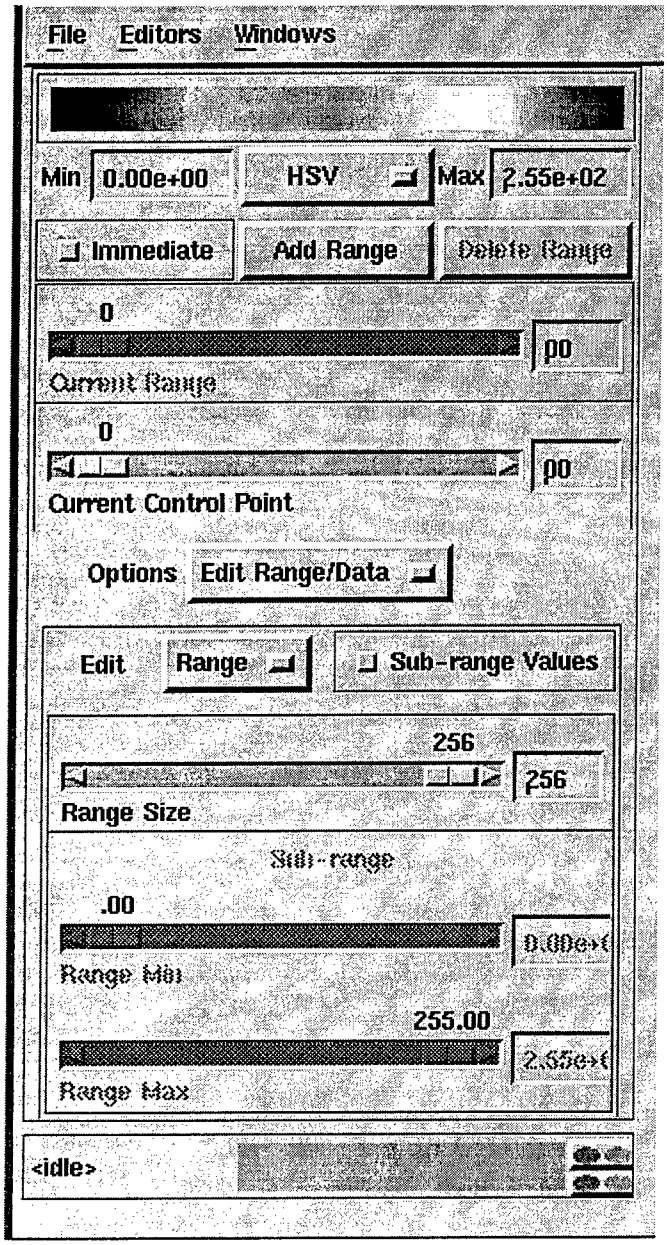

Figure 4: Datamap control panel

will be shaded entirely in one color. This can be taken care of but should be done carefully. It is not a good idea to delete the data map. There is a button at the bottom of the Uviewer window entitled "select object". It brings up a menu of the modules that are linked directly to the viewer. This makes it possible to change the properties of individual objects. It also makes it possible to destroy the project fairly easily if something is moved separately when it should not be. Select orthoslice in the object menu and datamap editor in the editors menu on the menu bar. The datamap appears in the viewer interface window (See Figure 4). The next modification depends on where the data are in the range. If the data consist of small values, on the lower end of the, an additional range will work well; select Add_Range. This gives the whole range of the current map to the colors in the reduced data range. There is a pop-up sub-menu in the middle of the editor box. One of those options is Edit Range/Data. It provides an interface that includes a sub-range. Toggle the box that gives a sub range. It has values from the file it read. Play with the min and max of those values until they correspond to the range of the real data. If the data are toward the middle of the range, add a sub-range, but not an extra range. Another option is to change the colors with the Edit Color sub-menu. Control point 0 (the slider above the menu) represents the data min while control point 1 represents the color at the data max. If the

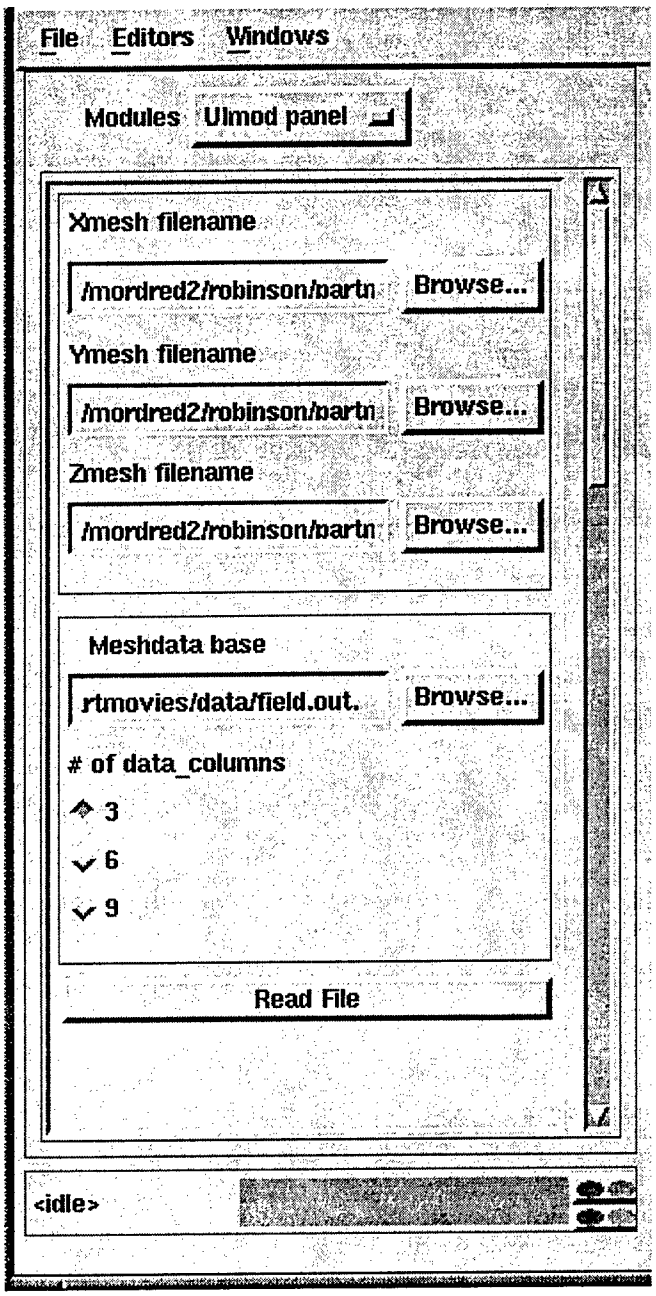

Figure 5: UI panel

256 range does not work for whatever reason, under Edit Range/Data is a slider that will reduce the colors in the range.

A very nice trick that allows other objects (such as the device geometry) to be seen through the slice may be found in the Object editor, under the Editors menu in the Uviewer. The orthoslice must still be selected. Under Properties.Surface are several sliders that control the surface properties of the object. One of these is opacity; reducing this makes the slice somewhat transparent so that it seems to be more a part of the geometry. The object menu can also change the color of the object and the jitter, which layers things in the viewer, allowing things to be seen or not seen through another object (this is often useful when working with particles).

In order to make the modules more user-friendly, user interfaces were added using the AVS User Interface (UI) kit. This kit allows the user to create an interface similar to those on the AVS modules. It provides a series of panels, buttons, sliders, and type-in areas to get the information to the modules that require it. Each module that was created for this project has its own interface so that it can be used with very little knowledge of AVS. For example, Figure 5 shows the UI for the macro which reads the electric field data.

Quadrilateral and contour plots have already been discussed, but there are many more visualization methods available in AVS. Many of the 3D plots can be found under Main.Mappers. The

annotation and graphing kit takes care of the 2D graphs. AGGraph creates a 2D line plot based on an array of y values. X values can be provided but are not necessary. AGGraph comes in various formats (cartesian, polar, bar charts, etc.) along with all sorts of axes and legends. There are some difficulties in combining an AGGraph with 3D images. Whenever a 2D graph is put in the same viewer with a 3D object, it blinks and then disappears. It turns out that this is a problem with the hardware rendering. It works fine with the Uviewer that supports 2D and 3D and with software rendering toggled.

An example of an application requiring the 2D graph is the changing power output of the device. Making this graph change in time (along with the other visuals) provided some unique challenges. The goal was to make it loop through the array of data so that it would be animated, presenting a problem that could not be fixed with the existing modules. The module that was developed used the count variable from the loop module to set the size of the array that would be read in. By giving the graph module the entire x array, but only the partial y array (up to the loop counter), it drew the graph as the loop incremented giving the impression of an animation. There is also a string variable that allows the color of the graph to be changed.

Another module that Dr. Eschenberg built is a TimeBar that represents the location (i.e. the time in the simulation) in the loop by changing the color of a bar from gray to red with the option of red to green at a certain value as it moves along. A small arrow moves ahead of the red section according to the loop count.

Lights, Camera, Action: Making movies with AVS

There are two ways of making a movie with AVS. One involves creating images in AVS one at a time and saving them as gif or jpg files and then using additional software to catenate the images into a movie. The other came built into the most recent edition of AVS. It does not work quite as well for data movies. It is really more for making movies of alterations to the view of the data set, such as a fade in or a rotation rather than altering the data itself. Things to consider before saving the images include lighting, which will not be as good in the image as it appears on the screen, so consider adding more light. The positioning needs to be correct as well; it is sometimes better to rotate and translate objects using the Transform editor (in the editors menu of the viewer) rather than moving them with the mouse. If there is

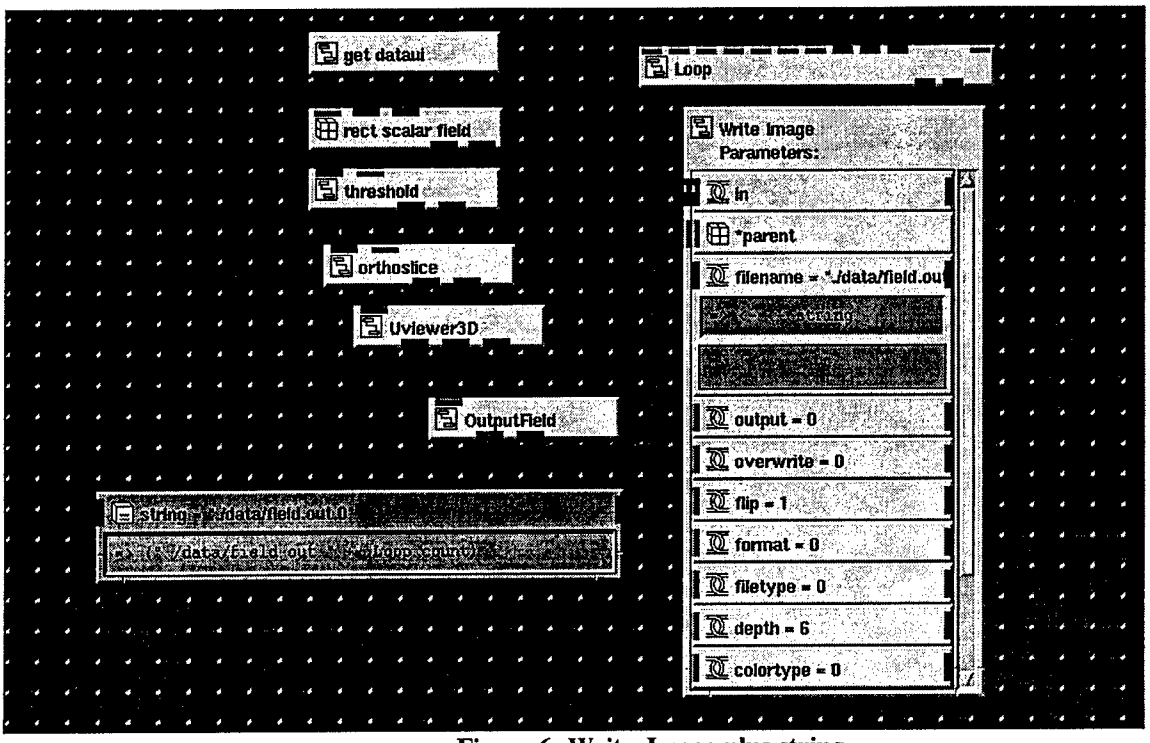

Figure 6: Write_Image plus string

a problem during the course of the animation (program crashing or spontaneous resizing of the image) then it is easy to return to the exact same settings.

Method 1

This method uses a Loop module and is appropriate for displaying data that change with time. An example *network* is shown in Figure 6. Under Main.IO is a module called Write_Image, which is exactly what it does. Its interface contains a slew of possibilities for the kind of image that can be exported. It does not automatically change the necessary options, like Bits per Pixel when the image type is changed. It also needs a filename, which is where AVS tricks become necessary. There may be another way to do this, but this works. A string from StandardObjects.parameters will change the filename as the loop increments. This syntax is very important. (See Figure 6)

=> ("/path/name." + .Loop.count)

This will access the count variable and attach it to the end of the file name with each iteration of the loop. Now the Write_Image module must be changed to read that string. Right clicking on the Write_Image module will bring up a menu. Parameters is the least confusing choice (see Figure 5). This displays (simply) what is inside the module. There will be a link (with an icon like a knot) called "filename".

Opening filename will reveal a reference to something within Write_Image. Delete it. In order to get its value from the string parameter, the reference should be changed to:

<-.<-.string.

That tells filename that it has to go up two levels and find an object named string to find its value. Hitting return inside the box will accept that value or bring up an error message. If an error message appears, adding another arrow, hitting return, and then deleting the arrow should work.

One noticeable thing about this *network* is that the Write_Image module will not connect to the Uviewer. This suggests that another module is required to connect them. Under Main.Viewers is a module called OutputField. It has a purple input that matches one of the outputs from the UViewer, and a black, blue, and green striped output that matches the Write_Image input. The OutputField module outputs an AVS *field* of the image that the UViewer displays, and the Write_Image module turns it into a picture. Once everything is absolutely perfect, and not going to break and leave random files all over the harddrive, the "dynamic" option under OutputField should be toggled. This will update the *field* every time the loop increments and causes Write_Image to output a file. This process will create a numbered series of images (gif, tif, or other) which can then be catenated by another program (e.g. Mediaconvert on the SGI) to create an animation.

Method 2

The other method, which came built in with release 3.4 of AVS/EXPRESS is the animator and its partner, image_capture. They do exactly what their names imply, animate something and then capture it. Image_capture will also generate a movie after it creates a series of image files in AVS format. These modules were intended to smoothly capture actions within the viewer window such as resizing, translating, or fading an object. The animator module requires something in the viewer to change for each frame.

The animator module does not require any hookups. It works by allowing the user to create a series of key frames. Once each frame is correct, click the generate frame button. If nothing has changed, it will not generate the frame. It will generate the frame, however, if something has moved and then moved back to its original position. This can become time consuming, but if the movie has to be done via these two modules, it can be done. The animator interface has a toggle that puts all of its interface into a separate window so that another interface can be open at the same time. The Transform interface (under the editors

menu) can change the positions of things numerically so that they can be changed back more easily. After all of the frames are generated, click the play button to see if everything went correctly. If it did not, it has to be done again.

The image_capture module plugs into the purple output on the UViewer. The module is normally inactive. The name of the directory where the files will be placed should be entered in the movie name field (include the final slash). With this module there is no choice, the files come out as avs files with an extension of .x. These are for some reason colored differently then the image in the viewer so some experimentation is required to get the desired colors in the movie. Toggle the capture mode from disk to memory to disk again to outsmart a known bug. To capture the animation, the mode needs to be set to capture from view. If anything obscures the view while it is running, it will not be happy. The next step is to run the animation and hopefully the files will be generated. If so, the button that generates a movie can be pressed. It will leave an MPEG called anim.mpg in the directory with the images. This can also produce single images. Whenever it is set to capture from view, it will create images of every change in the viewer.

Streamlines

Those are the majority of the modules that were developed at the Center for Plasma Theory and Computation, but there are many other visualization possibilities. For example, streamlines can be created using the same macro that gathered and indexed data for the orthoslice. Streamlines requires vector data. The data that comes from the Fill_up_array module comes in the form of what should be vector data, but in a 1D array. That array can be fed through a float that is forced with the object editor to be [n_x x n_y x n_z][3], and have a three element vector array which may then be used to create a field.

A few words on syntax

If a parameter (int, float, string) is going to be referencing something else, it needs a reference arrow (=>). If it is referencing a sister object: one on the same level, or one on a lower level, the path consists of a dot and the object name, which can be very long if the object is nested. If it is referencing a higher object, it needs a directional (up) arrow and a dot (<-.) for every level it needs to go.

From inside an object, a reference still needs a referencing arrow, but also needs as many arrows to get outside of the object it is nested in. Levels are separated by dots.

Values can be added by containing the string in quotation marks and adding the value reference with a "+".

Conclusion

In conclusion, the modules developed will assist the CPTC team by allowing them to create visuals and movies quickly and fairly painlessly with a program that can be very difficult to use. They now have the capability to animate 2D plots as well as incorporate them into movies. Electric and magnetic field data from ICEPIC may be read in without modifications and can then be used with all of the AVS modules after being converted to *field* format with the provided modules. This greatly increases the possible uses of these data. These modules were combined, along with ICEPIC data to create a movie which was shown at the AFOSR Mathematics and Computer Science Directorate Annual Review. That application also provides a template for future movies that can be made completely through the interfaces. In the near future, the computationalists at CPTC will, hopefully, use these modules so that they can be improved and eventually developed as stand-alone applications.

Acknowledgements

This work was performed in conjunction with work funded in part by the Air Force Office of Scientific Research Mathematics and Computer Science Directorate and the DoD High Performance Computing Modernization Program. AVS/EXPRESS is a product of AVS, Inc. ICEPIC was developed exclusively at the Center for Plasma Theory and Computation. Thanks to Kent Eschenberg and associates at CEWES MSRC for assistance and the use of their AVS modules. And special thanks to Captain Jerry Sasser.

References

[1] AVS/EXPRESS: User's Guide. Advanced Visual Systems Inc. Part number 320-0321-04. http://www.avs.com.

[2] James J. Havranek and Bradley J. Smith, "A Portable Parallel Particle in Cell Code," AIAA paper#96-0835 (Jan.1996).

[3] Raymond W. Lemke, et al, "Investigation of a Load-Limited, Magnetically Insulated Transmission Line Oscillator (MILO)," *IEEE Transactions on Plasma Science*, **25**, p. 364 (1997).

INVESTIGATING INTERFERENCE PATTERNS IN CELESTIAL IMAGES

Timothy Swierzbin

Chelmsford High School
200 Richardson Road
Chelmsford, MA 01863

Final Report for:
High School Apprenticeship Program
AFRL/Phillips Laboratory

Sponsored by:
Air Force Office of Scientific Research
Bolling Air Force Base, DC

And

Phillips Laboratory

August 1998

INVESTIGATING INTERFERENCE PATTERNS IN CELESTIAL IMAGES

Timothy Swierzbin
Chelmsford High School

Abstract

Research was conducted to characterize band C noise pattern interference in celestial images. Initial investigations focussed on the possibility of using one-dimensional fractals, such as the Cantor set, which appeared to be related to the observed interference pattern. However, because of certain restrictions to the boundaries of a Cantor set, the investigation did not yield desired results. Further studies using multi-fractals also did not produce useful results, but appeared to be a promising area for further examination. A mathematical approach was then applied in an alternative attempt to reproduce the pattern.

INVESTIGATING INTERFERENCE PATTERNS IN CELESTIAL IMAGES

Timothy Swierzbin

Visual clarity is important to obtain accurate information from a celestial image. The band C images that were examined in this study appeared fogged by interference, probably caused by an electronic error. In order to better understand interference pattern, a mathematical formula had to be found. Apart from understanding the pattern, a formula could also be used to construct a better filter for the interference. Upon initial examination, the pattern revealed traits that were similar to one-dimensional fractals. Further investigation using fractal geometry revealed evidence that the pattern could be in a class of fractals known as multifractals. However, the complexity of multifractals and time constraints prevented further study in this area. Instead, a final attempt, involving mathematical slopes, was used to approximate the pattern.

The pattern was composed of a series of high and low frequencies. These frequencies, when plotted as shown in Figure 1, appear to be clusters of line segments arranged in a self-similar pattern. One of the many definitions for a fractal is a pattern constructed from multiple iterations of a "self-similar" figure.

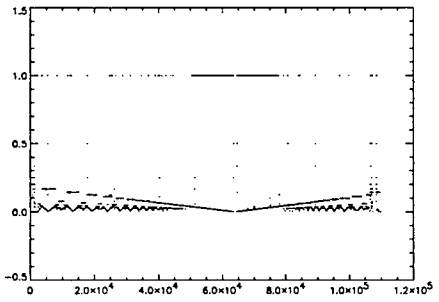

Figure 1. Plot of time vs. frequency.

The first attempt at solving the problem was to examine a fractal known as the Cantor Set. A Cantor Set is composed of only line segments that lie within the interval [0,1]. Figure 2, depicts how a

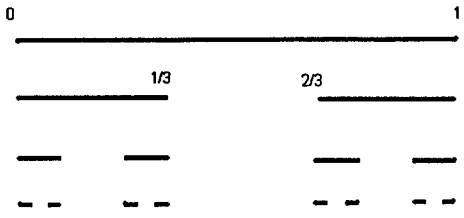

Figure 2. Four levels of the original Cantor set.

Cantor Set is constructed. First, the set starts with a single segment of length one. Then, the middle third of the segment is removed and two segments with a length of one-third are formed. The middle third of those two segments are removed and the pattern continues.

A regular cantor set did not resemble anything in the interference pattern, but when the set was modified by leaving out the end thirds, it resulted in a pattern that displayed similarities. When Compared to a section of the interference pattern, one can see the resemblance (Figure 3). Each pattern begins with a single segment, which then breaks into two segments, and then breaks into four. However, a Cantor set must remain continuous while the pattern is discrete. The interference pattern also does not

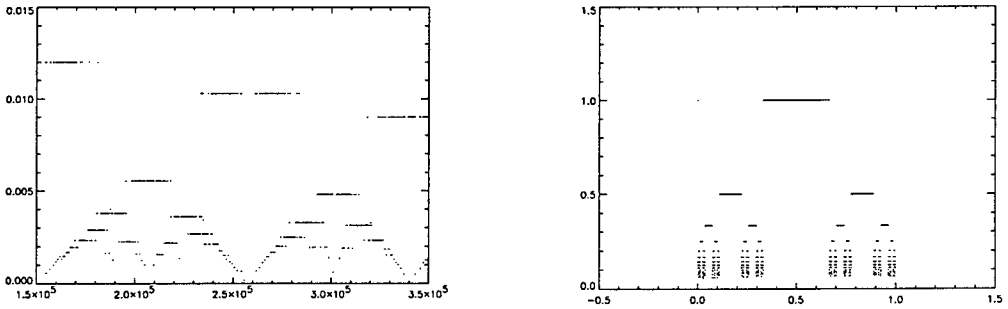

Modified Cantor set

Section of interference pattern

Figure 3. The modified cantor set compared to a magnified section of the original interference pattern.

completely follow the order that a segment splits in two. This led me to believe that I should not continue with my research on the Cantor set.

The study was continued by looking for other fractals that might be related to the pattern. To aide the efforts, the pattern's fractal dimension was calculated in the hope that it would match the dimension of a different type of fractal. The type of fractal dimension used was the self-similarity dimension. First, the number of self-similar sections were counted. Then, using one of the larger sections, it's scale relative to the complete pattern was found. Using the formula log (a)/ log (1/s) (Reference 1), where a is the number of self-similar pieces and s is the scaling factor, a fractal dimension for the section was calculated. Hoping that the fractal dimension would be the same throughout the entire pattern, the self-similar dimension for a smaller section was calculated in the same manner. However, the dimensions ranged between 1.812 and 1.17, which led me to an area of fractals known as multifractals. These are defined as a mix of fractals that contains a range of fractal dimensions (Reference 2). Unfortunately, basic multifractal mathematics were too complex to get any results from them, and the decision was made to graphically approximate the pattern.

The closest approximation achieved was from a program written by a co-worker (Reference 3). His program constructed a single line segment whose endpoints were then connected to a point

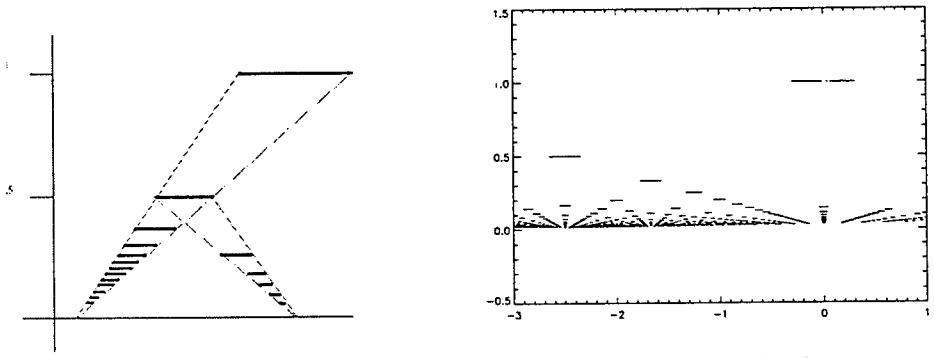

Figure 4. Left: shows method of construction. Right: shows final result

on the x-axis, left of the original segment. The slopes of the two lines connecting the endpoints with the x-axis were then calculated and segments were drawn at different levels within those lines. Each

new segment within the lines would then form two new lines with a point on the right. This pattern was repeated until a reproduction to the interference was produced. As can be seen in Figure 4, the new pattern has features resembling the interference pattern, but upon closer examination, there are many cross segments and extra segments that are not evident in the original pattern indicating that further work is needed before this technique can be used.

Because of a lack of time and the complexity of the problem, a mathematical formula for the pattern was not produced; however, the results obtained still appear promising and looking further into multifractals should prove to be of value. There is strong evidence that the interference pattern has a multifractal character.

A graphically-generated representation of the pattern may also be possible, but one may need to determine where an interference frequency exists at a certain time implying the need for applying probability to the problem.

Its function was to take an array of elements between 0 and 1 and calculate the level that an element exists. In order to do this, a type of recursive program was written. To determine the level an element exists, it had to pass a series of inequalities. If less than 1/3 an element would be sent to the left procedure, from there another set of inequalities would either send it to the right or left procedure, bumping the count on the level each time. When the program is finished it should give you a full array of levels that can be plotted with the array of elements. The final product will be a plot of a modified Cantor set.

The procedure is found under the name Cantor2.pro. Calling the procedure requires the command *cantor* followed by a set of parameters: num(an array of elements ranging from 0 to 1), n and d(numerator and denominator of scaling factor, and levels(returns an array of levels that corresponds to the array of elements in num. The full call looks like this *cantor,num,1,3,levels*. Be sure to save an array in num before passing it into cantor.

BIBLIOGRAPHY:

1. Peitgen, Heinz – Otto, et al. Fractals for the Classroom. Copyright 1992, Springer-Verlag New York, inc.

2. Bunde, Armin, et al. Fractals and Disordered Systems. Copyright 1991, Springer-Verlag Berlin Heidelberg.

3. Don Mizuno, private communication, AFRL/VSBC, 1998

COMMERCIAL POWER INTERFACE FOR THE ISACC ALARM SYSTEM

Arun K. Wahi

Albuquerque Academy
6400 Wyoming Blvd. NE
Albuquerque, NM 87109

Final Report for:
High School Apprenticeship Program
Air Force Research Laboratory:
Phillips Research Site

Sponsored by:
Air Force Office of Scientific Research
Bolling Air Force Base, DC

and

Air Force Research Laboratory

August 1998

COMMERCIAL POWER INTERFACE FOR THE ISACC ALARM SYSTEM

Arun K. Wahi
Albuquerque Academy

Abstract

An interface to monitor commercial power operation for the Sensaphone® Intelligent System for Automatic Control and Communication (ISACC) was developed. ISACC was already in place in the Cryogenic Technology lab to monitor experiments on the coolers and to notify a technician if conditions were out of bounds. ISACC could be programmed to delay notification until a given alarm had existed long enough for concern. OR Box Interfaces had been developed to combine alarm signals from five coolers into one of ISACC's limited alarm inputs. No system existed previously to notify a technician if commercial power failed; but because such a failure could cause expensive systems to terminate or operate out of bounds, the new interface replaced the existing relay box between the OR Interface and ISACC. In other words, the interface connected the existing systems and allowed either a power failure or an experimental condition to alarm ISACC. A one-hour delay of notification in which commercial power could be restored was delegated to ISACC's programming capability (rather than complicating the interface). Tests with a Fluke Digital Multimeter and ISACC alarm simulations indicated that the wiring was correct and that the interface functioned as intended. This paper illustrates the logic behind the circuitry of the interface.

COMMERCIAL POWER INTERFACE FOR THE ISACC ALARM SYSTEM

Arun K. Wahi

Introduction

The cryogenic technology lab operates on a commercial power system, an uninterrupted power source, and a power generator. In the event of a commercial power failure, the generator automatically replaces the commercial power sources to various systems. Once commercial power is restored, the generator automatically switches off.

Because the lab handles cryogenic coolers under experimental conditions, it is vitally important that a steady power supply be maintained. The current system, however, presents two major problems. First, the generator uses propane. The propane tanks hold a total of 48 hours' worth of gas. The frequency and duration of power failures are enough to warrant concern about exhausting the supply before commercial power can be restored. Second, the generator does not supply power to the air conditioning of two environments which together encompass five coolers. Lab personnel estimate that the most sensitive of these coolers would overheat after three hours without air conditioning. Thus, even a short power outage could cause significant and expensive damage to the equipment.

Should a power failure occur during working hours, one of the technicians would notice and report it to the civil engineering emergency desk, which would then work to restore commercial power in a reasonable amount of time. A failure at night, however, could go unnoticed. The worst-case scenario is that commercial power could fail during a long weekend, causing the generator to run out of propane before the next working day. The cumulative damage of total power loss to systems without the uninterrupted power source would cost several million dollars to amend. Therefore, the cost of the electronic components needed for an interface to monitor the commercial power is clearly justifiable.

Methodology

The interface can monitor commercial power from any wall outlet, so a common power cord will suffice for input. If the interface loses the signal from that cord, it then needs to produce an alarm which will notify a technician of a possible power outage. The obvious system to perform this task is the Sensaphone® Intelligent System for Automatic Control and Communication (ISACC). ISACC is already installed in the lab as an alarm system for the coolers. An OR Box Interface monitors signals from five independent coolers and sends an alarm to a relay box if any of the coolers exceeds its parameters. The relay box alarms ISACC via a nine-pin cable, which then dials certain telephone or pager numbers based

on a programmed need-to-know hierarchy (precisely what the commercial power interface intends to accomplish).

The original design for the interface included an output to one of the relay boxes described above. However, the tasks of the interface require all of the parts already in the relay box, so the new design combines both units to optimize a single box. This means the interface must output to ISACC via a nine-pin plug. It also requires an additional input from the OR Box Interface, which entails a W172DIP-5 relay receiving the signal from a nine-pin jack and relaying it to the nine-pin output plug.

A different relay is necessary to connect the power cord to a remaining set of pins on the output plug. ISACC should only alarm when the power cord does not produce a signal for a certain time. ISACC has a programmable recognition time ranging from two hundred (200) milliseconds to 4.5 hours. Lab personnel reason that a one-hour window in which power could be restored automatically would leave sufficient time for response without endangering any systems. Since the recognition delay is within ISACC's parameters, a time-delay relay is not necessary. Some relays could use the current from a 5V power supply to alarm ISACC; however, the IDEC RR2PU-120VAC relay contains a coil which closes the circuit when energized and opens the circuit in its de-energized state. This relay is therefore connected directly to the power cord to eliminate the expense of a power supply. A fuse between the relay and the power source is included for safety. The rough wiring, then, is as follows: the power cord enters the interface, the line passes through a 1A, 250VAC fuse to the IDEC relay, and the wires from the contact pins run to the pins of the nine-pin output plug.

In addition to a message from ISACC, a simple visual or audio signal could help technicians monitor commercial power during working hours. Use of a neon lamp as a visual signal is the most practical approach. Because there is no independent power supply in the circuit, the lamp must be wired in parallel to the IDEC relay coil. In this case, the lamp will indicate the normal operation of commercial power. The side benefit of the lamp's location is that if power fails and ISACC does not alarm, the technicians will know the breakdown in signal is with the relay or some point beyond.

The remaining feature in the final design is a bypass switch for the commercial power alarm. A switch that is normally open is located between the IDEC relay and the ISACC output. A technician can throw the switch if he is aware of a commercial power failure but wants ISACC to stop alarming.

The architecture of the interface is self-evident. Because the power cord contains noise, the OR Box input, W172DIP-5 relay, and ISACC output plug should be as far away from the power cord as possible. The two nine-pin connectors are therefore located on one side of the box opposite the side where the power cord and fuse enter. The lamp and switch must be visible and accessible, and the IDEC relay is too large to fit inside the box or near the cables, so these are located on the upper face of the box. The W172DIP-5 relay is placed on a circuit board held above the bottom of the box by a spacer, such that none of the parts on the upper face is in contact with the circuit board.

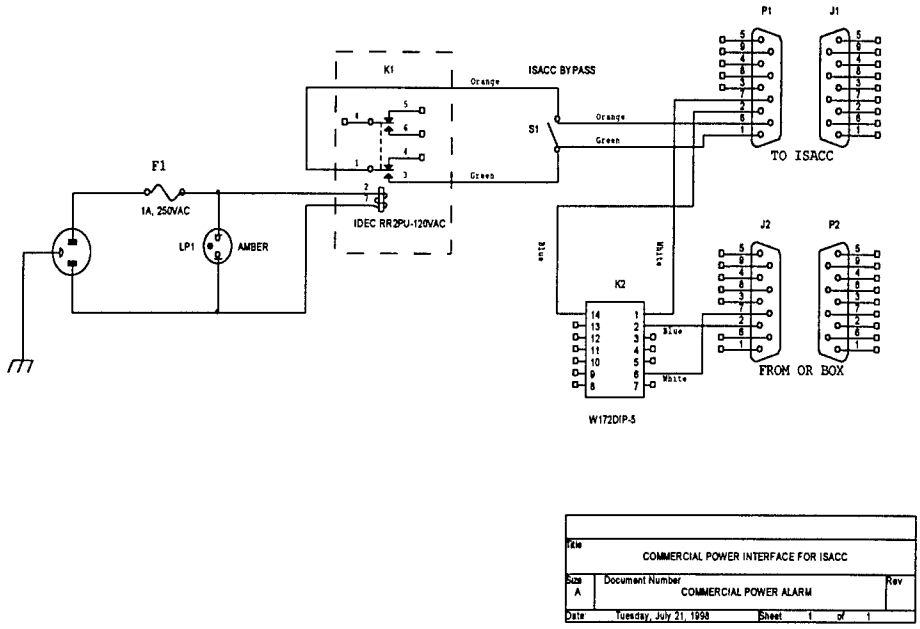

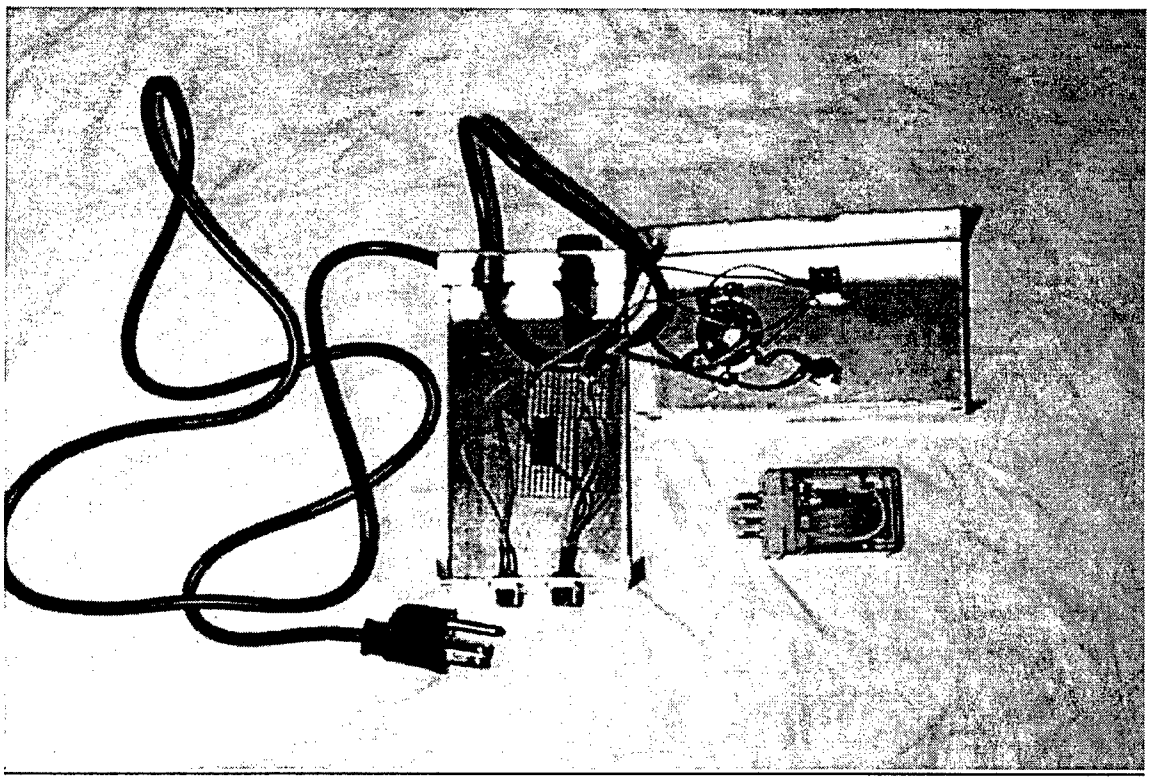

Commercial Power Interface: Internal w/ IDEC RR2PU-120VAC Relay

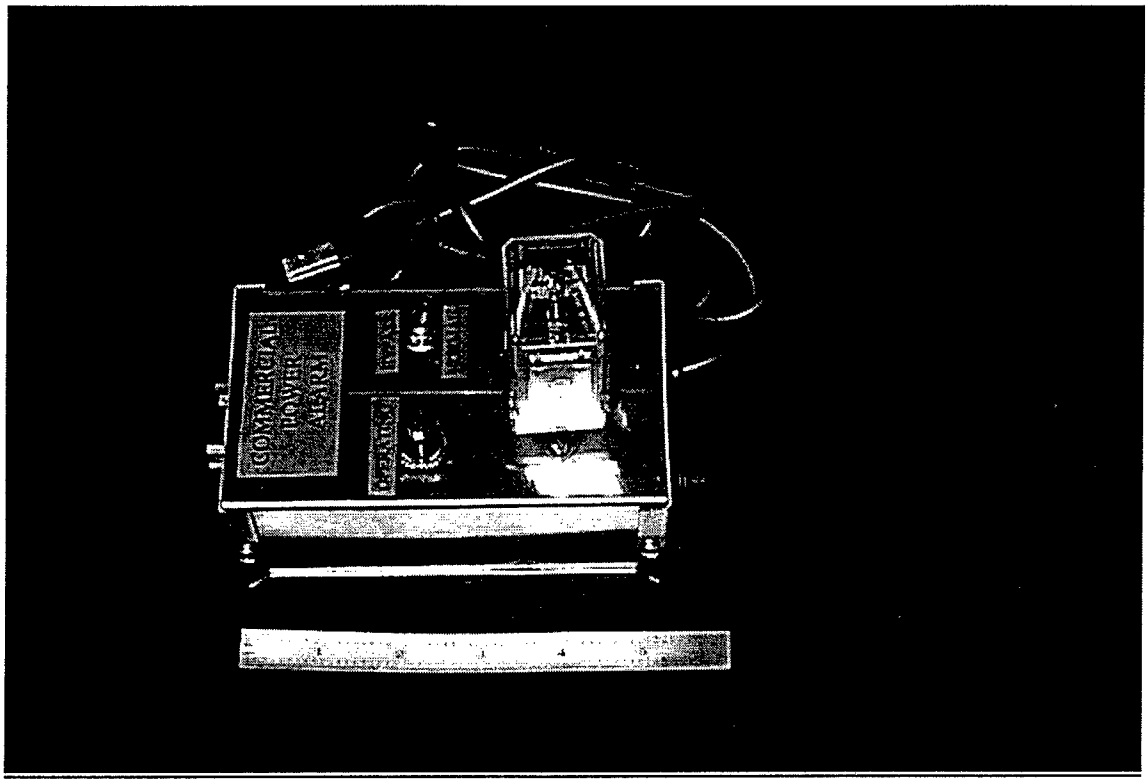

Commercial Power Interface: Top External

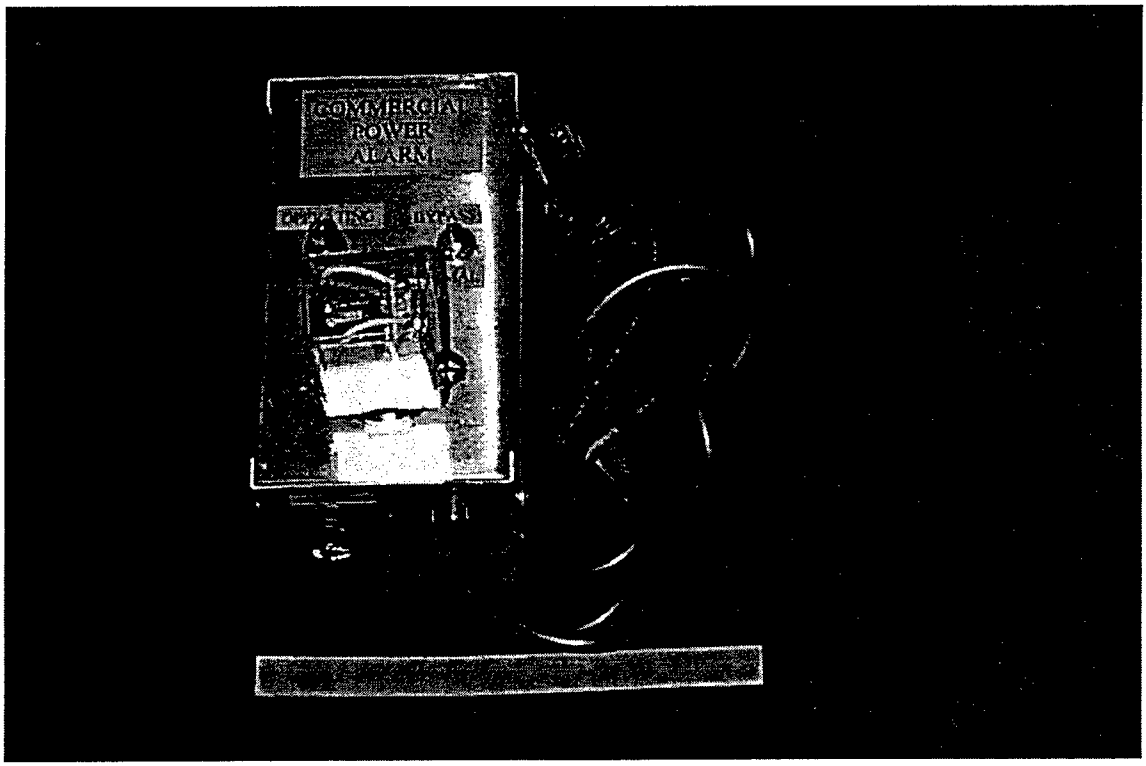

Commercial Power Interface: Top External

Results

The following tests were performed with a Fluke Digital Multimeter (DMM) to ensure correct wiring. Positive or negative results show whether or not the DMM showed a closed circuit. Whether a test should be positive or negative with or without a power source depends on the relay. Tests between *Line* or *Neutral* and anything grounded should be negative. Labels such as P1:1 refer to the part label in the wiring diagram and a pin number. *EPS* refers to a calibrated external power source used to simulate a signal from the OR Box Interface. *Line* and *Neutral* tests were performed on the male end of the power cord, whereas *Ground Pin* refers to any exposed wiring grounded to the inner box surface. "170 VAC to P3" indicates the only test in which the power cord was plugged into an outlet. The word *Bypass* indicates that the ISACC Bypass switch was thrown.

DMM + lead to P1:2, DMM - lead to P1:7 . . . positive

EPS + lead to J2:2, EPS - lead to J2:7, DMM + lead to P1:2, DMM - lead to P1:7 . . . negative

DMM + lead to Line, DMM - lead to Ground Pin . . . negative

DMM + lead to Neutral, DMM - lead to Ground Pin . . . negative

DMM + lead to P1:1, DMM - lead to P1:6 . . . negative

170VAC to P3, DMM + lead to P1:1, DMM - lead to P1:6 . . . positive

S1 Bypass, DMM + lead to P1:1, DMM - lead to P1:6 . . . positive

Sample Outputs from ISACC PC Monitor

Interface Plugged in to Commercial Power, Normal Position

ISACC>sho inp

Input	Name		Value	Status
IN01 =	"VACUUM	" =	Closed	OK
IN02 =	"CHILLER	" =	Closed	OK
IN03 =	"6020	" =	Closed	OK
IN04 =	"HUGHES	" =	Closed	OK
IN05 =	"3503	" =	Closed	OK
IN06 =	"Commercial Power"	=	Closed	OK
IN07 =	"New 24" Chamb 1	" =	Closed	OK
IN08 =	"New 24" Chamb 2	" =	Closed	OK
IN09 =	"New 24" Chamb 3	" =	Closed	OK
IN10 =	"New 24" Chamb 4	" =	Closed	OK
IN11 =	"36" Enviro	" =	Closed	OK
IN12 =	"36" Chamb 1	" =	Closed	OK
IN13 =	"36" Chamb 2	" =	Closed	OK
IN14 =	"3585	" =	Closed	OK
IN15 =	"Unknown Tabletop"	=	Closed	OK
IN16 =	"Creare SSC	" =	Closed	OK

Interface Unplugged, Normal Position

ISACC>sho inp

Input	Name	Value	Status
IN01 =	"VACUUM " =	Closed	OK
IN02 =	"CHILLER " =	Closed	OK
IN03 =	"6020 " =	Closed	OK
IN04 =	"HUGHES " =	Closed	OK
IN05 =	"3503 " =	Closed	OK
IN06 =	"Commercial Power" =	Open	ALARM
IN07 =	"New 24" Chamb 1 " =	Closed	OK
IN08 =	"New 24" Chamb 2 " =	Closed	OK
IN09 =	"New 24" Chamb 3 " =	Closed	OK
IN10 =	"New 24" Chamb 4 " =	Closed	OK
IN11 =	"36" Enviro " =	Closed	OK
IN12 =	"36" Chamb 1 " =	Closed	OK
IN13 =	"36" Chamb 2 " =	Closed	OK
IN14 =	"3585 " =	Closed	OK
IN15 =	"Unknown Tabletop" =	Closed	OK
IN16 =	"Creare SSC " =	Closed	OK

Interface Unplugged, Bypass Position

ISACC>sho inp

Input	Name		Value	Status
IN01 =	"VACUUM	" =	Closed	OK
IN02 =	"CHILLER	" =	Closed	OK
IN03 =	"6020	" =	Closed	OK
IN04 =	"HUGHES	" =	Closed	OK
IN05 =	"3503	" =	Closed	OK
IN06 =	"Commercial Power"	=	Closed	OK
IN07 =	"New 24" Chamb 1	" =	Closed	OK
IN08 =	"New 24" Chamb 2	" =	Closed	OK
IN09 =	"New 24" Chamb 3	" =	Closed	OK
IN10 =	"New 24" Chamb 4	" =	Closed	OK
IN11 =	"36" Enviro	" =	Closed	OK
IN12 =	"36" Chamb 1	" =	Closed	OK
IN13 =	"36" Chamb 2	" =	Closed	OK
IN14 =	"3585	" =	Closed	OK
IN15 =	"Unknown Tabletop"	=	Closed	OK
IN16 =	"Creare SSC	" =	Closed	OK

Conclusion

All wiring is correct -- nothing has been accidentally shorted. The commercial power alarm, the ISACC Bypass switch, and the OR Box Interface Relay all function as intended. The interface is interchangeable with the old two-chamber relay boxes. It has been installed and is in operation.

MODRTAN VALIDATION

Jeremy Wertheimer

Buckingham Browne & Nichols School
80 Gerry's Landing Road
Cambridge, MA 02138

Final Report for:
High School Apprenticeship Program
Phillips Laboratory

Sponsored by:
Air Force Office of Scientific Research
Bolling Air Force Base, DC

And

Phillips Laboratory

August 1998

MODTRAN VALIDATION

Jeremy Wertheimer
Buckingham Browne & Nichols School

Abstract

The objective was to test the accuracy of the computer model MODTRAN3.5 that predicted atmospheric transmittance and radiance. For each set of interferometer data, the recorded radiance, spectrally degraded to intervals between 525 cm^{-1} and 1795 cm^{-1}, was compared to the respective predictions from MODTRAN. The overall mean percent error was 0.22% and the overall average standard deviation of the percent error was 4.29%. The results indicated that MODTRAN was accurate enough to give a fairly good representation of atmospheric transmittance and radiance.

MODTRAN VALIDATION

Jeremy Wertheimer

Introduction

MODTRAN3.5 was a computer model that was able to predict the transmittance and radiance of the atmosphere. It used information about a specific atmospheric profile to predict radiance values using a band model approach. Another possible approach was a line by line determination of the atmospheric radiation. This would have been more accurate but much slower than that of MODTRAN. MODTRAN has, until now, never been validated for actual atmospheric conditions. If MODTRAN was accurate enough, it would give good estimations of atmospheric radiation and transmittance. This would make possible quick and accurate remote identification of surface properties from space based platforms.

Methodology

In order to find the accuracy of MODTRAN, it was necessary to compare its predictions against very accurate recorded radiance data. The ARM CART site in Lamont, Oklahoma gathered the necessary data during April of 1997 using a well-calibrated interferometer. This AERI (atmospheric emitted radiance interferometer) data was scanned and converted to the lower resolution of 4 wavenumber cm^{-1} half width at half maximum so that it matched a MODTRAN run at 8 cm^{-1} half width.

The AERI data was graphed with radiance on the y-axis and the wavenumber on the x-axis. When the measured part of the atmosphere was cloudless, the window region (about 800 cm^{-1} to 1300 cm^{-1}) was marked by a low radiance and an ozone peak around the 980-1080 cm^{-1} range [Figure 1a on the next page]. However, when there was high

atmospheric humidity or a cloud in the interferometer's line of sight, the radiance would go up in this region [Figure 1b]. MODTRAN was only compared to the relatively clear conditions. It would have been possible to simulate cloudy conditions with MODTRAN but adjusting MODTRAN until its output resembled the cloudy AERI data would have been counterproductive to the objective.

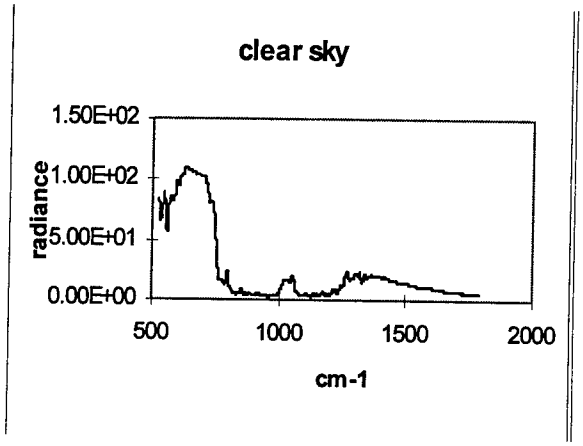

Figure 1a

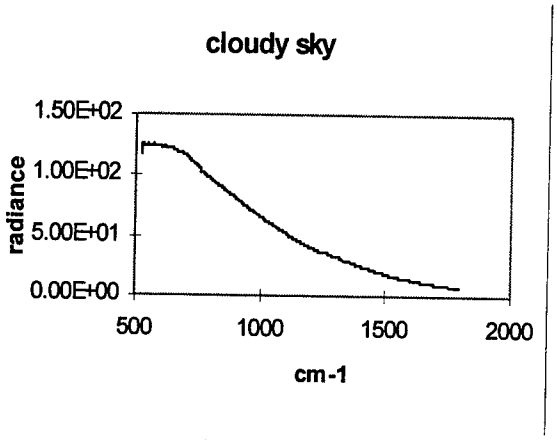

Figure 1b

Figure 1a/b: typical AERI radiance measurements. Figure 1a was a radiance measurement from a clear sky. Prominent features of the window region included, a CO_2 peak around 750 cm^{-1}, an O_3 peak around 1000 cm^{-1}, and a H_2O peak around 1300 cm^{-1}. Figure 1b was a radiance measurement from a cloudy sky. The window region has been filled in making it hard to see individual peaks. Only clear sky measurements, like the one displayed in Figure 1a, were used for the MODTRAN comparisons.

After finding a set of data with clear sky conditions, the radiosonde was used as an input for MODTRAN. The radiosonde was a stream of data from a weather balloon showing pressure, temperature, and relative humidity from the same date, time, and approximately the same place as the AERI measurement. The place was approximate because weather balloons have a tendency to drift off course on account of wind. Each MODTRAN radiance value was then compared to the AERI value of the same wavenumber in order to determine the error. [Table 1 on the next page is an example of the organization of the data and calculations.] Column A was the wavenumber (cm^{-1}),

Table 1

A	C	D	E	F	G	H
1790	5.49E+00	5.33E-07	5.4949E-07	1.62E-08	3.04%	3.04%
1791	5.47E+00	5.31E-07	5.47204E-07	1.62E-08	3.05%	3.05%
1792	5.44E+00	5.29E-07	5.44074E-07	1.52E-08	2.87%	2.87%
1793	5.36E+00	5.27E-07	5.35768E-07	8.84E-09	1.68%	1.68%
1794	5.20E+00	5.25E-07	5.19683E-07	-5.35E-09	-1.02%	1.02%
1795	4.96E+00	5.23E-07	4.95959E-07	-2.72E-08	-5.21%	5.21%
wavenumber	AERI	MOD	converted AERI	mean error	mean%error	mean abs%error
				5.859E-09	1.50%	3.85%
					stand derivation	
					5.53%	

Table 1: example of the last section of one of the 44 calculation tables containing spectrally degraded AERI data, MODTRAN predictions, and the resulting error calculations. Column A's range was always 525 cm^{-1} to 1795 cm^{-1} (part of the infrared spectrum). A detailed explanation of the statistics is in the text below.

column C was the AERI radiance data ([W/cm^2-ster-cm^{-1}]*10E7), column D was the MODTRAN radiance predictions (W/cm^2-ster-cm^{-1}), column E was the AERI data converted to the MODTRAN scale by being multiplied by 10^{-7}, and column F was the difference between the converted AERI data and the MODTRAN data. In other words, it was the relative error of the MODTRAN prediction calculated by an AERI radiance value minus the neighboring MODTRAN radiance value. The number at the bottom of the error column was the mean error. It was calculated by averaging the error column above it. Column G was the percent error of the MODTRAN prediction. Each column G cell was calculated by dividing the column F error in the same row by the MODTRAN prediction and then multiplying by 100 to get percent error. The second to bottom value in column G was mean percent error and the bottom value in this column was the standard deviation of the error percentages above it. Column H was the absolute value of the percent error in column G. The number at the bottom was the mean of the above positive errors. This mean absolute percent error value was calculated so that it was

possible to discern the extent to which the mean error was reduced by the canceling between positive and negative errors.

Results

Table 2

A	B	C	D	E	F	G	H	I
date	**time**	**notes**	**mean error**	**mean % error**	**mean absolute % error**	**standard deviation%**	**H_2O amount**	**CO_2 amount**
04/01/97	05	cloud						
	11	cloud						
	14	***clear***	7.48E-09	0.24%	3.39%	3.63%	2.7621E+03	2.7874E+02
	17	cloud						
	20	cloud						
04/02/97	05	cloud						
	11	cloud						
	14	***clear***	1.39E-08	0.98%	3.68%	3.05%	2.8424E+03	2.7935E+02
	17	cloud						
	20	cloud						
	23	cloud						
04/03/97	all	cloudy						
04/04/97	all	cloudy						
04/07/97	all	cloudy						
04/08/97	02	***clear***	-1.94E-09	1.13%	3.05%	4.62%	1.6350E+03	2.7910E+02
	05	cloud	4.96E-08	4.07%	5.04%	7.51%	1.9673E+03	2.7928E+02
	08	cloud						
	11	cloud						
	14	cloud						
	17	cloud						
	20	cloud						
	23	cloud						
04/09/97	all	cloudy						
04/10/97	all	cloudy						
04/11/97	all	cloudy						
04/12/97	all	cloudy						
04/13/97	02	***clear***	-3.14E-08	-2.96%	4.49%	6.20%	7.0215E+02	2.7983E+02
	05	***clear***	5.86E-09	1.50%	3.85%	5.53%	6.7147E+02	2.7985E+02
	08	***clear***	1.67E-08	2.78%	4.84%	7.35%	6.2595E+02	2.8001E+02
	11	***clear***	-6.50E-09	0.81%	3.66%	5.66%	6.7649E+02	2.8003E+02
	14	cloud						
	17	***clear***	-3.10E-08	-1.37%	3.79%	4.95%	8.0537E+02	2.8042E+02
	20	***clear***	-2.10E-08	-0.90%	3.44%	4.72%	8.7534E+02	2.8019E+02
	23	***clear***	invalid data					invalid data

A	B	C	D	E	F	G	H	I
date	**time**	**notes**	**mean error**	**mean % error**	**mean absolute %error**	**standard deviation%**	**H_2O amount**	**CO_2 amount**
04/14/97	02	***clear***	invalid data					invalid data
	05	***clear***	-5.45E-09	0.34%	3.54%	5.28%	6.5117E+02	2.7997E+02
	08	***clear***	-5.04E-07	0.04%	3.32%	4.72%	6.6074E+02	2.7995E+02
	11	***clear***	-3.20E-08	-1.83%	3.93%	5.07%	8.1165E+02	2.7998E+02
	14	***clear***	-1.80E-08	-1.52%	3.73%	5.34%	8.6652E+02	2.7976E+02
	17	***clear***	-3.10E-08	-1.36%	3.54%	4.71%	9.9561E+02	2.7970E+02
	20	***clear***	-1.50E-08	-0.70%	2.92%	4.17%	1.0813E+03	2.7909E+02
	23	***clear***	-2.30E-08	-1.74%	3.18%	4.52%	1.0491E+03	2.7841E+02
04/15/97	14		invalid data					
	17	smlCld	3.76E-07	18.57%	18.57%	17.39%	1.0491E+03	2.7841E+02
	20	***clear***	5.04E-08	2.72%	3.33%	4.66%	1.7709E+03	2.7836E+02
04/16/97	02	***clear***	3.20E-08	0.90%	2.42%	3.29%	1.9820E+03	2.7887E+02
	05	***clear***	4.37E-08	1.94%	2.91%	3.95%	2.2290E+03	2.7958E+02
	08	cloud						
	11	cloud						
	14	cloud						
	17	smlCld						
	20	smlCld						
	23	***clear***	6.31E-08	3.00%	3.59%	4.66%	1.6332E+03	2.8048E+02
04/17/97	02	***clear***	-4.04E-09	-0.83%	2.42%	3.36%	1.6349E+03	2.8068E+02
	05	***clear***	-2.17E-08	-1.76%	2.83%	3.81%	1.5665E+03	2.8048E+02
	08	cloud						
	11	cloud						
	14	smlcld	6.34E-08	3.43%	4.11%	5.42%	1.8152E+03	2.8090E+02
	17	smlCld	1.07E-07	5.20%	5.51%	6.49%	1.6341E+03	2.8067E+02
	20	haze	6.23E-08	2.79%	3.40%	4.29%	1.7694E+03	2.8004E+02
	23	***clear***	4.34E-08	1.50%	2.91%	3.75%	1.8134E+03	2.7907E+02
04/18/97	02	***clear***	-2.42E-08	-1.55%	2.73%	3.61%	1.8744E+03	2.7880E+02
	05	***clear***	2.48E-08	0.33%	2.61%	3.62%	1.7336E+03	2.7834E+02
	08	***clear***	-4.45E-09	-0.31%	2.31%	3.29%	1.6896E+03	2.7641E+02
	11	***clear***	2.25E-08	0.99%	2.08%	2.82%	2.1390E+03	2.7779E+02
	14	smlCld						
	17	smlCld						
	20	cloud						
	23	cloud						
04/19/97	02	smlCld	9.15E-08	3.93%	4.24%	5.38%	2.0317E+03	2.7605E+02
	05	***clear***	-3.90E-09	-0.45%	2.23%	3.37%	2.1581E+03	2.7637E+02
	08	***clear***	-5.06E-08	-2.28%	4.12%	5.51%	2.3009E+03	2.7638E+02
	14	***clear***	-1.38E-08	-0.56%	2.30%	3.25%	2.1444E+03	2.7671E+02
	17	***clear***	3.13E-08	1.19%	2.38%	3.47%	2.1414E+03	2.7696E+02
	20	haze	8.33E-08	3.20%	3.59%	4.49%	2.2924E+03	2.7654E+02

A	B	C	D	E	F	G	H	I
date	**time**	**notes**	**mean error**	**mean % error**	**mean absolute %error**	**standard deviation%**	**H_2O amount**	**CO_2 amount**
	23	smlCld						
04/20/97	02	***clear***	2.73E-08	0.28%	2.29%	3.06%	2.1942E+03	2.7619E+02
	05	cloud						
	08	***clear***	2.48E-08	0.86%	2.15%	3.03%	2.5788E+03	2.7583E+02
	14	cloud						
	17	cloud						
	20	***clear***	1.04E-07	3.51%	3.75%	4.25%	2.4474E+03	2.7491E+02
	23	***clear***	6.91E-08	2.20%	2.82%	3.92%	2.4388E+03	2.7504E+02
04/21/97	02	***clear***	2.05E-08	0.71%	2.76%	4.17%	1.8097E+03	2.7509E+02
	05	haze	-3.68E-08	-1.88%	3.39%	4.58%	1.9588E+03	2.7556E+02
	08	cloud						
	11	cloud						
	14	cloud						
	17	cloud						
	20	cloud						
	23	cloud						
04/22/97	all	cloudy						

Table 2: results of all MODTRAN predictions compared to the AERI data. Table 2 included the date, time and comparison statistics for each data set that was recorded in clear sky conditions. Cloudy measurements were generally not analyzed. An explanation of the organization is in the text below and an explanation of the math is contained in the Methods section earlier in the paper.

The results of all 20 days of data were organized in Table 2 [above]. Column A contained the date on which the data for the calculations following it were collected and column B was the time rounded down to the hour on a 24 hour clock. Column C contained notes on the suspected conditions of that time or day. "*Clear*" signified clear sky conditions and a valid set of comparison calculations. "Cloud" indicated that the window region of the AERI data was filled in [see Figure 1b]. "SmlCld" indicated that the window region was beginning to fill in. "Haze" signified that there was a slight rise of radiance in the window region and a high relative humidity was contained in the radiosonde data. A day in which all the AERI data was invalid on account of clouds was indicated by the time of "all" in column B and "cloudy" in column C. Columns D, E, F,

and G represent mean error, mean percent error, mean absolute percent error and the standard deviation of the percent error respectively. The numbers came directly from the process described in the Methods section. H_2O amount and CO_2 amount in columns H and I came from the radiosonde data. They were recorded there in case they had any bearing on the accuracy of MODTRAN.

In the 20 analyzed days, there were 36 sets of data taken in clear sky conditions. The average mean percent error from these was 0.22%. The fact that this number was so close to zero was expected because the positive and negative error values should have almost canceled each other out. The average mean absolute percent error was 3.15% which was lower than expected, given the possible modeling and measurement errors. MODTRAN was not as accurate as a line by line (LBL) determination of the atmospheric radiance when both models use the same atmospheric conditions. The LBL calculations usually led to a mean absolute percent error about 1% lower than that of a MODTRAN run. However, the standard mode of operating a line by line determination (without aerosols) led to much poorer results by roughly a factor of two. The overall MODTRAN average standard deviation of the percent error was 4.29% which was not terrible but could be better.

Analysis

It was possible to organize the 36 sets of clear sky comparisons in several different ways. The simplest way was to create bar graphs with each of the 36 bars representing one value from each of the 36 data sets. Figures 7, 8, and 9 [appended at the end of this paper] were organized that way. Figure 7 showed the mean percent error of each data set, Figure 8 showed the mean absolute percent error, and Figure 9 showed the

standard deviation of the percent error. Table 3 served as a legend for Figures 7, 8, and 9 to show which of the 36 data collection times went with which x-axis number. Figure 7 indicated that the mean percent error was usually more positive than negative since the range was from -2.96% to 3.51%. Also there were 21 positive values and only 15 negative values. This meant that the MODTRAN predictions were usually slightly below the AERI measurements. This could have been blamed on clouds or aerosols that were not accounted for in the MODTRAN model.

The mean absolute percent error values in Figure 8 were between 2.08% and 4.84%. This was fairly good. This meant that the mean error values in Figure 7 were not just low because they were canceling each other out. The general shape of the standard deviation values in Figure 9 (standard deviation) resembled the shape of Figure 8 (mean absolute percent error). From these bar charts, a relatively large mean absolute percent error usually, but not always, meant that the same data would have a relatively large standard deviation. This was expected because as the accuracy of MODTRAN drops, the standard deviation should rise.

In order to find the affect of relative humidity on the accuracy of MODTRAN, Figure 10, on the next page, compared the mean absolute percent error to the water amount. It was not clear as to whether the accuracy and the water amount were directly related. In Figure 10, as the water amount went up, the error seemed to go down in a linear fashion. This may indicate that MODTRAN was a better model at higher water amounts. However, it was known that at very high water amounts, MODTRAN must be adjusted before it can give accurate predictions. There was not enough data to decide

whether the points at the high water amounts around 2.5E3 are outliers or the beginning of the breakdown of MODTRAN's predictions.

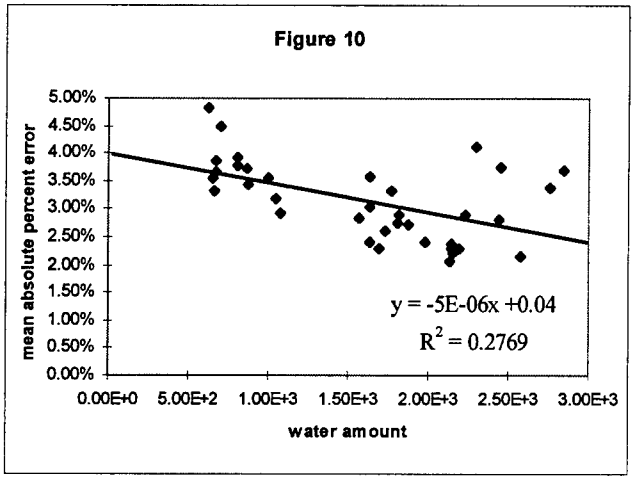

Figure 10

Figure 10: plot of the relationship between water amount on the x-axis and mean absolute percent error on the y-axis with a fitted line and a R^2 value. This graph showed the affect that water amount has on the accuracy of MODTRAN. From the fitted line, it appeared that the mean absolute percent error goes down as water amount goes up but this could not continue forever. Also, the R^2 value was too low to make the fitted line useful. The result of water's affect on MODTRAN was inconclusive in this study.

Conclusion

The final outcome of this experiment was that MODTRAN3.5 was proven to be fairly effective in simulating real world atmospheric radiance. Compared to very accurate radiance data, it had an overall mean percent error of 0.22% due to cancellation, a mean absolute percent error of 3.15%, and a mean standard deviation of 4.29%. The relationship between water amount and accuracy was inconclusive.

Table 3 (legend)

number	date	time
1	4/1/97	14:00
2	4/2/97	14:00
3	4/8/97	2:00
4	4/13/97	2:00
5		5:00
6		8:00
7		11:00
8		17:00
9		20:00
10	4/14/97	5:00
11		8:00
12		11:00
13		14:00
14		17:00
15		20:00
16		23:00
17		20:00
18	4/16/97	2:00
19		5:00
20		23:00
21	4/17/97	2:00
22		5:00
23		23:00
24	4/18/97	2:00
25		5:00
26		8:00
27		11:00
28	4/19/97	5:00
29		8:00
30		14:00
31		17:00
32	4/20/97	2:00
33		8:00
34		20:00
35		23:00
36	4/21/97	2:00

Table 3: legend for Figures 7, 8, and 9. The left-hand column contained the numbers from the x-axis of the following 3 figures. Each number was matched with the corresponding date and time of day that the ARM CART site in Oklahoma obtained the data set. Times are rounded down to the hour in order to facilitate analysis by a computer. Dates apply to all data sets on the same row and below until the next date.

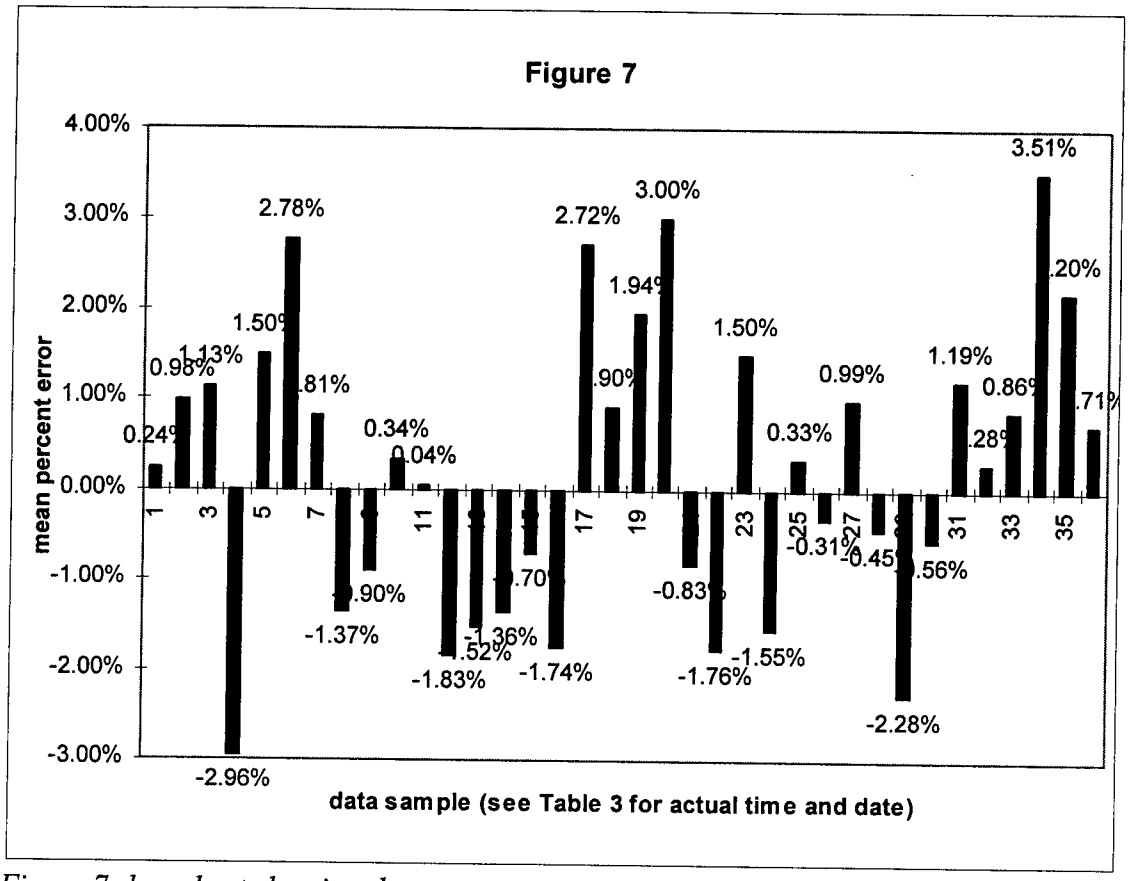

Figure 7: bar chart showing the mean percent error of each data set. Since the range, mean, and median lean toward the positive side and there are more positive then negative values, a typical AERI measurement was higher than its corresponding MODTRAN3.5 prediction. Perhaps there was some aerosol present in the atmosphere that was unaccounted for by MODTRAN.

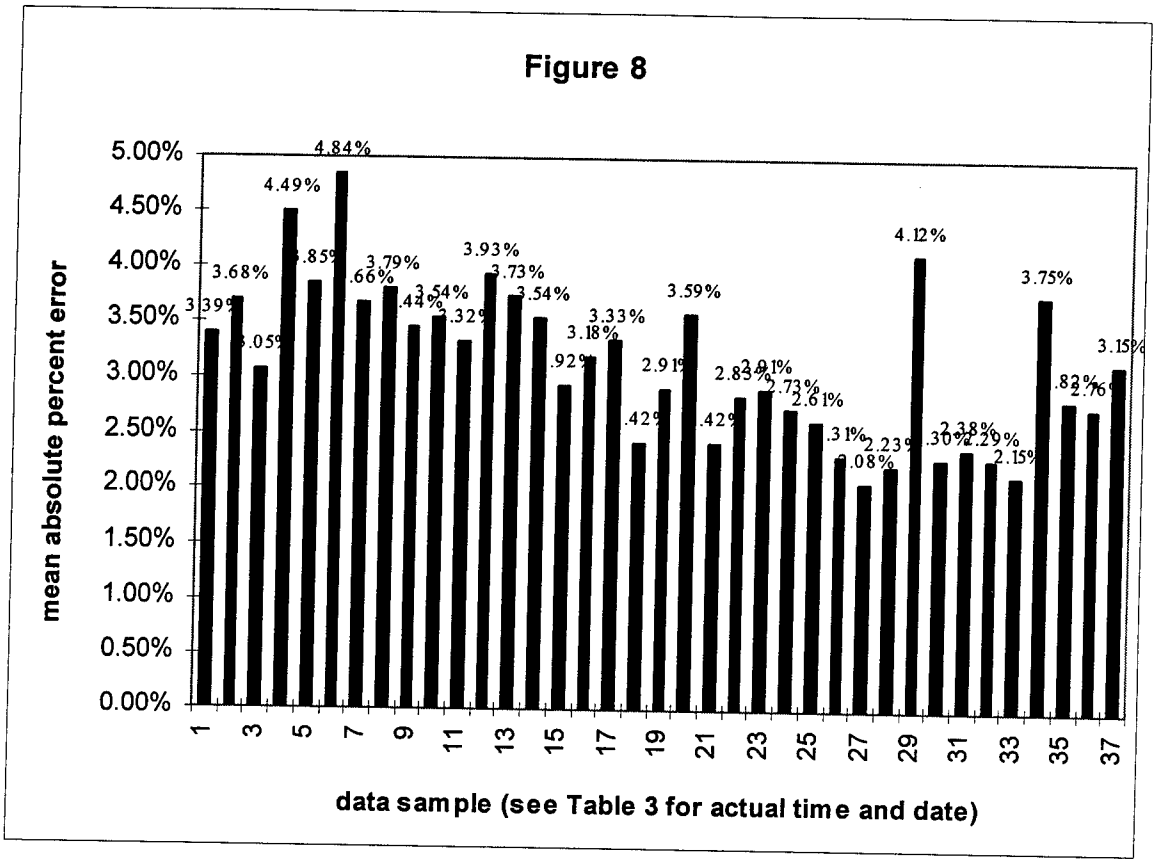

Figure 8: bar chart showing the mean absolute percent error of each data set. The range, from 2.08% to 4.84%, was not perfect but was not a significant cause for concern. The mean was 3.15% and the median was 3.12% so Modtran was fairly accurate when the canceling between positive and negative values was taken into account.

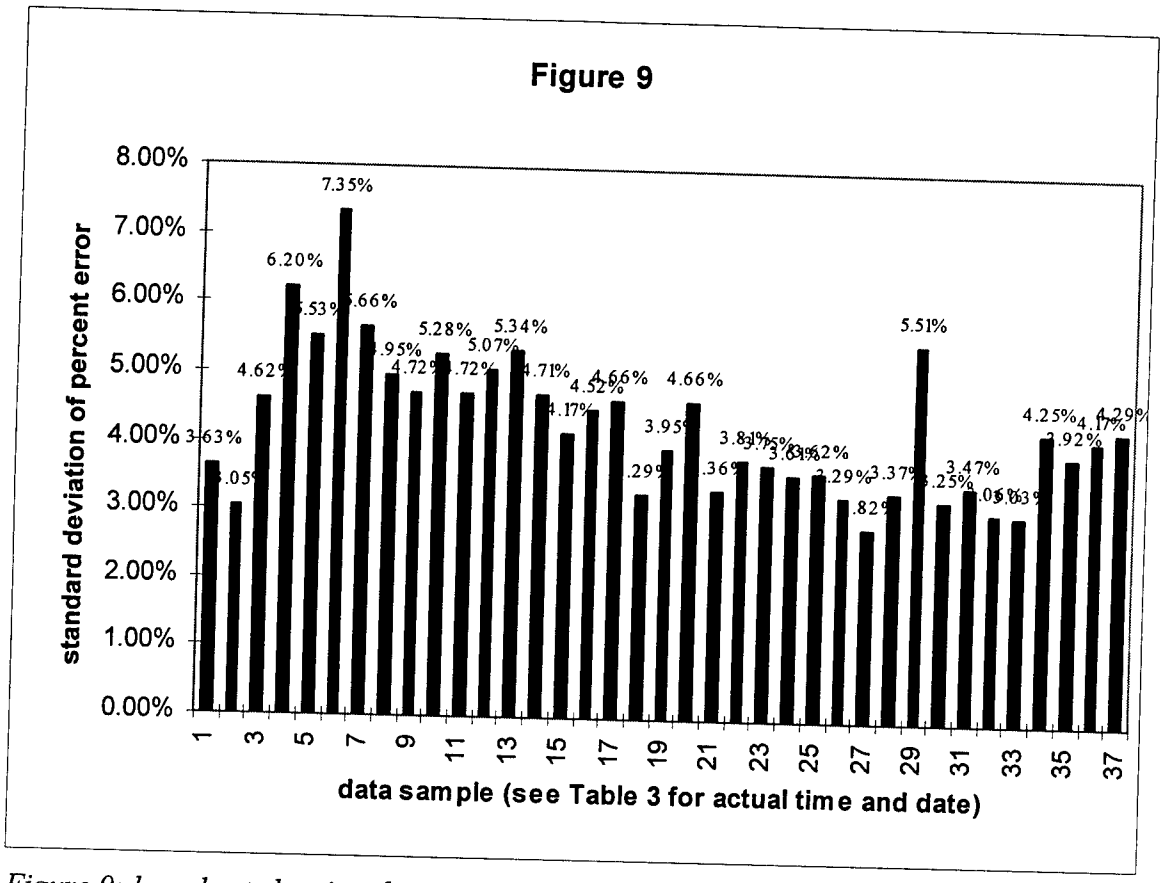

Figure 9: bar chart showing the standard deviation of the percent error values from each data set. The mean standard deviation was 4.29% and the median was 4.17%. These values showed the slight inconsistency of the MODTRAN model. The error values were usually spread out since MODTRAN was never perfect and when the radiance was very low, the percent error goes up even when MODTRAN was off by the same amount. The error values can sometimes climb as high as 30% for wavenumber values around 900 cm^{-1}. See Figures 10a, b, and c for examples of this.

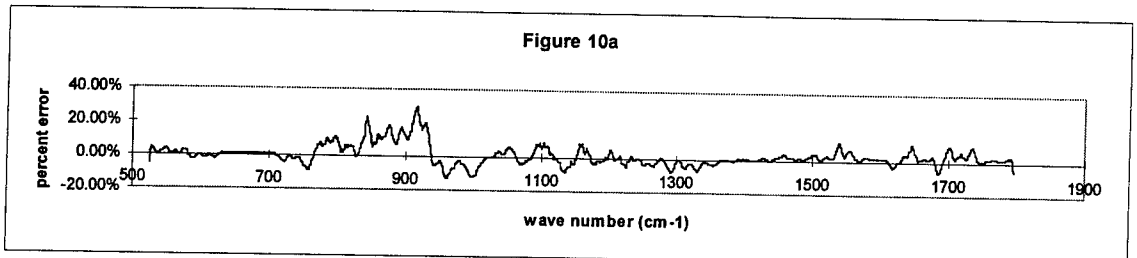

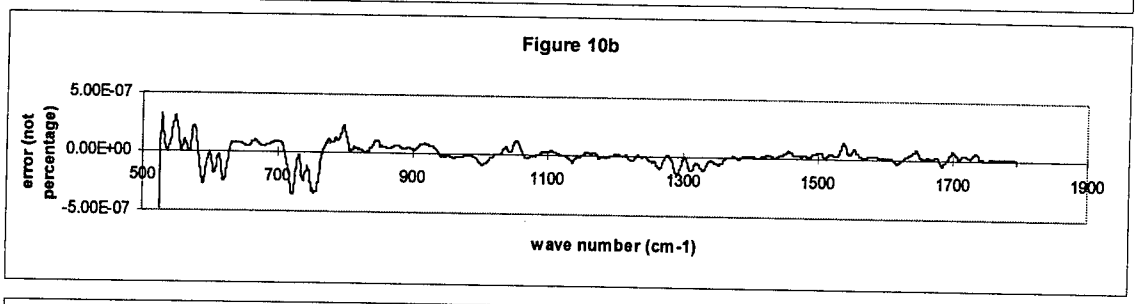

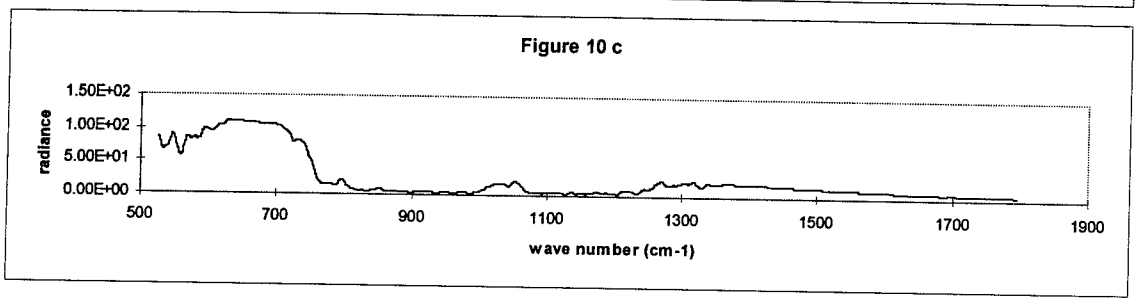

Figures 10 a/b/c: Comparisons of different ways of looking at error from the same set of data. There were two ways to calculate over all error. The first was to find the percent error (see Figure 10a) which was calculated in column G of table 1. The second was to find the actual error (sometimes called the absolute error but having nothing to do with the absolute value function) which was done in column F of Table 1. The advantage of working with percent error was that error from different data sets could then be compared without worrying about one data set having an overall higher radiance than the other. However, the drawback was that, when the MODTRAN radiance value was low as it was around 900 cm^{-1} in Figure 10c, the percent error was high as in Figure 10a at then same wavenumber. This was because the percent error was calculated by dividing the actual error by the MODTRAN prediction. Conversely, when the MODTRAN radiance value was high, as in the $C0_2$ band around 750 cm^{-1}, the actual error was high because there was more room for MODTRAN to make an error.

Summer Work Projects

Jeremy L. White

Sandia Preparatory School
532 Osuna Road N.E.
Albuquerque, NM 87113

Final Report for:
High School Apprentice Program
Phillips Laboratory

Sponsored by:
Air Force Office of Scientific Research
Bolling Air Force Base, DC

and

Phillips Laboratory

January 1995

Summer Work Projects

Jeremy L. White
Sandia Preparatory School

Abstract

During my tenure at Phillips Laboratory as part of the High School Apprenticeship Program I worked on a series of projects. The first of these projects was designing a web page for the Component Characterization Group of the Space Electronics and Protection Branch. The next project on which I worked was using computer programming to aide in the operation of an Aracor irradiation device. I also learned of some of the effects of high energy electron irradiation on plexiglass.

Summer Work Projects

Jeremy L. White

The summer research program has been an incredible experience for me, even for my second time participating in it. I learned a great deal of information which I may not even see when I attend a university next school year. This program has also greatly enhanced my academic qualifications. Some of the tasks that I was given included the construction of a web page and the use of computer programming to assist in the calibration of an irradiation device. Another event that occurred during my summer research was an explanation and demonstration of the "Lichtenberg Tree" effect.

The first task which was assigned to me during my summer research program was to assist in building a web page for the Component Characterization Group at Phillips Laboratory. This web page had already been started by Dr. Harald Schone prior to my arrival at the Laboratory. Thus, a template for some of the pages had already been created. This template was for the pages that contained the biographical information of the various members of the group. However, most of the biographical information was yet to be gathered and transferred to the web page with the exception of Dr. Schone. Most of the work that I did for those pages was transferring the biographical information, which was written up and submitted to me by the members of the group, to the pages. It was also necessary to compress the member's images using an image conversion piece of software. After the information was formatted, I then linked the pages to each member's email account. There were several other pages, which I either designed or modified by manipulating the color settings, text format, or picture layout. This part of my experience took approximately two and a half weeks of my time at the lab.

The second, and most interesting project for me, was working with the Aracor irradiation device. This device is used to irradiate electronic equipment, such as microprocessors and ram, which are intended for use in space, or any other high radiation environment. This device, unfortunately, requires calibration before use, no matter if it has been one day or one month since it was last used. This process is very time consuming, or so I heard; I was never actually witness to this procedure. The solution to dealing with this

time consuming calibration process was employing computer programming to take care of it. A special add-on card for the computer allowed the machine to be controlled from the computer. Fortunately, this card came with a library of functions which allowed a program written in Quick Basic to control the Aracor. This program was worked on prior to my involvement with the effort. As this was my first experience at writing a real program with any computer programming language, I was not asked to finish the program alone. Before I actually worked on this program, I learned the basics of the language by reading a book about Quick Basic and through looking at the help files built into the compiler, and completed practice programs which were created by Dr. Harald Schone to teach me how to program. After this brief learning experience, I went to work on the program with Mr. Donovan Curley. The first task that was given to me was writing a sub program which would be run whenever an error was detected while the main program was running. Error trapping statements were a necessary addition to the program, as the machines (the computer and the Aracor) may not always function properly, and a person would not be monitoring the process, hence the purpose of the computer program. The purpose of this sub program was to stall the main program until a knowledgeable person would take notice that there was a problem, find out what it is, and fix it. This was not an easy task due to the location of the computer. The computer was located such that the monitor was facing one of the outer walls of the laboratory. Due to this, the monitor was not visible to any person in the room, unless he or she was working right next to the computer. As a result, I was forced to use more than just a visual warning system. As the computer had no sound card, and would not recognize the one which we (Donovan Curley and I) attempted to install, I had to use the PC speaker, which had limited capabilities. Luckily, I found some help files in the compiler on using sound, and learned how to make a tone similar to an alarm or police siren. This speaker was not very loud of course, and was even more quiet when Windows® 95 was running. With Window® 95 off, fortunately, the siren was loud enough to catch the attention of a person entering the laboratory, even when the air-conditioner was on. I used a series of loops to repeat this siren, and flash a message on the screen until someone came by to see what was wrong. The message was just a general message however, but it served its purpose of alerting anyone nearby to an error. After completing this sub program, I began to assist Donovan Curley in completing the rest of the program

by writing some code for the calibrations required for a month or more of idle time for the Aracor and by helping to fix bugs in the existing code. When the end of the summer research program came, the program was nearly finished, and only needed some cleaning up and minor additions before being used to calibrate the Aracor.

The last and perhaps the most exciting event of the summer research program for me was learning about the "Lichtenberg Tree" effect. This part of my research was more for my personal benefit than anything else. What we did for this little experiment was to cut and polish some one-half inch thick plates of plexi-glass using saws, sand paper and a blow torch. We then drilled a small hole, parallel to and one-eighth of an inch below the surface of the plate. Then a small metal pin was inserted into the hole. After creating the plates, we bombarded them with electrons using the Dynamitron 1MeV linear electron accelerator. The result of this bombardment is the "Lichtenberg Tree" effect. When the plate is shot with electrons, the electrons come to rest in the plate due to insufficient energy to penetrate all the way through. This depth was one-eighth of an inch for the plexi-glass. The accumulation of the electrons causes the formation of local electric fields, which when exceed the insulating strength of the plexi-glass, or when the field pattern is disturbed by a small hole, such as the one we created, a discharge occurs. The electrons all migrate to the hole and pass out of the plexi-glass. The plexi-glass is ruptured in this process, and small tunnels are created in the plexi-glass which lead to the hole. The resulting pattern is very similar to that of a tree, only on a relatively two dimensional plane. This pattern is also very beautiful, especially when one side of the plexi-glass is coated with dark colored spray paint such as black.

On the whole, this program has brought many benefits with it for me. Learning how to make a web page was not only fun, but it may very well be an invaluable skill as the use of the internet increases. It could be useful even if it is just to make a personal web page for fun. Learning how to program in Quick Basic has helped me a great deal in school even though I am not using that particular language. I am currently enrolled in a C++ programming class, and because of the knowledge that I gained about programming this summer I am nearly a month ahead of all but one other student in the class, who has been programming in that language for a couple of years. Also, as a result, my teacher has been giving me extra

reading assignments apart from the rest of the class which is spreading the gap between me and the rest of the class even more quickly. I have also come to enjoy programming a lot, and have a compiler at home now. As for the experiment with the "Lichtenberg Tree" effect, it was probably one of the most interesting learning events in my life so far, and has furthered my interest in electricity and atomic level chemistry and related areas of physics, which I am also currently studying at school. This research program has been one of the best experiences in my life so far, and has inspired interest in future work at a laboratory.

References

The information used for this report was obtained through discussions with the following people from the Component Characterization group within the Space Electronics and Protection Branch of Phillips Laboratory, Kirtland Air Force Base, New Mexico: Capt. Ken Merkel, Mr. Joe Chavez, Mr. Bill Kemp, Dr. Harald Schone, Mr. Donovan Curley.